Fusion of radar data from multiple MIMO systems to achieve higher angular resolution

Anusha Ravish Suvarna

TU Delft

Fusion of radar data from multiple MIMO systems to achieve higher angular resolution

by

Anusha Ravish Suvarna

to obtain the degree of Master of Science
at the Delft University of Technology,
to be defended publicly on Wednesday August 18, 2021 at 09:00 AM.

Student number:	5009936	
Project duration:	October 1, 2020 – August 18, 2021	
Thesis committee:	Prof. DSc. Alexander Yarovoy,	TU Delft, supervisor
	Dr. Raj Thilak Rajan,	TU Delft
	Dr. Jianping Wang,	TU Delft, daily supervisor
	Arie Koppelaar,	NXP Semiconductors

This thesis is confidential and cannot be made public until August 31, 2022.

TU Delft

Abstract

In today's automotive applications, radar is widely used to estimate the target position and velocity with respect to the radar position. Estimating the position of the target in terms of range and velocity is fairly advanced and accurate. However, resolving two closely spaced targets in the azimuth domain which have the same range and relative radial velocity as seen from the radar is still a very challenging problem that needs to be addressed. The azimuth resolution that can be achieved by a radar sensor is directly proportional to the number of antenna elements in the radar, that is increasing the number of elements improves the resolution capability. But increasing the aperture of the single radar mounted on the automobile is not desirable as it is cost ineffective and not easy to fit in the design of the automobile. Thus a study is performed on combining the data from multiple radar sensors which are distributed over the fascia of the car along the horizontal axis. In this thesis, methods to achieve higher angular resolution in azimuth using multiple radar sensors is presented.

The system design and geometry for a distributed system consisting of FMCW radar sub-systems is studied along with the signal model for the same. The interpretation of near field and far field region around the radar sensors is presented. In this thesis, the Range-Doppler processing of the data is performed first and the snapshot related to the range and Doppler bin where the target is detected is extracted to perform the Direction of Arrival (DOA) estimation. This is done as it is computationally efficient and the DOA estimation can be performed on every snapshot and hence the changes in the target position can be detected faster. The signal model for DOA estimation using single sensor and distributed sensors is provided for single snapshot case. Sparse signal processing technique is chosen to estimate the DOA in this thesis as it has better performance and certain advantages in DOA estimation of target using single snapshot compared to other methods like Beam forming or MUSIC. The theory behind compressive sensing technique is discussed along with the concept of block sparsity to fuse the data from multiple sensors. A new algorithm called Block Focal Under determined System Solver (FOCUSS) is proposed to incoherently combine the data from multiple sensors in order to achieve a better performance. This method benefits from the spatial diversity gain by combining the data from multiple sensors. However, the resolution improvement achieved by the incoherent combining of the data from multiple sensors is still limited by the largest aperture of the sub-system used and hence a way to coherently combine the data from multiple sensors is presented. Coherent FOCUSS algorithm is proposed which combines the data from multiple sensors coherently and the virtual aperture of such combining is given by the separation between the sensors and hence it can achieve very high resolution in azimuth. Such a method has some drawbacks when the target is non-isotropic or the distance between the sensors is too large, which is also discussed in this thesis. A method called Fusion FOCUSS is introduced to overcome some of the drawbacks of coherent processing, whose resolution capability is in between that of Block FOCUSS and Coherent FOCUSS.

Simulations are performed to evaluate the performance of the proposed algorithms and for comparison purpose the results obtained from Block Orthogonal Matching Pursuit (BOMP) algorithm is provided. Monte Carlo runs are performed for different scenarios consisting of varying SNR, target phase and baseline of the distributed system. The performance of the algorithms with varying SNR values is presented. The penalty incurred in performing coherent processing on a non-isotropic target is discussed. The problem of off-grid targets is studied and a possible solution for the same is implemented as discussed in literature. Results obtained by performing an experimental evaluation in the anechoic chamber to study the performance of Block FOCUSS is presented along with the explanation of results. We also propose some ideas for future work to further investigate the problem.

Acknowledgements

I would like to thank **NXP Semiconductors, Eindhoven**, for giving me the opportunity to pursue my thesis in collaboration with **TU Delft**. I would like to thank my supervisors and mentors from TU Delft and NXP respectively, for playing a crucial role in the completion of my thesis.

Foremost, I would like to thank my supervisor **Prof. DSc. Alexander Yarovoy** for providing me the opportunity to pursue my thesis in his research group, Microwave Sensing, Signals and Systems. He has constantly believed in me and encouraged me tremendously in this eventful journey. He has not only shown keen interest in my thesis but also ensured that I took care of my physical and mental health. This was much needed in this unfortunate time, where the Covid pandemic has forced us all to work from home and has limited the human interaction on day-to-day basis. He also ensured that I was on the right track in my thesis during our regular meetings and has guided me throughout. He has been a constant source of energy and encouragement for all the students.

I would like to express my gratitude to daily supervisor **Dr. Jianping Wang** for his extreme patience and guidance during my thesis. I thoroughly enjoyed the technical discussions with Dr. Jianping during my research. He has been a great guide, answering all my technical queries and helping me take important decisions. He has not only been a technical guide during my thesis but has also provided me with great insights and knowledge into the technical community and has been a good friend who has helped me make the informed decisions in the next steps of my career. He has always been humble and helped me in solving the problem effectively, which enabled me to tie a lot of loose ends.

I would like to thank my **NXP** mentor **Arie Koppelaar**, who has been a tremendous support. Even though we met briefly in person only once before I started my thesis, it was extremely easy to work with Arie. He was always available to answer my questions and have ad hoc discussions about the research. He has patiently listened to my thoughts and questions, and helped me proceed in the right direction. He has been extremely encouraging to try out different ways, constantly providing ideas and feedback to help better my work. The guidance and support that I have received from Arie has helped not only in improving the quality of thesis but also my technical abilities.

I would like to express my thanks to **Feike Jansen** from **NXP**, for always challenging and encouraging me to do better. He has provided very valuable insights into the vastness of the problem that we are trying to solve in this thesis. He always made me look at the bigger picture and at the same time helped me realize all the nooks and corners of a given problem. He encouraged me to understand the concepts completely before working on solutions. This has made me grow as a researcher and has taught me in approaching a given problem in a more systematic way. He encouraged me to not be limited by the industry limitations and has enabled me to think beyond the limited scope when approaching a problem.

My research would not have been complete without experimental validation of the proposed algorithms. Thanks to **Pascal Aubry** from **TU Delft** for facilitating and helping me perform the necessary experiments in the TU Delft lab.

Last but not the least, I would like to thank all my friends in the Netherlands and friends across the globe, who ensured my well being and have been a constant source of support. I would like to express my utmost gratitude to my family. Even though we were separated by geographies, they have constantly encouraged me throughout my Masters and believed in me, which has kept me going in these challenging times. Special thanks to my little nephew who filled this tough time with his enthusiasm and laughter.

Anusha Ravish Suvarna
Delft, August 2021

Contents

List of Acronyms

ADC Analog to Digital converter.

AF Ambiguity Function.

BOMP Block Orthogonal Matching Pursuit.

BP Basis Pursuit.

BPDN Basis Pursuit Denoising.

BW Bandwidth.

CS compressive sensing.

DOA Direction of Arrival.

DOD Direction of Departure.

DTW Detection Window.

FA False Alarms.

FFT Fast Fourier Transform.

FMCW Frequency Modulated Continuous Wave.

FOCUSS Focal Under determined System Solver.

FOV Field of View.

MIMO Multiple Input Multiple Output.

MLW Main Lobe Width.

MSE Mean Square Error.

PFA Probability of False Alarm.

PR Probability of Resolution.

PRI Pulse Repetition Interval.

RCS Radar Cross Section.

RMSE Root Mean Square Error.

SLL Side Lobe Level.

SNR Signal-to-Noise Ratio.

ULA Uniform Linear Array.

List of Symbols

α	Ratio of bandwidth over FMCW chirp duration
$\dagger$	symbol used to define Moore-Penrose inverse
λ	Wavelength of the carrier frequency
$\mathbf{A}$	Steering matrix or sensing matrix in CS domain
$\mathbf{a}$	Steering vector
$\mathbf{N_s}$	Number of grid points in search grid (number of dictionary elements in CS)
$\mathbf{n}$	Noise vector
$\mathbf{W}$	Weighting matrix
$\mathbf{x}$	Source vector that needs to be estimated
$\mathbf{y}$	Measurement vector
Ψ	DOA of target with respect to sensor M2
τ	Round trip delay
θ	DOA of the target with respect to centre of the distributed system
φ	DOA of target with respect to sensor M1
A	Complex amplitude of the target
B	Baseline
d_m	Distance of a sensor from origin (half the baseline)
f_c	Carrier frequency of the radar waveform
K	Number of targets present
L	Number of virtual apertures in a distributed system
M	Number of radar sub-systems in a system
$M1$	The left sensor
$M2$	The right sensor
N	Number of virtual elements in a single sensor
N_{mc}	Number of experiments in each Monte Carlo trial
N_{Rx}	Number of receivers in a single sensor
N_{Tx}	Number of transmitters in a single sensor
Q	number of scatterers comprising a target
R	Range of the target from center of the distributed system
$R1$	Range of the target from sensor M1
$R2$	Range of the target from sensor M2
T	Pulse repetition time

1 Introduction

In this chapter, an introduction to the Direction of Arrival (DOA) estimation problem is provided along with the current state of art study. The motivation to solve the problem of DOA estimation in automotive radar with the use of distributed system is given in Section 1.1. The research objective of the thesis which is to achieve high resolution DOA estimation along with the novelty in this thesis is given briefly in Section 1.2. Section 1.3 discusses the current state of art in distributed radar and discusses the gaps in the existing methods. An outline of the thesis structure is presented in Section 1.4. Section 1.5 concludes the Chapter.

1.1. Motivation

In the last decade the interest in safety of drivers, passengers, pedestrians and other road users has increased significantly with the growth in automotive industry and economy of the nations. Radars play an important role in this as they can be used for detection of pedestrians, cyclists, other automobiles and in estimating other road objects. Radar is not sensitive to lighting and weather conditions and is used to measure the line of sight distance, radial velocity and angular position of the remote objects. Radar was initially used in applications like distance warning, crash avoidance and has now evolved into being used in multiple applications like automatic emergency brake, blind spot detection, adaptive cruise control or lane change assistant [1]. Nowadays, automotive radars operate at a frequency range of 24 GHz or 76 - 81 GHz and a research on higher frequency bands over 100 GHz is ongoing [2]. Also typically a bandwidth ranging from 100 MHz to 1 GHz is used, based on the target application. Radar in automotive application is mainly used to estimate the distance to the target, the radial velocity of the target relative to the movement of the automobile and the angular location that the target has relative to the car. With advances in signal processing techniques and improvement in hardware used in radar, the estimation of distance or range of the target and the velocity estimation has been improved over the years. However, resolving targets in the angular domain, called Direction of Arrival (DOA) estimation, is still a challenging task because it requires spatial sampling of the reflected signals. Though there have been plenty of study and literature available in this regard, there is still a lot of scope to further improve on the DOA estimation of the targets in a cost-effective way.

The angular resolution that can be achieved is inversely proportional to the antenna array size of the radar used. One of the ways to achieve higher resolution capability is to simply increase the array size in the radar, but this is cost ineffective and not easy to fit in the design of the automobile. This type of design is also not desirable by automobile manufacturers as placing a single large radar unit on the fascia of the automobile might impact the aesthetics of the automobile. Hence, in this thesis we look for a way to combine the data from multiple smaller radar units that are spread out on the fascia of a car. Having multiple radar units that are distributed across the fascia will benefit from the spatial diversity gain as discussed in [3]. Distribution of the radar sensors on the car fascia can increase the resolution as it provides a larger virtual aperture. However, combining the data from multiple sensors can be challenging in different ways. When an extended target like a car is present in the near field of the radar, it can appear as a non-isotropic target to the system under consideration. The Radar Cross Section (RCS) observed by individual sensors can be different for such extended targets and the target will be perceived incoherently by the radar sensors [3]. In this thesis a study to increase the angular resolution of the DOA estimation by developing radar algorithms to combine data from multiple such radar systems will be performed.

1.2. Research objective and Novelty

High resolution in DOA estimation can be achieved by having an antenna array with large aperture. But, constructing a very large array has practical limitations in cost and size. Hence, smaller radar sub-systems can be used instead and the data from these sub-systems can be combined to form a large virtual aperture. The objective of the thesis is to improve angular resolution of an automotive radar system by combining the data from multiple radar sub-systems that are distributed on the fascia of the automobile. Combining data from multiple radar sub-systems is studied and presented in literature in the automotive radar applications [4]. The current state of art employs a single radar sensor to perform parameter estimations on targets in the surrounding area of the automobile. Multi-static mode of operation of the radar using multiple radar sensors is a topic that is relatively new in automotive radar application [4] and needs further exploration. There have been some studies with incoherent combining of the data from multiple radar systems [5], but they do not consider the isotropic property of target in choosing the best processing technique. For a distributed system, due to its larger spatial extension, it has a higher probability of observing a target in the near field of the system. Especially, nearby targets will be seen under a different angle by the individual radar sensors and therefore a different RCS might be experienced. Targets that are observed isotropically need to be processed differently than those that are experienced in a non-isotropical way. In this thesis we propose a method for coherent processing of the target as well as incoherent processing. Since, one does not a-priori know whether the target is isotropic or non-isotropic in the given Field of View (FOV), both processing techniques will be impacted if one makes a wrong assumption. The quantification of this impact is a novel topic.

Exploring algorithms that exploit sparsity in the signal model to solve the DOA estimation problem using multi-static signals is also an under explored domain. The approach of carrying out Range-Doppler processing on received radar data, quantizes targets in the range and Doppler domain. After Range-Doppler processing, DOA estimation is carried on these Range-Doppler bins that contain sufficient energy. This is the method commonly used in automotive radar because of its low-complexity nature. For this reason the same processing steps are followed, and it is beyond the scope of this thesis to depart from this mode of operation. Because of latency, it is desirable for the automotive use case to carry out DOA estimation using data collected from a single system cycle (single snapshot DOA estimation). In this thesis estimating DOA of targets using compressive sensing (CS) algorithms for single snapshot are provided. A new block sparsity CS algorithm is proposed which is an extension of Focal Under determined System Solver (FOCUSS) algorithm, called the Block FOCUSS. Block FOCUSS performs an incoherent combination of the data from multiple sensors using block sparsity. We can further benefit from the entire virtual aperture of the distributed system by coherently fusing the data from multiple sensors. Since we operate at millimetre wavelengths, even a small displacement in the target position with respect to a sensor can lead to a large change in phase of the waveform that is perceived by the sensor. This makes it difficult to combine the signals coherently. In this thesis a new algorithm called Coherent FOCUSS is proposed for combining the data coherently from multiple sensors by compensating for the phase difference that occurs due to the path length difference of the signal towards the sensors. Further, an algorithm to fuse the coherent and incoherent processing of data is proposed using modified FOCUSS called Fusion FOCUSS. As per our knowledge this is the first time the Block FOCUSS (B FOCUSS) and Fusion FOCUSS, variants of FOCUSS algorithm is being discussed. Also it is the first time coherent combining of data from multiple radar sub-systems to achieve higher angular resolution is discussed using the phase compensation method.

1.3. Literature review

In this section, the current state of art of the problem of DOA estimation using radar is discussed along with its application in distributed radars. The literature study is divided into two main parts. In the first part a study performed on the different methods of DOA estimation is presented. In the second part, the literature studied on DOA estimation using distributed radars is discussed.

1.3.1. DOA estimation algorithms

In this subsection, a literature overview for single radar DOA estimation algorithms is provided. The three methods that are well known are the non-parametric methods (beam forming), parametric methods (MUSIC, ESPRIT) based estimation and the sparse signal processing methods. The traditional beam forming method is well studied and is also used widely in communication and sensing to estimate the DOA of the targets [6]. In this method the resolution capability is limited by the single target spectral main-lobe width, which is proportional to the aperture of the array. In order to achieve a resolution of 2° a sensor with large aperture

of ~60 times the wavelength is necessary. However to use this method it is not necessary to have a prior knowledge on the number of sources present in the scene, but it is difficult to determine the number of targets present from the beam forming spectrum.

Next set of methods are based on parameter estimation or also called as the sub-space methods. In these methods the signal sub-space and the noise sub-space are separated to estimate the signal parameters and thus correct estimation of number of sources present in the signal is important. If the number of sources assumed or estimated is wrong then the results can suffer from inaccuracy [7]. Two main algorithms in this method are MUSIC and ESPRIT. The MUSIC algorithm is based on analyzing the covariance matrix of the received signals and the signal and noise sub-space are separated to estimate the signal [7]. While using MUSIC, if the rank of the covariance matrix is not sufficient then separating signal sub-space from noise sub-space is not possible, thus there needs to be pre-processing steps that should be performed to improve the rank of the covariance matrix. Methods like Forward Backward spatial smoothing is proposed in literature to improve the rank of the covariance matrix [8].ESPRIT estimates the signal parameters via the rotational invariance techniques, it exploits the invariant structure of the stacked smoothed matrix in spatial domain to estimate the DOA [9]. In this thesis we are interested in estimating the DOA using a single snapshot. These methods usually require more than one snapshot in order to achieve optimal performance. There is literature that proposes estimating the DOA by MUSIC using single snapshot [10], but it is not straightforward and the performance is not optimal. Instead of sequential Range-Doppler DOA processing, one can also try to jointly estimate 2 or 3 parameters. The joint estimation of range and DOA to achieve super resolution is proposed in [11] which combines Discrete Fourier Transform with MUSIC algorithm for the Ultra Wide band MIMO automotive radar angle-range imaging. But this requires the use of multiple snapshots.

Sparsity based algorithms are comparatively new in the field of automotive radar, but literature is widely available on different algorithms to estimate the DOA using this technique. These are sparsity based algorithms which estimate the sparse signal from an under determined system of equations [12]. An advantage of this method is that prior knowledge of number of targets is not necessary. Sparse signal processing algorithms can be broadly classified into two main categories with grid based algorithms and grid less based algorithms [13]. Some of the grid based algorithms are BPDN, MP, OMP and FOCUSS, while there are also grid-less algorithms that are present [13]. Another advantage of sparsity based algorithms is the performance of these algorithms in estimating the DOA using a single snapshot is good [14] and has no additional steps (like fixing the rank of covariance matrix for MUSIC). The algorithms discussed in this Section are all super resolution algorithms. Considering these advantages, in this thesis we employ sparsity based algorithms to solve the DOA estimation problem. Furthermore, there has been a lot of study performed on the array design itself, where sparse arrays are employed [15]. Estimating the DOA of targets in automotive radar application through CS algorithm is explained in detail in [12].

1.3.2. DOA estimation with a distributed system

Using a distributed system to perform the DOA estimation provides lot of advantages. In [3], it is shown that with non-coherent processing, a target's RCS spatial variations can be exploited to obtain a diversity gain for target detection and for estimation of various parameters, such as angle of arrival and Doppler. Signals received by the system can be processed to yield high resolution estimates of angle of arrivals of radar targets by combining the data from multiple sensors. Multiple radars suitably placed can also be operated in multi-static mode of operation which provides more data and thus improves the estimation accuracy of DOA. In [3] the RCS of the complex target and the signal model is provided along with the relation between the correlation of the signal and the distance between the sensors and also to the distance of the target from the sensors. It states that complex targets can be modelled using a large number of scatterers and have a diverse RCS patterns which varies as a function of angle. This angular variation needs to be accounted for in the combined processing of data from multiple sensors.

Estimating range, velocity and DOA of targets using CS in distributed radar units have been discussed in literature in multiple applications including passive wireless LAN radar network [16], ground surveillance radar network [17] and Multiple Input Multiple Output (MIMO) radar with widely separated antennas [18]. There are also other algorithms that are employed for distributed radar networks separated by large distances. One such system is LOFAR which combines the data from multiple radio telescopes in a central processing system by collecting all the data from telescopes that are spread over large distances [19]. But these methods require precise synchronization and also a robust central processing system, also as the sensors themselves are fixed in the ground the challenges faced by these systems are different than a sensor mounted on a moving car. However, there have been research that proves that synchronization between radar sensors spread out on

the automobile is feasible as shown in [20]. There are also studies performed where the radars are placed on a ship, to provide Multi-function Array Radar (MFAR) antenna, that provides high-resolution high-speed data collection simultaneously [21]. This system consists of multiple receivers spread out on a large ship while a transceiver system is employed to transmit the signals. Target localization performed by non coherent combining of data from multiple sensors which use single transmitter and multiple receivers that are distributed is discussed in [22]. In this publication the block sparsity method is used to combine the data from multiple sensors. In [23] a coherent imaging method is provided from distributed radar sensors which models the time uncertainty as an unknown time delay in the optimization problem. A CS algorithm called FISTA is employed to solve this optimization problem, however in this paper they do not consider the non-isotropic property of the targets. They always consider that the targets are in the far field region and the sensors see the same RCS of the target.

In [24], a method to perform 2D MUSIC to estimate the position of the target is presented. This proposes a method to estimate the Range-DOA using MUSIC by combining the data from a distributed system by combining the covariance matrix from multiple sub-systems. This is an incoherent fusion of data to perform joint DOA estimation. Along with the use of MUSIC the thesis also provides a CS based algorithm called C-SALSA to estimate the range and DOA of the target. However the joint estimation of range and DOA requires multiple snapshots, which loses the advantage of performing single snapshot DOA estimation. Also, performing joint Range-DOA estimation requires higher memory, but in single snapshot DOA estimation only the detected targets from Range-Doppler processing is saved in memory and thus a large saving in memory can be achieved. Thus we do not consider the joint estimation method in this thesis.

There is also some research performed in Fraunhofer Research Institute (FHR) on distributed systems for automotive applications [5] [25] [15]. A study is performed on incoherent combining of the data from multiple radar sensors separated by a certain distance, in this case the resolution is limited by the aperture of the largest sub-array present in the system. Performance analysis is done for multiple array configurations and even for sparse sub-arrays with apertures larger than the equivalent uniform linear array. They make use of a CS based algorithm called Block Orthogonal Matching Pursuit (BOMP) to combine the data from multiple sensors. BOMP is a greedy algorithm but it is computationally efficient when compared to other sparsity based algorithms. But in this literature only the incoherent combining of the scene is discussed and thus the resolution that can be achieved is limited. Also a comparison study of different CS based algorithms is provided in [15] which shows that there are other algorithms like FOCUSS which perform better than OMP, thus using FOCUSS to combine the data from multiple sensors can provide better resolution. We explore this algorithm further in this thesis to perform block sparse estimation of DOA in Chapter 3. We also explore a method to perform coherent combining and a mix of coherent and incoherent combining of the data from multiple sensors to obtain higher angular resolution as discussed in Chapter 4.

1.4. Outline of thesis

This thesis consists of total six chapters and the remainder of the thesis is as follows. The system model and signal model of the distributed system that is used in this thesis is explained in Chapter 2. The near field behaviour in relation to a distributed system is discussed along with the isotropic properties of targets. This chapter also provides an overview of Range-Doppler processing performed on the data and the extraction of the single snapshot after Range-Doppler processing. The signal model for DOA estimation of a distributed system is discussed and the compressive sensing theory needed to estimate the DOA is provided. Chapter 3 discusses the block sparsity method to combine the data from multiple sensors. The FOCUSS algorithm is explained and a new algorithm called Block FOCUSS which is an extension of FOCUSS is presented. Block FOCUSS incoherently combines the data from multiple sensors. Chapter 4 discusses the necessary coherent conditions in order to perform coherent fusion of the data from multiple sensors. The phase difference observed at the sensors due to the path length difference of the signal from the target is discussed. A new method to perform DOA estimation, called Coherent FOCUSS is presented. The new algorithm accounts for the phase difference that occurs due to the path length difference in the signal model. The drawbacks of this method for a distributed system with large baseline and therefore increased sparsity, is explained. A new method is proposed whose resolution capability is between the coherent and incoherent algorithms called the Fusion FOCUSS. This algorithm provides a way to combine the coherent and incoherent apertures of the distributed system. In Chapter 5, the performances of the several FOCUSS variants are determined and compared to the BOMP algorithm which is considered as state of the art. Comparisons are done on basis of Monte Carlo simulations. An evaluation of the algorithm performance for varying Signal-to-Noise Ratio

(SNR) is performed and the results are presented. The penalty incurred in performing coherent processing on a non-isotropic target is discussed. As the CS algorithms used in this thesis are grid based algorithms, they suffer from off-grid problems, which is discussed as well and a solution discussed in literature is provided to overcome this problem. Along with simulations, an experimental evaluation of the performance of the proposed algorithms is performed in an anechoic room. The results obtained by these experiments are presented and the measurements are discussed. Chapter 6 summarizes the work done in this thesis along with the key outcomes. In this chapter we also propose some ideas for future work to further investigate and continue the work on DOA estimation for distributed systems.

1.5. Conclusions

To improve the safety of traffic participants, there is a strong motivation to improve the performance of radar sensors in the car. With increased demand for safety and advances in autonomous driving, it becomes more important to resolve targets with high resolution. Enhancing the resolution of the DOA estimation by using distributed radar sensors is promising and methods to perform coherent fusion of the data from multiple sensors is an area that needs to be explored. Coherent distributed radar is an upcoming technology in the automotive radar domain. A literature survey discusses the current state of the art in DOA estimation techniques for single sensor and for distributed sensors. It is shown that there are methods to tackle the DOA estimation problem for a distributed system, but there is still room for improvement. No literature was found that proposes coherent processing of the data from multiple sensors when the target is in the near field, which is addressed in this thesis. To solve the problem of achieving high resolution DOA estimate using distributed sensors, two main methods are proposed in this thesis which are coherent processing and incoherent processing of the data. A novel Block FOCUSS algorithm is proposed for performing incoherent processing of DOA estimation of targets. Also, a novel way of coherent processing of the data is proposed using Coherent FOCUSS algorithm. This algorithm coherently combines the data obtained from multiple sensors by accounting for the observed phase difference in the definition of the sensing matrix. Further, an algorithm to fuse the coherent and incoherent processing of the data is proposed using modified FOCUSS called Fusion FOCUSS.

2

System and signal model

In this chapter, a system consisting of multiple radar sub-systems is discussed. A general signal model is provided which is further used in the DOA estimation algorithm. The system operation and signal model for all the configurations are discussed. In Section 2.1 the geometry of the system is presented. In Section 2.2 RCS of targets in near field and far field region of the imaging scene is studied. Section 2.3 gives signal model for a complex scatterer, an overview of Range-Doppler processing of signals and extraction of snapshot after Range-Doppler processing. Section 2.4 provides the generic signal model for DOA estimation of the target. Further it discusses different modes of operation of the system and the signal model for each of those configurations. It also provides the basics of compressive sensing techniques and the optimization problem in terms of CS. Section 2.5 mentions the system assumptions made in the scope of this thesis and a conclusion is provided in section 2.6.

2.1. System definition

In this thesis, a system is defined as a collection of multiple radar sub-systems. Please note that the term sensor is used interchangeably with sub-systems in the entire thesis. A sub-system or sensor considered in this

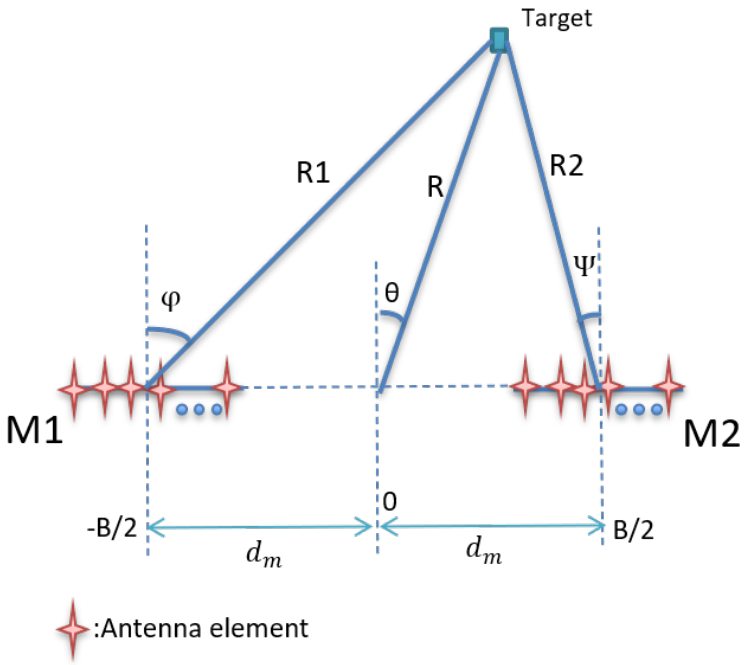

Figure 2.1: System setup

thesis is always a radar with a Multiple Input Multiple Output (MIMO) configuration unless mentioned otherwise. Each radar sub-system is assumed to comprise of N_{Tx} transmitters and N_{Rx} receivers, which forms a virtual array comprising of total $N_{Tx} \cdot N_{Rx}$ receiver elements (N_{TxRx}). Unless mentioned the transmitters and receivers in the MIMO are always spaced in such a way that the equivalent virtual array forms a Uniform Linear Array (ULA). The effective aperture of such a ULA is equivalent to $(N_{Tx}N_{Rx}) \cdot \lambda/2$, where λ is wavelength of the signal. In this thesis we only discuss the system consisting of 2 radar sensors, but the same geometry of the setup can be used for multiple radar sensors as the equations can be translated according to the placement of these sensors. There is a central processing unit which interacts with all the sub-systems and combines the data obtained from these radar sensors.

A system consists of 2 radar sub-systems as depicted in Fig 2.1. The radar sub-systems are called M1 (left sensor) and M2 (right sensor), separated by a distance of B, which is also referred to as the baseline of the system. The positions of the radar sub-systems are indicated as B/2 and -B/2 indicating the distance between them to be B. The center of the distributed system is considered to be at the origin marked as 0. The distance of radar sub-system from the center is also given as d_m, such that $B = 2 \cdot d_m$.

If a target is present at range R from center of the system as shown in Fig 2.1, from system geometry, it can be seen that it is present at range R_1 from sensor M1 and at range R_2 from sensor M2. The DOA of the target with respect to M1 is considered to be φ, with respect to M2 it is ψ and with respect to center of the distributed system it makes an angle of θ.

From the geometry of this system, the following relation between the range and DOA of the target can be derived as

$$\mathrm{R}_1 = \sqrt{\mathrm{R}^2 + \mathrm{d}_\mathrm{m}^2 + 2\mathrm{R}\mathrm{d}_\mathrm{m}\sin(\theta)} \tag{2.1}$$

$$\mathrm{R}_2 = \sqrt{\mathrm{R}^2 + \mathrm{d}_\mathrm{m}^2 - 2\mathrm{R}\mathrm{d}_\mathrm{m}\sin(\theta)} \tag{2.2}$$

$$\varphi = \arcsin\left(\frac{R\sin(\theta) + d_m}{R_1}\right) \tag{2.3}$$

$$\psi = \arcsin\left(\frac{R\sin(\theta) - d_m}{R_2}\right) \tag{2.4}$$

Using Eqs 2.1 - 2.4, if the position of the target in range and azimuth is known with respect to center of the system, its range and DOA from the individual radar sensors can be derived. These equations are used to define a common grid perspective for the system, which is discussed in Section 2.3.

To get some insight into how the range difference as seen from M1 and M2 sensor varies, a plot is provided which shows how the difference between $R1$ and $R2$ varies for a given target position in x and y co-ordinate system. The plot is provided for varying target positions in x and y co-ordinates from -80 m to 80 m along the

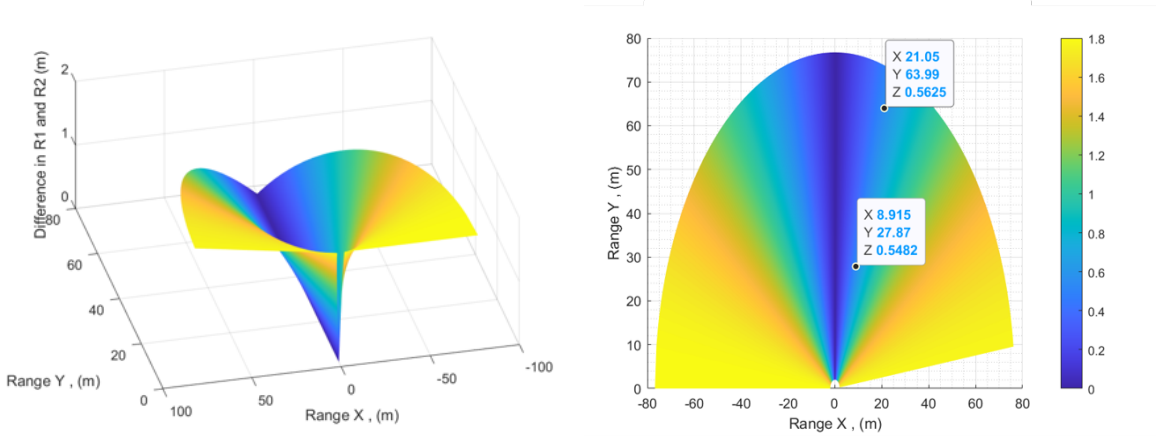

(a) 3D plot (b) 2D projection

Figure 2.2: Difference in Range $R1$ and $R2$ for baseline of 1.8m for every target position in x-y co-ordinates. (a) 3D plot showing the difference in ranges. (b) 2D projection of the plot in (a)

x axis and 0 to 80 m along the y axis, the radar sensors are placed on either side of the origin. The Fig 2.2 shows the difference between R_1 and R_2 plotted as a function of target in x and y co-ordinates. The baseline (B) used between the 2 sensors is 1.8 m and the waveform with carrier frequency 78 GHz and bandwidth of 250 MHz is considered. For a bandwidth of 250 MHz the range resolution obtained is ~0.6 m, hence any range difference less than this number will see the target in the same range bin. The plot also marks two points as references which shows the region where the difference in range is about 0.6 m in Fig 2.2 (b), it can be observed that as the position of the target in y axis moves away from origin, the broadside angle where the target falls in the same range bin also increases. As the targets are moved away from broadside the range difference between the 2 sensors increase and thus the targets will be resolved in range.

2.1.1. Near field and far field definition

For a point target the reflected wave received from the target is a spherical wave, but at large distance from the sensor (far-field) this can be approximated with a planar wave. The distance which determines when a wave can be approximated as a planar wave is given by Fraunhofer distance [26] as shown below

$$\text{Fraunhofer distance} \sim \frac{2D^2}{\lambda}$$

D : Aperture of the radar sensor

λ : wavelength of the signal

If distance of the target from the radar sensor is greater than Fraunhofer distance then the waves received can be approximated as planar waves and the target is said to be in the far field region. If distance of the target is lesser than Fraunhofer distance then the target is said to be in the near field region of the radar [26]. The Fraunhofer distance is directly proportional to the aperture of the radar being used, i.e., as the aperture increases probability that the target is in the near field region increases for a given target position.

As radar is operated in the mm-wave frequency range (~76 GHz to 81 GHz) the Fraunhofer distance for a uniform MIMO with 3 transmitters and 4 receivers is around 28 cm. This means that the target is almost always in the far field region as seen by individual radar sensors [27]. But when a distributed system is present with a virtual aperture equal to the baseline B as shown in Fig 2.1 the Fraunhofer distance is determined by baseline separation B. Hence for large baseline separations the far field assumption of the target as seen from the entire distributed system might not be valid. It needs to be noted that the target is still in the far field region as seen by just sensor M1 or M2 in Fig 2.1, but it might not be in the far field region for the whole system with aperture B. When the target is not in the far field then the received wave reflected from the target is no longer planar and is spherical, hence the linear relationship in phase along all the sensors in the distributed sensor is lost. But the linear relationship within a single sensor M1 or M2 still holds good as the far field assumption hold good for the sub-systems. Thus when the targets are in near field, we need to consider that the targets DOA as seen by the sensors is different and this needs to be taken into account in the combined DOA estimation.

2.2. Isotropic property of targets

A complex target is made up of multiple scatterers and has varying Radar Cross Section that changes with center frequency and aspect angle. Consider a target to be made up of Q scatterers with varying complex amplitude, then an example realization of RCS of a target randomly placed inside the perimeter of a 20 cm x 20 cm space can be depicted as shown in Fig 2.3. If the two radar sensors M1(left sensor) and M2(right sensor) are separated by a baseline separation, then DOA of the target as seen by M1 and M2 is not the same as discussed in Section 2.1. From Fig 2.3 it can be seen that if the DOA of the target is even slightly different, then a different RCS of the target is observed (represented as Left and Right lines in the figure). Such targets are said to be non-isotropic in the field of view of the radar system. If the target is isotropic in the field of view of the radar system then the RCS seen by the system is same across both M1 and M2 sensors. Note that further on in the thesis report when the target is mentioned to be isotropic or non-isotropic, it is always in reference to the field of view (FOV) of the radar and does not mean that the target has the same property for 360°view. In this thesis the FOV of the system is defined as the overlapping region of the view of both the radar sensors.

Consider an extended target with a complex RCS. In this scenario the signal received by the antenna elements can be seen as coherent reception (for isotropic targets) or incoherent reception (for non-isotropic targets) based on the distance between the antenna elements and the distance of the target to the system. The target with complex RCS can be considered as a radiating object with beam-width of $R\lambda/\Delta x$, can be

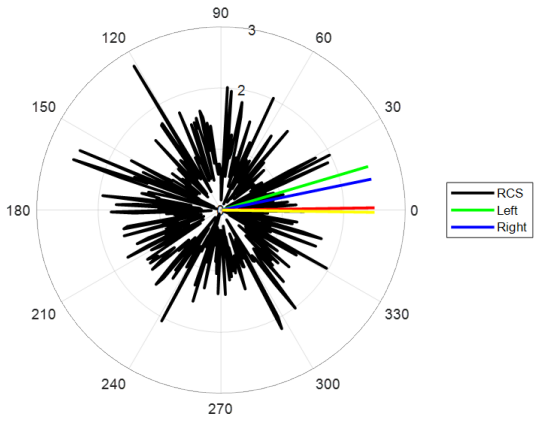

Figure 2.3: RCS of an extended target (20cm x 20cm) made up of Q(100) scatterers

derived by extending [28, Example 5.3.3]. If the antennas are located in an area defined by the projection of the beam of the reflecting object on the antenna array, then the signal received from the target is correlated, else the signals received by the different radars are mutually uncorrelated [3]. This can be given analytically as explained in [3] as follows, the target response observed from the left and right most antennas in the array is uncorrelated if the equation below is satisfied

$$B > \frac{R\lambda}{L} \tag{2.5}$$

B: Aperture of the antenna array
R: Range of the target from the Rx antenna
L: the length of the target (the occupied target length)

The signal received is correlated if the distance between the antenna elements (B) is less than the beam width which is given in Eq 2.5. For sub-systems the aperture is much smaller when compared to the distributed system, hence from Eq 2.5 it is seen that for a distributed system it is more difficult to receive correlated signals while for individual sub-system the signal might still be correlated. Fig 2.4 shows an illustration on how the scattered beam form the target is received at the radar system. Right image shows that the radar system receives the same beam for an isotropic target, making the received signal to be correlated. Left image shows that the radar system receives different beams for a non-isotropic target, making the received signal to be uncorrelated as per Eq 2.5.

To understand what the Eq 2.5 means for different baselines and length of the target, some simple plots are made which vary the range (R) and length (L) of the target for a carrier frequency of 78 GHz. Based on the baseline used a classification is performed to determine if the signal received from the target is correlated or not. From Fig 2.5 it is shown that as the length of the target increases the probability that the signals are correlated reduces, also when the range of the target from the radar increases the probability that the signals are correlated increases. As the baseline reduces we see the region where the signals are correlated

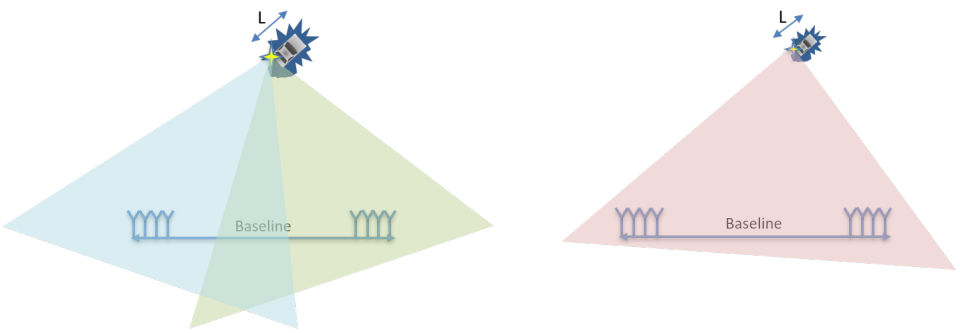

Figure 2.4: Non-isotropic scatterer (Left) ; Isotropic scatterer (Right)

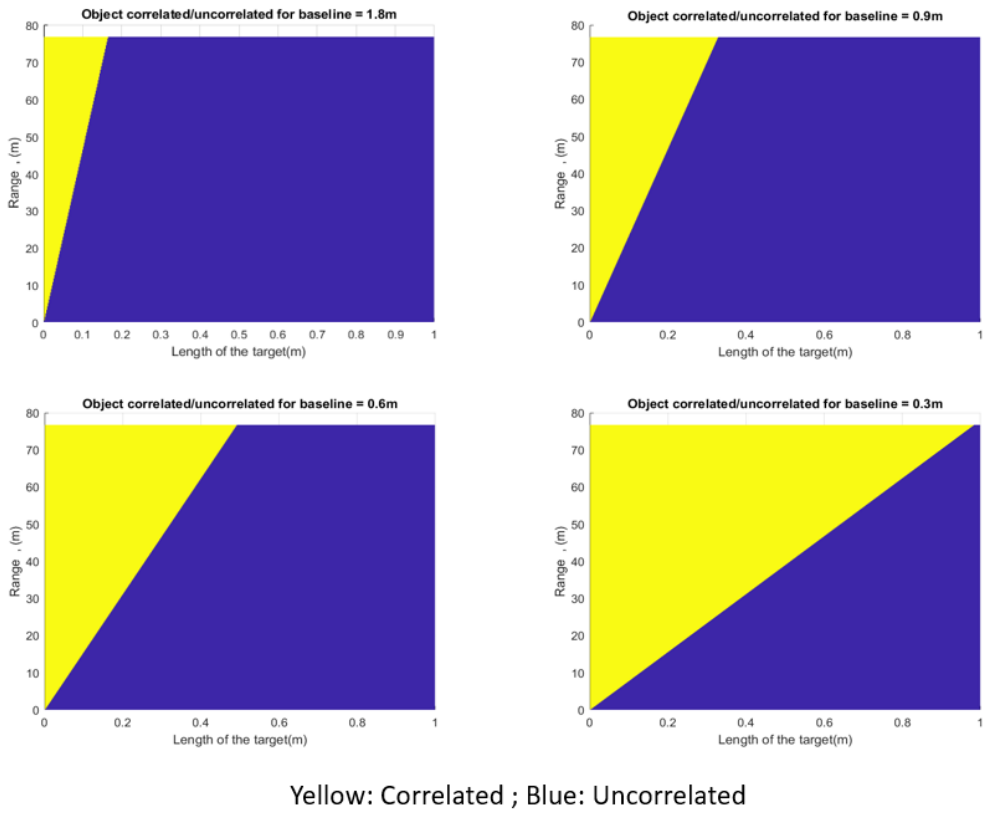

Figure 2.5: Region of correlated signal as a function of Range and length of target for different baseline values

increases and the region of non correlated signals reduce. This can be seen as the reduction of slope of the line between the 2 regions in the plots as the baseline reduces. This is an important plot that helps us determine if coherent or incoherent processing needs to be performed on the received signals. Note that when performing incoherent processing one can benefit from the non correlated signals as they provide a diversity gain in space [3], where as while performing coherent processing if the signals are non correlated then it can lead to errors. Hence it is important to understand the property of the target before determining the right processing technique which is not an easy step.

2.3. Signal model

Automotive radar applications widely use Frequency Modulated Continuous Wave (FMCW) waveform for the operation of radar even though there are multiple waveforms available, as FMCW waveform has many advantages. It is simple to implement in the hardware as the Analog to Digital converter (ADC) in the receiver operates at a beat sampling frequency, lower than the frequency deviation in the FMCW ramp. It is also low cost and the pulse radiation with high peak power is not present [29]. The signal model for the system discussed in previous Section 2.1 is discussed here. The assumption that the transmitted signals from different transmitters are independent and also the noise at each receiver element is Gaussian independent noise [30] is made. Further, it is to be noted that the position of all the sensors are known and each sensor is coherent in itself. If the sub-systems are fully synchronized then multi-static mode of operation can be used, if not mono-static configuration is used. The signal models for both these configurations are discussed. The perfect synchronization between the radar sub-systems is relatively not easy, however it is not impossible. In[20] it is discussed on how the synchronization between the radar sub-systems can be achieved.

Dechirp operation is performed on the received signal of a FMCW MIMO sensor and the signal is digitized with the help of ADC in the receiver [31]. The dechirped FMCW signal obtained by a single antenna element for a point target can be written as follows

$$s(t) = A\exp(j2\pi\alpha\tau t)\exp\left(-j2\pi\left(f_c\tau + \frac{1}{2}\alpha\tau^2\right)\right) \tag{2.6}$$

$$\alpha = \frac{\text{Bandwidth } (BW)}{\text{Chirp duration } (T)}$$

In Eq 2.6, A is the complex amplitude of the target which consists of effects of target RCS, propagation loss, amplitude of transmitted signal and antenna loss, Tau (τ) is the time delay with which the radar waveform is received from the target after transmission (called the round trip delay), f_c is the carrier frequency of the FMCW waveform and α is the ratio of bandwidth (BW) over FMCW chirp duration. For a system consisting of multiple antennas and multiple sub-systems the Eq 2.6 can be extended to incorporate a variable n which represents the index of virtual channels formed for the radar system, given by Eq 2.7 for a sensor with Single Input Multiple Output sensor. By employing a coding scheme such as Time division multiplexing or Doppler division multiplexing this system can be extended to work as Multiple Input Multiple Output where each virtual channel can be distinguished. For example if a single MIMO sensor is present then the number of virtual channels is $N_{Tx}N_{Rx}$. A system consisting of 2 such MIMO sensors will have $4 \cdot N_{Tx}N_{Rx}$ virtual channels if the system is fully synchronized. $2 \cdot N_{Tx}N_{Rx}$ of these virtual channels correspond to the mono-static responses and $2 \cdot N_{Tx}N_{Rx}$ of them to the bi-static responses, which is further explained in Section 2.4.2

$$s(t,n) = A\exp\left(j2\pi\alpha\tau_n t\right)\exp\left(-j2\pi\left(f_c\tau_n + \frac{1}{2}\alpha\tau_n^2\right)\right) \tag{2.7}$$

In Section 2.2, it is shown that the response received from a target is made up of multiple complex valued signal with different gain and phase for each scatterer. A target comprising of Q scatterers [3] can be modelled by extending the Eq 2.7 of a point target to include the effect from Q scatterers in the target as in Eq 2.8

$$s(t,n) = \sum_{q=1}^{Q} A_q \exp\left(j2\pi\alpha\tau_{q,n} t\right)\exp\left(-j2\pi\left(f_c\tau_{q,n} + \frac{1}{2}\alpha\tau_{q,n}^2\right)\right) \tag{2.8}$$

In above Equation, A_q is the complex valued response from each reflection point. The targets will have different time delay (τ_n) for each virtual antenna. Though the (τ_n) within each sub-system is comparable for point targets, each individual scatterer for extended target has a slightly different (τ_n) and hence the sum over Q scatterers will have different sum for each antenna pair n, this is the non-isotropic aspect of the extended target that is modeled in Eq 2.8.

Further, the equation for an imaging scene consisting of K extended targets can be represented as given in Eq 2.9

$$s(t,n) = \sum_{k=1}^{K}\sum_{q=1}^{Q} A_{k,q} \exp\left(j2\pi\alpha\tau_{q,k,n} t\right)\exp\left(-j2\pi\left(f_c\tau_{q,k,n} + \frac{1}{2}\alpha\tau_{q,k,n}^2\right)\right) \tag{2.9}$$

The time delay observed between each antenna element for each target is different as depicted in Eq 2.9.

The above equation can be extended for multiple chirps, which is denoted by the slow time variable mT, where T is the pulse repetition time and m represents the chirp number in the slow time. This is given by the below Eq 2.10.

$$s(t,mT,n) = \sum_{k=1}^{K}\sum_{q=1}^{Q} A_{k,q} \exp\left(j2\pi\alpha\tau_{q,k,n,mT} t\right)\exp\left(-j2\pi\left(f_c\tau_{q,k,n,mT} + \frac{1}{2}\alpha\tau_{q,k,n,mT}^2\right)\right) \tag{2.10}$$

The time delay observed between each chirps for each target is different as depicted in Eq 2.10.

2.3.1. Range Doppler estimation

Range and Doppler estimation of the target present in the field of the radar is performed on the dechirped received FMCW waveform. Range estimation is performed in order to determine the distance of the target from the radar and Doppler estimation is done to determine the relative radial velocity of the target. Processing of the received FMCW waveform is done in order to estimate the range and velocity of the target [29]. After dechirping process of the FMCW waveform a beat signal is produced with a frequency which is the difference between the transmit frequency and the received frequency. The beat frequency comprises of propagation delay of the waveform which is used to determine the range of the target respectively [32].

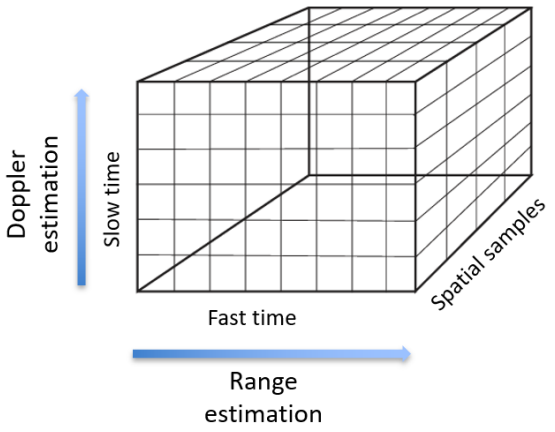

Figure 2.6: Radar data cube

Radar transmits a sequence of chirps (pulses) and receives a sequence of chirps reflected back from the target. The singular data values collected from radar after dechirping of all the received chirps from all the antennas are saved in the radar data cube format [32] as depicted in Fig 2.6.

The samples acquired within a chirp are referred to as fast time samples. It represents the sampling in fast range. They are used to estimate the range of the target as these samples will have the reflected signal back from the target, whose delay can be used to estimate the range of the target (for example, by doing Fast Fourier Transform (FFT) along the fast time axis, along variable t in Eq 2.10 we can estimate the range). The complex-valued baseband samples from different pulses from the same range bin are represented along the slow time axis. The Pulse Repetition Interval (PRI) determines the amount of chirps (or pulses) sent per second. Typical PRIs are much longer than the fast-time sampling interval. Because of the long sampling intervals, samples taken across multiple pulses are referred to as slow time. Processing data in the slow-time dimension (along variable mT in Eq 2.10) allows us to estimate the Doppler spectrum at a given range bin. Coherent integration over multiple pulses by means of FFT will give us the shift in Doppler frequency

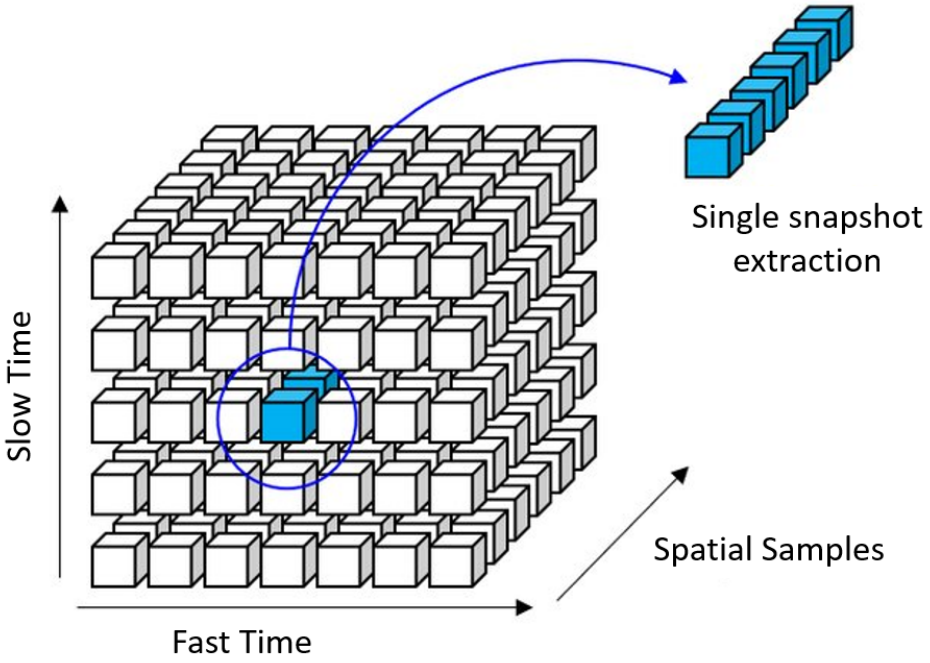

Figure 2.7: Extracting spatial samples after Range Doppler processing from radar data cube [33]

experienced by a moving object as the phase changes over time. The spatial samples are collected based on the number of transmitter receiver pairs present as they represent the reflections from an object in the spatial dimension. This is used mainly for estimating DOA in the automotive radar applications. Based on the delay between arrival of signals as seen from one receiver antenna to another, the DOA can be estimated.

The beat frequency (or beat signal) is produced by demodulation of the received chirp. The beat signal can be analysed with an FFT to determine which frequencies are present in the beat signal (a beat frequency corresponds with a time-of-flight and hence with a target at a certain range). By determining the beat frequency, the time-of-flight and thus the range of a target is estimated. To determine the Doppler frequency of the target a second FFT is performed along the slow-time samples (along the chirps) of the data. In automotive radar applications usually a 2D-FFT is performed along the fast time and slow time dimension of the radar data in order to determine the range and Doppler of the target [34]. The range resolution and Doppler resolution is determined by bandwidth of the FMCW waveform and integration time of the FMCW chirps respectively [34]. Once the target is localized in range bin and Doppler bin after Range-Doppler processing of the signal, the spatial samples corresponding to a Range-Doppler bin can be extracted to perform the DOA estimation of the target, Fig 2.7 [33]. The extracted spatial samples together are called a snapshot. For a MIMO sensor consisting of N_{Tx} transmitters and N_{Rx} receivers, a snapshot consists of $N_{Tx}N_{Rx}$ spatial samples.

In this thesis, going forward when we discuss about DOA estimation, note that the DOA estimation is always done after Range-Doppler processing and also on one snapshot obtained after Range-Doppler processing. Single snapshot DOA estimation is preferred in automotive applications as it has very low latency, since it calculates the DOA for every snapshot individually [35]. Low latency is an important requirement in automotive applications due to safety requirements, which enables the automobile to act in time when needed. In addition to this it also benefits from the processing gain achieved from Range-Doppler processing performed prior to DOA estimation.

2.4. DOA estimation method

After Range-Doppler processing is performed on received data, target detection is performed and the snapshot corresponding to the range and Doppler bin which contains the target is extracted to obtain the spatial samples, Fig 2.7. DOA estimation is performed on these extracted snapshots. In the section the signal model for DOA estimation using single sensor and distributed sensor is discussed along with the signal model to perform DOA estimation.

2.4.1. DOA estimation for Single system

The impinging wave-front on the antenna array has a linearly increasing time delay when the target is located in the far field of the antenna array for a ULA with respect to the first element, as depicted in Fig 2.8. This constant delay between the arrival of the wave-front can be translated into a phases shift when the signal is sufficiently narrow band from one antenna element to the other [6]. The Fig 2.8 shows a Uniform Linear Array (N elements) with separation between the elements as d, $Rx0$ is the first element and is used as the reference element, the time delay of arrival of the wave-front on the consecutive array elements is a function of path length as shown in the Fig 2.8. This path length difference translates to corresponding phase shift between the signals received by array elements.

If the received samples after Range-Doppler processing of N-receiver array elements are represented as **y**,

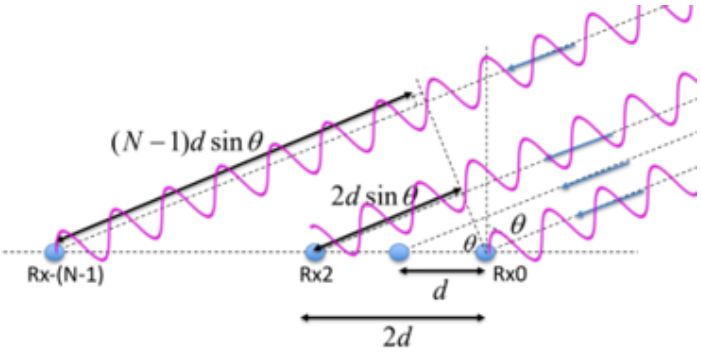

Figure 2.8: Impinging wave-front on a ULA from target

then the signal model for the received samples for K targets can be gives as

$$\mathbf{y} = \mathbf{A}_k\mathbf{x} + \mathbf{n} \tag{2.11}$$

$$\mathbf{y} \in \mathbb{C}^{N\times 1}; \mathbf{x} \in \mathbb{C}^{K\times 1}; \mathbf{A}_k \in \mathbb{C}^{N\times K}$$
$$\mathbf{A}_k = [\mathbf{a}(\theta_1)\,\mathbf{a}(\theta_2)\ldots.\mathbf{a}(\theta_K)]$$
$$\mathbf{a}(\theta) : \text{steering vector}$$
$$\mathbf{x} : \text{impinging source vector} ; \mathbf{n} : \text{noise vector}$$

The steering vector $\mathbf{a}(\theta)$ represents the impinging signal from the target present at an angle θ from the array elements, which is given as Eq 2.12

$$\mathbf{a}(\theta) = \left[1, e^{j2\pi\frac{d\sin(\theta)}{c}}, e^{j2\pi\frac{2d\sin(\theta)}{c}}, \ldots, e^{j2\pi\frac{(N-1)d\sin(\theta)}{c}}\right]^T \tag{2.12}$$

To perform DOA estimation of the target, a steering matrix or beam-forming matrix $\mathbf{A}$ is defined, whose columns consists of steering vectors as defined by Eq 2.12 for all possible DOA of targets in the defined Field of View. The given FOV region is divided into N_s grid points with certain spacing between each grid point. The steering vector is defined for each of these grid points, which constitute the columns of the matrix $\mathbf{A}$, refer to Eq 2.13.

$$\mathbf{A} = [\mathbf{a}(\theta_1)\,\mathbf{a}(\theta_2)\ldots\mathbf{a}(\theta_{\mathrm{Ns}})] \tag{2.13}$$

$$\mathbf{A} \in \mathbb{C}^{N\times N_s}$$
$$N_s : \text{number of grid points in search grid}$$

For example, if the FOV is -90° to $+90^\circ$, the grid points separated by 1° will have 181 columns in the steering matrix $\mathbf{A}$. In this thesis the targets are assumed to be on the grid for the signal model consideration unless mentioned otherwise. A search is made along these points to find the DOA's of the targets in the FOV. In this definition steering matrix $\mathbf{A}$ is made up of all possible target positions in the defined FOV.

The signal model for the DOA estimation is gives by Eq 2.14

$$\mathbf{y} = \mathbf{A}\mathbf{x} + \mathbf{n} \tag{2.14}$$

$$\mathbf{y} \in \mathbb{C}^{N\times 1}; \mathbf{x} \in \mathbb{C}^{N_s\times 1}; \mathbf{A} \in \mathbb{C}^{N\times N_s}$$

DOA estimation algorithms like beam-forming, MUSIC, ESPRIT, compressive sensing algorithms etc., can be further employed to estimate the DOA of the targets using Eq 2.14,

2.4.2. DOA estimation for Distributed system

In the previous section, the signal model for a single radar system was discussed. This can be extended to a system consisting of multiple sub-systems. Consider a system explained in Section 2.1, consisting of 2 sub-systems separated by a baseline separation of B, Fig 2.1. In this thesis we consider that each sub-system is made up of antenna elements in a MIMO configuration with N_{Tx} transmitters and N_{Rx} receiver elements. The total receiver array elements consists of $N_{Tx}N_{Rx}$ virtual elements, let this be represented as $N(= N_{Tx}N_{Rx})$. From Fig 2.1 it is seen that if a target makes an angle θ to the center of the distributed system, then the angle that the target makes with respect to sensor M1 (ϕ) and sensor M2 (ψ) can be calculated by Eq 2.1 - 2.4 as the range of the target is approximately known after Range-Doppler processing. As the near field model needs to be considered for the target as shown in Section 2.2, the angle that the target makes with respect to the 2 sensors is different. In this case a small difference in the range of the target from 2 sensors can cause a change in the phase of the received signal from target as received by the 2 sensors [36]. Hence the two mono-static responses that are received by the 2 sensors can have different phases and this can impact the DOA measurement. If the target is in motion then this also has an effect on Doppler estimate, but in this thesis we consider only stationary targets and hence ignore this effect.

- **Mono-static configuration**

  When the system is operated in the mono-static configuration, the transmitter and receiver are both co-located, thus the Direction of Departure (DOD) and Direction of Arrival of the wave is the same, ref

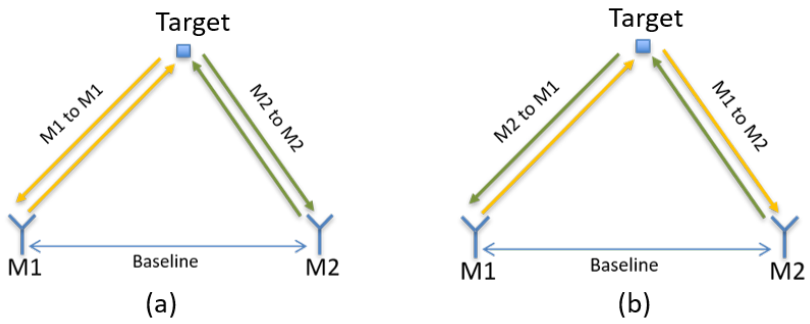

Figure 2.9: (a): Mono-static response and (b): Bi-static response

Fig 2.9. Using Eq 2.1 - 2.4 the grid points in the sensing matrix **A** defined for the target as a function of θ as explained in Eq 2.13 is translated to the angles φ and ψ. The two sensing matrix $\mathbf{A}(\varphi)$ and $\mathbf{A}(\psi)$ are derived from the angle θ used in defining the sensing matrix **A** in Eq 2.13 as shown in Eq 2.15 and Eq 2.16.

$$\mathbf{A}_1 = \left[\mathbf{a}(\varphi_1)\,\mathbf{a}(\varphi_2)\ldots\mathbf{a}(\varphi_{\mathrm{Ns}})\right] \tag{2.15}$$

$$\mathbf{A}_2 = \left[\mathbf{a}(\psi_1)\,\mathbf{a}(\psi_2)\ldots\mathbf{a}(\psi_{\mathrm{Ns}})\right] \tag{2.16}$$

$$\mathbf{A_1}, \mathbf{A_2} \in \mathbb{C}^{N\times N_s}$$

N_s : number of grid points in search grid

Note that every column in matrix $\mathbf{A_1}$ and $\mathbf{A_2}$ are steering vectors pointing to the target present in the same location, corresponding to DOA θ as seen from the center of the distributed systems. In this manner a common grid is defined for the entire system, where the corresponding DOA from sensor M1 and M2 are estimated for every DOA point defined by the system center as shown in Fig 2.1.

If $\mathbf{y}_1$ and $\mathbf{y}_2$ are the snapshots obtained from sensor M1 and M2 respectively after Range-Doppler processing, and they sense the target as $\mathbf{x}_1$ and $\mathbf{x}_2$, then the signal model for the mono-static configurations is given as in Eq 2.17 and 2.18.

$$\mathbf{y}_1 = \mathbf{A}_1\mathbf{x}_1 + \mathbf{n}_1 \tag{2.17}$$

$$\mathbf{y}_1 \in \mathbb{C}^{N\times 1}; \mathbf{x}_1 \in \mathbb{C}^{N_s\times 1}; \mathbf{A}_1 \in \mathbb{C}^{N\times N_s}$$

$$\mathbf{y}_2 = \mathbf{A}_2\mathbf{x}_2 + \mathbf{n}_2 \tag{2.18}$$

$$\mathbf{y}_2 \in \mathbb{C}^{N\times 1}; \mathbf{x}_2 \in \mathbb{C}^{N_s\times 1}; \mathbf{A}_2 \in \mathbb{C}^{N\times N_s}$$

- **Multi-static configuration**

  When the system is operated in the bi-static (or multi-static for higher number of sensors) configuration, the transmitter and receiver elements are not co-located, thus the DOD and DOA of the wave are different, ref Fig 2.9. In Fig 2.9 when M1 is transmitting and M2 is receiving the DOD is given by φ and DOA is given by ψ. The sensing matrix **A** is thus defined as the Kronecker product of DOD and DOA as shown in Eq 2.19 and Eq 2.20. $\mathbf{A_3}$ is used to represent the sensing matrix of the bi-static response when M1 is transmitting and M2 is receiving; $\mathbf{A_4}$ is used to represent the sensing matrix of the bi-static response when M2 is transmitting and M1 is receiving.

$$\mathbf{A}_3 = \left[\mathbf{a}_{M1M2}(\varphi_1 \otimes \psi_1)\,\mathbf{a}_{M1M2}(\varphi_1 \otimes \psi_2)\ldots\mathbf{a}_{M1M2}(\varphi_{\mathrm{Ns}} \otimes \psi_{\mathrm{Ns}})\right] \tag{2.19}$$

$$\mathbf{A}_4 = \left[\mathbf{a}_{M2M1}(\psi_1 \otimes \varphi_1)\,\mathbf{a}_{M2M1}(\psi_2 \otimes \varphi_2)\ldots\mathbf{a}_{M2M1}(\psi_{\mathrm{Ns}} \otimes \varphi_{\mathrm{Ns}})\right] \tag{2.20}$$

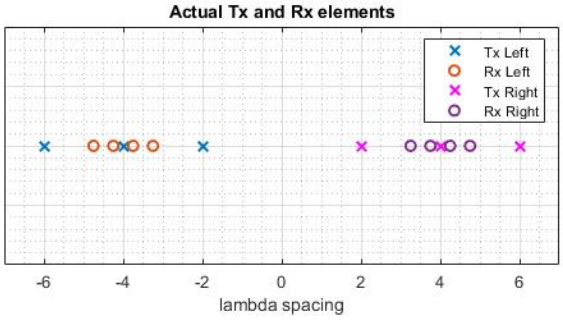

Figure 2.10: Position of array elements in sensors M1 and M2

$$\mathbf{A}_3, \mathbf{A}_4 \in \mathbb{C}^{N \times N_s}$$
$$N_s : \text{number of grid points in search grid}$$

The steering vectors $\mathbf{a}_{M1M2}(\varphi \otimes \psi)$ is the bi-static response with M1 transmitting and M2 receiving, which is calculated as the Kronecker product give by Eq 2.21. An example of the element positions in the distributed system with sensors M1 and M2 is depicted in Fig 2.10. The element positions are marked in the x axis in terms of wavelength used. Sensor M1 is positioned around -4λ and M2 is positioned around +4λ, the position of each antenna element in the sensor is shown in the figure as well. Let Tx_1 and Rx_1 be the transmitters and receivers in M1 sensor, Tx_2 and Rx_2 be the transmitters and receivers in M2 sensor, then

$$\mathbf{a}_{M1M2}(\varphi \otimes \psi) = \mathbf{a}_{Tx1}(\varphi) \otimes \mathbf{a}_{Rx2}(\psi) \tag{2.21}$$

$$\mathbf{a}_{Tx1}(\varphi) = exp\left(j2\pi \mathbf{d_{Tx1}} \sin(\varphi)\right)$$
$$\mathbf{a}_{Rx2}(\psi) = exp\left(j2\pi \mathbf{d_{Rx2}} \sin(\psi)\right)$$
$$\mathbf{d_{Tx1}} : \text{array containing Transmitter element positions for M1}$$
$$\mathbf{d_{Rx2}} : \text{array containing Receiver element positions for M2}$$

The steering vectors $\mathbf{a}_{M2M1}(\psi \otimes \varphi)$ is the bi-static response with M2 transmitting and M1 receiving, which is calculated as the Kronecker product give by Eq 2.22.

$$\mathbf{a}_{M2M1}(\psi \otimes \varphi) = \mathbf{a}_{Tx2}(\psi) \otimes \mathbf{a}_{Rx1}(\varphi) \tag{2.22}$$

$$\mathbf{a}_{Tx2}(\psi) = exp\left(j2\pi \mathbf{d_{Tx2}} \sin(\psi)\right)$$
$$\mathbf{a}_{Rx1}(\varphi) = exp\left(j2\pi \mathbf{d_{Rx1}} \sin(\varphi)\right)$$
$$\mathbf{d_{Tx2}} : \text{array containing Transmitter element positions for M2}$$
$$\mathbf{d_{Rx1}} : \text{array containing Receiver element positions for M1}$$

Note that in Eq 2.22, the DOD and DOA are interchanged and hence the beam-steering vectors are also reversed compared to Eq 2.21.

If $\mathbf{y}_3$ is the snapshot obtained after Range-Doppler processing with M1 transmitting and M2 receiving, the target is observed as $\mathbf{x}_3$, then the signal model for this bi-static configuration is given as in Eq 2.23.

$$\mathbf{y}_3 = \mathbf{A}_3\mathbf{x}_3 + \mathbf{n}_3 \tag{2.23}$$
$$\mathbf{y}_3 \in \mathbb{C}^{N \times 1}; \mathbf{x}_3 \in \mathbb{C}^{N_s \times 1}; \mathbf{A}_3 \in \mathbb{C}^{N \times N_s}$$

If $\mathbf{y}_4$ is the snapshot obtained after Range-Doppler processing with M2 transmitting and M1 receiving, the target is observed as $\mathbf{x}_4$, then the signal model for this bi-static configuration is given as in Eq 2.24.

$$\mathbf{y}_4 = \mathbf{A}_4\mathbf{x}_4 + \mathbf{n}_4 \tag{2.24}$$
$$\mathbf{y}_4 \in \mathbb{C}^{N \times 1}; \mathbf{x}_4 \in \mathbb{C}^{N_s \times 1}; \mathbf{A}_4 \in \mathbb{C}^{N \times N_s}$$

2.4.3. Problem formulation for DOA estimation using compressive sensing

Compressive sensing is a fairly new topic in the field of automotive radar, however there is various literature available that explains the concepts involved in compressive sensing in detail [37] [38] [39] [12]. In this section the important concepts needed in estimation of DOA of the targets using compressive sensing techniques are discussed. Recalling the generic signal model for DOA estimation of a radar system, Eq 2.14 we have

$$\mathbf{y} = \mathbf{A}\mathbf{x} + \mathbf{n}$$

Here the sensing matrix can be seen as comprising of a sensing matrix Φ and a representation basis Ψ, i.e., $\mathbf{A} = \Phi\Psi$. Ψ works as a selection matrix that selects the required M rows out of N available rows. For the radar scenario the representation basis is chosen to be spike representation basis i.e., $\Psi = \mathbf{I}$ (Identity matrix). Hence here $\mathbf{A} = \Phi$ and is called the sensing matrix [12].

In the above equation, the sensing matrix $\mathbf{A}$ has more number of columns than rows, as there are limited number of receiver elements in the radar sensor, whereas the FOV is divided into grid points covering the entire FOV as finely as needed. Here FOV represents the overlapping perceivable region of the 2 sensors in the azimuth domain. We consider the overlapping region of the radar sensors due to the assumption that is made in Section 2.5 that the target is observable by both the sensors. This makes Eq 2.14 an under-determined system of equations as there are less equations than unknowns. Such an under-determined system of equations has infinitely many solutions and cannot be solved in regular least squares manner [40]. Note that the columns of the sensing matrix are called as atoms and the grid points that determine the DOA of the targets is referred to as dictionary of the sensing matrix. This is a grid-based definition of the CS problem which assumes that the target is on one of the defined grids in the sensing matrix [13]. Compressive sensing theory proposes that a unique solution to this under-determined system of equation can be found if, the vector $\mathbf{x}$ that needs to be estimated is sparse [37] i.e., the number of non-zero elements in $\mathbf{x} \ll N_s$, where N_s is the number of columns in $\mathbf{A}$ and the sensing matrix has good coherence properties. The number of non-zero elements in a vector is called the cardinality of a vector, $card(\mathbf{x}) = K$ implies that the vector $\mathbf{x}$ has only K non-zero elements. As long as $K \ll N_s$ a unique solution can be found to Eq 2.14 using compressive sensing techniques. The condition of sparsity for a guaranteed unique recovery of $\mathbf{x}$ is given by coherency of the sensing matrix, $\mathbf{A}(\mu)$. $\mathbf{A}(\mu)$ depends on design of the sensing matrix which should be such that the columns (or atoms) of $\mathbf{A}$ are nearly orthogonal to each other. Note that this value provides a sufficient recovery for the unique recovery of sparse signal but is not a necessary condition [41]. Calculation of this value and the impact it has on the solution is discussed in detail in Appendix A.

Moreover, the vector $\mathbf{x}$ that is to be estimated here represents the number of targets present in the angular domain (azimuth) after Range-Doppler processing as discussed in Section 2.3 and this is considered sparse as most targets are already resolved in the range and Doppler dimension.

Fig 2.11 shows a pictorial representation of Eq 2.14 without noise $\mathbf{n}$. $\mathbf{y}$ is the received data samples from N receiver antenna elements, $\mathbf{A}$ is the sensing matrix and $\mathbf{x}$ is the source vector that needs to be estimated. In this figure, the $\mathbf{x}$ shown has cardinality of 3($K = 3$) i.e., there are 3 non-zero values and the rest of the elements

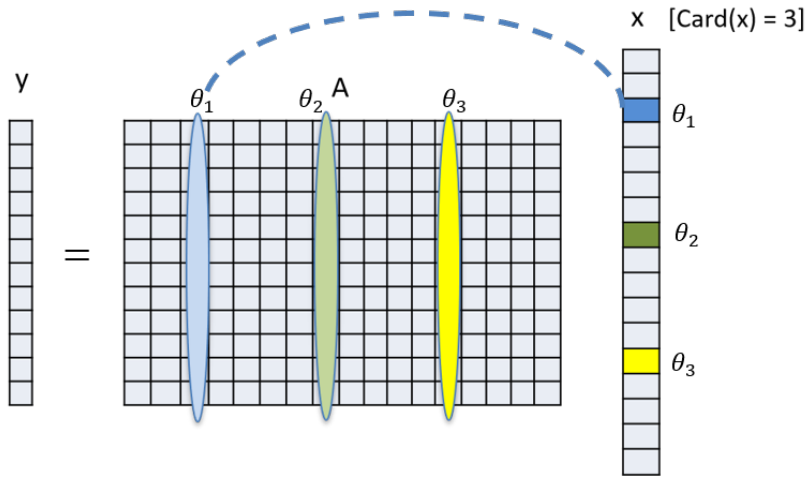

Figure 2.11: Pictorial representation of equation to estimate DOA without additive noise

are zero. This represents 3 targets in the FOV of the radar with DOA (θ_1, θ_2 and θ_3) equivalent to the DOA defined by the corresponding columns in defining the sensing matrix. The problem is now to estimate which columns of **A** contribute to the source vector **x** given the measurement vector **y**. Once the columns of **A** that contribute in estimating the non-zero value in **x** is known, we can extract the DOA corresponding to that particular column of **A** [39]. Fig 2.11 implies that measurement vector **y** can be well approximated by linear combination of K atoms in the sensing matrix **A** [13].

2.4.4. Optimization problem statement

The optimization problem without noise to solve for **x** in Eq 2.14 is given by the l_0-norm optimization as follows

$$\hat{\mathbf{x}} = \arg\min_{\mathbf{x}} \|\mathbf{x}\|_0 \text{ s.t. } \mathbf{y} = \mathbf{A}\mathbf{x} \tag{2.25}$$

l_0-norm is given as the number of non-zero values in a vector. However, l_0- norm is NP hard to solve and not a convex problem. Hence, the optimization problem can be relaxed to use l_1- norm. l_1- norm is a convex function and also promotes sparsity [37]. The optimization problem can thus be written as

$$\hat{\mathbf{x}} = \arg\min_{\mathbf{x}} \|\mathbf{x}\|_1 \text{ s.t. } \mathbf{y} = \mathbf{A}\mathbf{x} \tag{2.26}$$

In general, the p-norm of a vector is defined as

$$\|\mathbf{x}\|_p = \sqrt[p]{\sum |\mathbf{x}_i|^p} \tag{2.27}$$

As l_0- norm promotes sparsity but is NP hard to solve, a l_p- norm can be used where the value of p is chosen to be 0 and 1. This will take the results closer to the sparse solution. Introducing noise to this optimization problem defined in Eq 2.26 we get the following regularization problem usually known as the Least Absolute Shrinkage and Selection Operator (LASSO) [13].

$$\hat{\mathbf{x}} = \arg\min_{\mathbf{x}} \lambda\|\mathbf{x}\|_1 + \|\mathbf{A}\mathbf{x} - \mathbf{y}\|_2^2 \tag{2.28}$$

In Eq 2.28, $\lambda > 0$ is the optimization parameter which needs to be chosen appropriately based on standard deviation of the Noise [42].

2.5. System assumptions for scope of thesis

Given the extent of the scope of distributed radar a number of assumptions are made to focus on the core problem of DOA estimation in distributed radar setups. The following assumptions are made in this thesis

- The responses obtained in a single sub-system is correlated among all the receiver elements contained in that sub-system.
- The targets are considered to be in the near field region of the system. However, it is shown that the target can be considered to be present in the far field region as seen from a single sub-system.
- The targets are visible by all the sub-systems present in the system.
- Stationary objects are considered i.e., the relative velocity of the target is considered to be zero.
- Targets are resolved only in range and azimuth, and we do not consider elevation estimation in the thesis.
- The imaging domain is considered sparse in the angular domain (for the given FOV in automotive radar this is a valid assumption as there will be fewer targets that fall in the same range and Doppler bin after Range-Doppler processing).

2.6. Conclusions

In this chapter, the system design and signal model is discussed for the distributed radar system. The system geometry is studied for a system consisting of two sensors and the target position is parameterized with respect to the center of the distributed system. The equations are presented which can be used to obtain the range and DOA of the target with respect to each radar sensor, which will be used to determine the common grid while combining the data from multiple sensors. The statistical scattering property of the target is studied when the target is in the near field and the far field region. It is observed that the target RCS can change based on the observation angle and also the distance of the target to the radar. Hence, coherent processing of the data to estimate DOA is not possible in all scenarios. Also, based on the distance of the target from the radar, the target is either in near field or far field of the radar. Through illustrations it is shown that, for larger baseline separation the probability that the target is in the near field region is higher, for the given position of the target. Thus, we need to consider the near field model in order to estimate the DOA from a distributed system. The signal model for a complex scatterer is discussed and a generic signal model is given for DOA estimation using a single radar along with a brief overview of Range-Doppler processing, for a FMCW waveform. The single snapshot extracted after Range-Doppler processing is used for the estimation of DOA. This is further extended to obtain the signal model for mono-static and bi-static configurations of the distributed system, which depends on the DOD and DOA of the target. Compressive sensing theory is discussed in brief which says that if the signal to be estimated is sparse, then the signal can be recovered successfully with lesser number of measurements than the unknowns. The optimization problem in terms of l_1-norm optimization is provided as this norm promotes sparsity and helps to recover the original signal. System assumptions considered in the thesis are presented.

3

Generalized Block FOCUSS algorithm

This chapter introduces a new generalized Block FOCUSS algorithm to estimate the DOA of targets by combining the responses from multiple radar sub-systems. This method can be applied for both mono-static and multi-static configurations of the system and for the near-field and the far-field region. Section 3.1 discusses how sparsity in the solution space can be exploited in a distributed system using the principle of block sparsity to combine the data from sub-systems. Section 3.2 introduces the existing FOCUSS algorithm and shows how it can be extended to Block FOCUSS to solve the problem of data fusion. In Section 3.3 a comparison is done between existing BOMP algorithm and Block FOCUSS algorithm, and the performance of Block FOCUSS is also discussed. Section 3.5 concludes this chapter.

3.1. Block sparsity of distributed system

In Chapter 2, Section 2.4.3 formulates the DOA estimation problem for a single radar sensor as a compressive sensing problem. To fuse the data from multiple radar sensors, it is important that the block sparsity concept is understood.

Consider the system defined in Section 2.1 (Fig 2.1), it consists of two sensors that are looking at the same imaging scene, i.e., a target present is visible to both the sensors. A system consisting of 2 sensors looking at the same target scene can be depicted as shown in Fig 3.1 (Fig borrowed from [43]). 2 mono-static and 2 bi-static responses are received from such a system as explained in Section 2.4.2 based on the system coherency. Since the 2 sensors are looking at the same target scene and their sensing matrix is defined for a common grid perspective as mentioned in Section 2.4.2 the four vectors are sparse at the same location. These four vectors are said to be jointly sparse or that they share the same support [13].

It is to be noted that when vectors are considered to be block sparse (sparse at the same location), it means that the non-zero values occur in the same position in the vector $\mathbf{x}$ but it does not mean that the non-zero value is the same in all the vectors. This is a very important point because for targets that are perceived in a non-isotropic fashion by individual sub-systems, the RCS seen by each sensor can be different and thus we cannot assume that the non-zero value in all vectors $\mathbf{x}$ is the same [43]. This is a general problem formulation that can therefore work on both isotropic and non-isotropic targets and can also be used on sub-systems which are mutually incoherent (in which case bi-static response is unavailable).

Also, in Fig 3.1 only two measurement vectors are depicted for the mono-static responses, this can be easily extended for multiple measurement vectors. For example if the bi-static responses of the system are considered as well then there will be four measurement vectors ($\mathbf{y}_1, \mathbf{y}_2, \mathbf{y}_3$ and $\mathbf{y}_4$) that are sparse in the same location.

There are algorithms like Block Orthogonal Matching Pursuit (BOMP) which can be used to solve the optimization problem that considers the signal to be estimated is block sparse as discussed in [43] [44]. This algorithm extends the existing OMP algorithm to consider that the signal to be estimated is block sparse. In this thesis we propose a new method to estimate the signal which is an extension of an alternative algorithm with higher performance, FOCUSS [42].

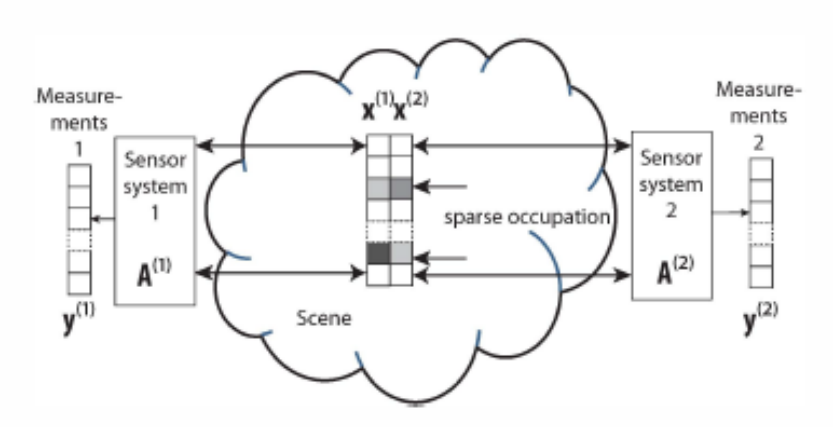

Figure 3.1: Block sparsity principle [43]

3.1.1. Optimization problem for block sparse signal

In Section 2.4.4, the CS optimization problem for a single radar sensor to solve for $\mathbf{x}$ was given by Eq 2.28. The optimization problem to solve for $\mathbf{x}$ of the distributed system can be given as shown in Eq 3.1, where L is the number of virtual apertures that are available ($L = 4$ for 2 MIMO sensors i.e., 2 mono-static apertures and 2 bi-static apertures), $\mathbf{x}$ vector is sparse at the same location for all the snapshots (block sparse).

$$\hat{\mathbf{x}} = \arg\min_{\mathbf{x}_1,..\mathbf{x}_L} \sum_{l=1}^{L} \left\| \mathbf{y}_l - \mathbf{A}_l \mathbf{x}_l \right\|_2^2 + \lambda \|\mathbf{x}\|_{2,1} \tag{3.1}$$

Here $\mathbf{y}_l, \mathbf{x}_l$ and $\mathbf{A}_l$ represents measurement vector, source vector and sensing matrix respectively for each aperture $l (l = 1, \ldots, L)$. Note that $\mathbf{A}_l$ is defined for each aperture in the common grid perspective as discussed in Eq 2.15, 2.16, 2.19 and 2.20. To understand what $\|\mathbf{x}\|_{2,1}$ is let's consider a matrix $\mathbf{X}$ comprising of the vectors $\mathbf{x}_1, ..\mathbf{x}_L$ as columns of the matrix. Then the matrix $\mathbf{X}$ is given as

$$\mathbf{X} = \begin{pmatrix} x_1^{(1)} & x_2^{(1)} & \cdots & x_L^{(1)} \\ x_1^{(2)} & x_2^{(2)} & \cdots & x_L^{(2)} \\ \vdots & \vdots & & \vdots \\ x_1^{(N)} & x_2^{(N)} & \cdots & x_L^{(N)} \end{pmatrix} \tag{3.2}$$

$$\mathbf{X} \in \mathbb{C}^{N \times L}$$

N : number of array elements in a single sensor (N_{TxRx})

Each row in $\mathbf{X}$ corresponds to a point on the grid and each element in the row corresponds to the target RCS seen by the responses from different sensors [44]. A vector $\mathbf{v}$ is constructed by taking the l_2 norm along the rows of $\mathbf{X}$ as shown below

$$\mathbf{v} = \begin{pmatrix} l_2\left(x_1^{(1)} & x_2^{(1)} & \cdots & x_L^{(1)}\right) \\ l_2\left(x_1^{(2)} & x_2^{(2)} & \cdots & x_L^{(2)}\right) \\ \vdots & \vdots & & \vdots \\ l_2\left(x_1^{(N)} & x_2^{(N)} & \cdots & x_L^{(N)}\right) \end{pmatrix} \tag{3.3}$$

The l_2-norm of a vector is defined as square root of the sum of absolute squares of its entries, thus the l_2 norm of a row of $\mathbf{X}$ is given as

$$l_2\left(x_1^{(n)}, x_2^{(n)}, \cdots, x_L^{(n)}\right) = \sqrt{\sum_{l=1}^{L} \left| x_l^{(n)} \right|^2} \tag{3.4}$$

Thus the $\|\mathbf{x}\|_{2,1}$ norm can be given from Eq 3.3 as

$$\|\mathbf{x}\|_{2,1} = \|\mathbf{v}\|_1 \tag{3.5}$$

The fusion of data from multiple snapshots is done while calculating the $\|\mathbf{x}\|_{2,1}$ norm of the data, which promotes row sparsity (block sparsity) in $\mathbf{X}$ [44]. It is important to note that the matrix $\mathbf{X}$ is not explicitly constructed at any point in solving the algorithm, it is just used here for the understanding of $\|\mathbf{x}\|_{2,1}$ norm.

3.2. FOCUSS

Focal Under-determined System Solver(FOCUSS) is one of the on-grid high resolution algorithms that can be used to solve the compressive sensing problem. There are multiple solvers that are available in literature that can be used to solve the CS problem to estimate the DOA of the target using a single sensor. Some of these algorithms are Orthogonal Matching Pursuit (OMP), Basis Pursuit (BP), Basis Pursuit Denoising (BPDN) and NESTA. In [25] a comparison is provided between these algorithms. It is shown that FOCUSS is a good choice which is robust to noise, provides a high resolution estimation and at the same time not as computationally demanding as NESTA. It is a good balance between greedy algorithms like OMP and BPDN which are very fast but provide lower resolution estimation and the NESTA algorithm which provides higher resolution compared to OMP but is very slow in time.

In Eq 3.1, the optimization problem is given in terms of l_1-norm optimization as l_1-norm promotes sparsity. FOCUSS algorithm however uses l_p-norm (Eq 2.27) instead of l_1-norm, where $0 < p < 1$ [42], which also promotes sparsity. The optimization problem to solve for block sparse signal using Block FOCUSS can thus be written as

$$\hat{\mathbf{x}} = \arg\min_{\mathbf{x}_1,..\mathbf{x}_L} \sum_{l=1}^{L} \left\|\mathbf{y}_l - \mathbf{A}_l\mathbf{x}_l\right\|_2^2 + \lambda\|\mathbf{x}\|_{2,p} \tag{3.6}$$

FOCUSS is based on the iterative re-weighted least squares technique and was originally designed to obtain a sparse solution by successively solving least squares optimization problem and is widely used to deal with compressive sensing problems. The advantages of FOCUSS are its relative low computation and stable results; only a few iterations tend to be enough to achieve a rather good approximating solution [42]. The choice of parameter p is dictated by the speed of convergence and sparsity of the solution generated. Values of $p \leq 1$ give sparse solutions, hence for sparse reconstruction p lies in $[0,1]$. The convergence rate is given as $2-p$, thus the algorithm converges faster for smaller values of p, but there is a higher likelihood to get trapped in the local minima [42]. In practice the default value of $p = 0.8$ have been found to represent a good compromise between speed of convergence and quality of the generated sparse solution [45].

FOCUSS algorithm consists of two parts [42]:

1. Find a low-resolution estimate of the sparse signal
2. Prune this solution to a sparse solution.

A weighting matrix $\mathbf{W}$ is constructed in each iteration of the algorithm using the p-norm of the data vector that is estimated. The algorithm stops when the following criteria is satisfied

$$\frac{\|\hat{\mathbf{x}_k} - \hat{\mathbf{x}}_{k-1}\|_2}{\|\hat{\mathbf{x}}_{k-1}\|_2} < \delta \tag{3.7}$$

In Eq 3.7, k represents the current iteration number in the algorithm, $\hat{\mathbf{x}}_{k-1}$ and $\hat{\mathbf{x}}_k$ represent the estimated signal in $(k-1)^{th}$ and k^{th} iteration respectively. δ is chosen as 10^{-8} by default in this thesis, it is a user selected parameter and can be changed to fine tune for faster convergence [45].

The steps involved in FOCUSS algorithm for a single snapshot is explained in detail in the following Section 3.2.1. It is followed by the steps involved in performing Block FOCUSS algorithm for multiple apertures, which is introduced for the first time in literature as per our knowledge in Section 3.2.2.

3.2.1. FOCUSS algorithm

In order to understand the working of FOCUSS algorithm, lets consider a signal model for a single sensor without noise, the optimization problem for this in terms of l_p-norm can be written as

$$\hat{\mathbf{x}} = \arg\min_{\mathbf{x}} \|\mathbf{x}\|_p \text{ s.t. } \mathbf{y} = \mathbf{A}\mathbf{x} \tag{3.8}$$

Algorithm 1 FOCUSS algorithm for a single snapshot (noiseless case)

1: Initialize $k = 0$; $\mathbf{W}_0 = \mathbf{I}$; $\delta_t = 10^{-8}$; $\delta_0 = 1$; λ = noise variance
2: **while** $\delta_k > \delta_t$ **do**
3: $k = k + 1$
4: $\mathbf{q}_k = (\mathbf{A}\mathbf{W}_{k-1})^{\dagger}\mathbf{y}$
5: $\mathbf{x}_k = \mathbf{W}_{k-1}\mathbf{q}_k$
6: $\mathbf{W_k} = \mathrm{diag}\left(\|\mathbf{x}_k\|_p\right)$
7: $\delta_k = \frac{\|\mathbf{x}_k - \mathbf{x}_{k-1}\|_2}{\|\mathbf{x}_{k-1}\|_2}$

FOCUSS algorithm finds the weighted minimum norm $\|\mathbf{W}^{-1}\mathbf{x}\|$, where $\mathbf{W}$ is a weighting matrix which satisfies the following equation

$$\mathbf{x} = \mathbf{W}(\mathbf{A}\mathbf{W})^{\dagger}\mathbf{y} \tag{3.9}$$

$\dagger$: symbol used to define Moore-Penrose inverse

We can re-write Eq 3.9 by introducing a vector $\mathbf{q}$ that satisfies the equation

$$\begin{gathered}\mathbf{x} = \mathbf{W}\mathbf{q} \\ \text{where, } \hat{\mathbf{q}} = \arg\min_{\mathbf{q}} \|\mathbf{q}\|_p \text{ s.t. } \mathbf{y} = \mathbf{A}\mathbf{W}\mathbf{q}\end{gathered} \tag{3.10}$$

The optimization problem is now defined for a new vector $\mathbf{q}$, Note that $\|\mathbf{q}\| = \|\mathbf{W}^{\dagger}\mathbf{x}\|$, thus the optimization objective in Eq 3.10 is preserved.

If we solve the above Eq 3.10 for estimating $\mathbf{q}$, then $\mathbf{x}$ can be estimated by substituting the value of $\mathbf{q}$ in Eq 3.10.

$\mathbf{W}$ is the weighting matrix which is calculated from the p-norm of the solution of $\mathbf{x}$ obtained from previous iteration in the algorithm. If the algorithm has k-iterations then for the k^{th} iteration $\mathbf{W}$ is calculated as follows

$$\mathbf{W}_k = diag\left(\|\mathbf{x}_{k-1}\|_p\right) \tag{3.11}$$

$$\mathbf{W} \in \mathbb{C}^{N_s \times N_s}$$

$$\mathbf{W}_k = \begin{pmatrix} \left|\mathrm{x}_{k-1;1}\right|^{\mathrm{p}} & 0 & \cdots & 0 \\ 0 & \left|\mathrm{x}_{k-1;2}\right|^{\mathrm{p}} & \cdots & 0 \\ \vdots & \vdots & \ddots & \vdots \\ 0 & 0 & \cdots & \left|\mathrm{x}_{k-1;N_s}\right|^{\mathrm{p}} \end{pmatrix}$$

For the initialization of $\mathbf{x}$ before the start of the algorithm, in this thesis we chose to initialize it as the least square solution of the problem $\mathbf{y} = \mathbf{A}\mathbf{x}$ by setting $\mathbf{W}_0$ to the Identity matrix $\mathbf{I}$ [42].

In summary, the FOCUSS algorithm is explained in Algorithm 1

For the signal model with noise, the regularization problem can be found by applying the Tikhonov regularization as seen in Eq 3.12. The parameter λ dictates the regularization, which determines the trade-off between finding a sparse solution and convergence of the problem [46]. The regularization problem stated in Eq 3.10 can be written as

$$\hat{\mathbf{q}}_k = \arg\min\left(\|\mathbf{A}\mathbf{W}_k\mathbf{q} - \mathbf{y}\|_2^2 + \lambda\|\mathbf{q}\|_p\right) \tag{3.12}$$

In Eq 3.12, the $\|\mathbf{A}\mathbf{W}_k\mathbf{q} - \mathbf{y}\|_2^2$ part controls the error of the solution and the p-norm of $\mathbf{q}$ controls the sparsity. Based on this regularization problem the step 4 in Algorithm 1 can be modified as shown below for a signal model with noise.

$$\begin{gathered}\text{Step 4}: \mathbf{q}_k = \mathbf{A}_k^H\left(\mathbf{A}_k\mathbf{A}_k^H + \lambda\mathbf{I}\right)^{-1}\mathbf{y} \\ \text{Where } \mathbf{A}_k = \mathbf{A}\mathbf{W}_k \text{with} \lambda \geq 0\end{gathered}$$

To see how the solution is minimized, we can understand by seeing the objective that is minimized, which is

$$\left\|\mathbf{W}^{\dagger}\mathbf{x}\right\|^2 = \|\mathbf{q}\|^2 = \sum_{i=1,w_i\neq 0}^{N}\left(\frac{x_i}{w_i}\right)^2 \tag{3.13}$$

In Eq 3.13, the relatively large entries in **W** reduce the contribution of corresponding elements in **x** to the cost and vice versa [42]. By multiplying the weighting matrix **W** with sensing matrix **A** FOCUSS selects the columns of A that best represents the solution vector **x**, or in turn the DOA of the targets and hence less error prone compared to greedy algorithms. In FOCUSS the cost function is implicitly generated in the process of computation and not explicitly specified [42].

3.2.2. Block FOCUSS algorithm

In Section 3.2, the optimization problem for multiple apertures which are sparse at the same location (block sparse) was provided in Eq 3.6. In this Section a modification of Algorithm 1 (discussed in previous Section 3.2.1) to include block sparsity of multiple snapshots is provided.

Looking at Algorithm 1 it is seen that **x** is used only in Step 6 in the calculation of the weighting matrix **W**. Hence the FOCUSS algorithm can be modified to incorporate the block sparsity of multiple snapshots by modifying this step. Since we assume that the vectors $\mathbf{x}_l$ (l varies from $1,\ldots,L$) for L apertures is sparse in the same locations, the combined estimate of $\mathbf{x}_l$'s is obtained in each iteration as the 2-norm solution to give a single **x** from all the $\mathbf{x}_l$'s. Step 6 of Algorithm 1 can thus be replaced by the following step for Block FOCUSS algorithm.

$$\text{Step 6}: \mathbf{W}_k = \text{diag}\left(\|\mathbf{x}_k\|_{2,p}\right)$$
$$\text{Where } \|\mathbf{x}_k\|_{2,p} = \|\mathbf{v}\|_p \text{ ; from Eq 3.5}$$

Hence an additional step will be added in Step 6, where we also calculate the 2-norm of $\mathbf{x}_m$ and then calculate the Weighting matrix **W**. The steps involved in Block FOCUSS algorithm to solve for Block sparse signals of multiple snapshots is shown in Algorithm 2. The noiseless case is considered for easy comparison with Algorithm 1. The steps involved for the signal model with noise is also discussed in detailed in Algorithm 3. In this case the value for λ is chosen as the minimum of the noise variances from all the apertures.

Algorithm 2 Block FOCUSS algorithm for multiple apertures (noiseless case)

1: Initialize $k=0$; $\mathbf{W}_0=\mathbf{I}$; $\delta_t=10^{-8}$; $\delta_0=1$
2: **while** $\delta_k>\delta_t$ **do**
3: $k=k+1$
4: **for** $l=[1,2,\ldots L]$ **do**
5: $\mathbf{q}_{k,l}=(\mathbf{A}_l\mathbf{W}_{k-1})^{\dagger}\mathbf{y}_l$
6: $\mathbf{x}_{k,l}=\mathbf{W}_{k-1}\mathbf{q}_{k,l}$
7: Calculate $\mathbf{W}_k\rightarrow\|\mathbf{v}_k\|_2$ for all $x_{k,l}(l=1,\ldots,L)$ from Eq 3.3
8: Calculate $\mathbf{W}_k\rightarrow\mathbf{W_k}=\text{diag}\left(\|\mathbf{v}_k\|_p\right)$
9: $\delta_k=\frac{\|\mathbf{x}_k-\mathbf{x}_{k-1}\|_2}{\|\mathbf{x}_{k-1}\|_2}$

Algorithm 3 Block FOCUSS algorithm for multiple apertures (with noise)

1: Initialize $k=0$; $\mathbf{W}_0=\mathbf{I}$; $\delta_t=10^{-8}$; $\delta_0=1$; $\lambda=$ noise variance
2: **while** $\delta_k>\delta_t$ **do**
3: $k=k+1$
4: **for** $l=[1,2,\ldots L]$ **do**
5: $\mathbf{q}_{k,l}=\mathbf{A}_{k,l}^H\left(\mathbf{A}_{k,l}\mathbf{A}_{k,l}^H+\lambda\mathbf{I}\right)^{-1}\mathbf{y}_l$ Where $\mathbf{A}_{k,l}=\mathbf{A}_l\mathbf{W}_k$ with $\lambda\geq 0$
6: $\mathbf{x}_{k,l}=\mathbf{W}_{k-1}\mathbf{q}_{k,l}$
7: Calculate $\mathbf{W}_k\rightarrow\|\mathbf{v}_k\|_2$ for all $\mathbf{x}_{k,l}(l=1,\ldots,L)$ from Eq 3.3
8: Calculate $\mathbf{W}_k\rightarrow\mathbf{W_k}=\text{diag}\left(\|\mathbf{v}_k\|_p\right)$
9: $\delta_k=\frac{\|\mathbf{x}_k-\mathbf{x}_{k-1}\|_2}{\|\mathbf{x}_{k-1}\|_2}$

3.3. Performance and comparison of Block FOCUSS with BOMP

In this thesis, we will compare the proposed Block FOCUSS algorithm with state of the art BOMP algorithm for fusion of data from multiple radar sensors. Hence it is important to understand how the two algorithms work. In Section 3.2 a detailed explanation of FOCUSS and Block FOCUSS is given. Detailed steps involved in the implementation of BOMP algorithm are discussed in [44]. There are some small errors in the algorithm steps discussed in [44] and hence the steps involved are given in Algorithm 4 after corrections.

It is important to understand the working of BOMP algorithm. Block OMP or BOMP is an extension of a greedy algorithm called OMP. OMP is a greedy algorithm and thus a fast algorithm in obtaining a sparse solution. OMP can be extended to BOMP by combining the estimated vector $\mathbf{x}$ at each iteration from all the apertures by performing a 2-norm of the vectors (or along the rows of matrix $\mathbf{X}$, Eq 3.2). In every iteration of the algorithm the matched filter response is obtained and the strongest target(with highest energy) in the scene is declared as a target. The residue after the estimation from the previous iteration is calculated and in the next iteration it tries to find the next possible strongest source present in the residue by finding the matched filter response with this residual signal. Each iteration thus adds the next strongest source vector to the list of declared targets, making the algorithm greedy in nature. The iteration ends when the residue goes below a certain defined threshold or the number of targets to be estimated is known a prioiri. In the ideal case, the algorithm takes K iterations if K targets are present in the imaging scene.

Thus, it becomes very important to define a right threshold for the algorithm, else we might end up with lot of false targets detected which are of lower energy from the left over residue. This threshold can change from one system to another and needs to be fine tuned for the given system. Also, the performance of the algorithm for low SNR is not as good as it is for higher SNR values [45]. Another important point to be noted is that BOMP suffers from ghost targets being detected, reason being if there is an error in the initial target estimation the algorithm tries to find another target in the left over residue in the following iteration. Hence, there are some limitations with this algorithm.

On the other hand Block FOCUSS is an extension of the FOCUSS algorithm which is also algorithmically very efficient and is robust for noise in comparison with OMP [45]. The computational efficiency of FOCUSS can be improved by replacing the pseudo-inverse step with a computation of Singular Value Decomposition (SVD) of $\mathbf{WA}$ as explained in [47]. Further improvement in computational efficiency can be considered

Algorithm 4 BOMP algorithm for multiple apertures

1: Initialize $k = 0; \mathbf{r}_l = \mathbf{y}_l$; δ_t = user defined threshold for stoppingthe algorithm; I = null set
2: **while** $\delta_k > \delta_t$ **do**
3: $k = k + 1$
4: **for** $l = [1, 2, \dots L]$ **do**
5: Matched filter response: $\mathbf{m}_{k,l} = \mathbf{A}_l^H \mathbf{r}_{k,l}$
6: Construct a vector for L apertures and for N grid points in dictionary as

$$\zeta = \begin{pmatrix} \ell_2\begin{pmatrix} m_1^{(1)} & m_1^{(2)} & \cdots & m_1^{(L)} \end{pmatrix} \\ \ell_2\begin{pmatrix} m_2^{(1)} & m_2^{(2)} & \cdots & m_2^{(L)} \end{pmatrix} \\ \vdots \quad \vdots \quad \vdots \\ \ell_2\begin{pmatrix} m_N^{(1)} & m_N^{(2)} & \cdots & m_N^{(L)} \end{pmatrix} \end{pmatrix}$$

7: Find the index n of the maximum entry of ζ (thereby identifying the pixel on the grid with the highest energy value) and merge n into an index set $I_k = I_{k-1} \cup \{n\}$
8: Construct a partial sensing matrix $\mathbf{E}_{k,l}$ which only constitutes the columns of $\mathbf{A}_l$ listed in I_k.
9: Compute the complex weights $\mathbf{w}_{k,l}$, which is the least square solution of the over determined linear equation

$$\mathbf{y}_l = \mathbf{E}_{k,l}\mathbf{w}_{k,l}$$
$$\text{i.e., } \mathbf{w}_{k,l} = \text{pinv}(\mathbf{E}_{k,l})\mathbf{y}_l$$

Here, vector $\mathbf{w}_{k,l}$ lists the reflectivities of the targets found in the index set I_k.
10: Find the residual signal $\mathbf{r}_{k,l}$

$$\mathbf{r}_{k,l} = \mathbf{y}_l - \mathbf{E}_{k,l}\mathbf{w}_{k,l}$$
$$\delta_k = \|\mathbf{r}_{k,l}\|_2$$

through hardware acceleration to improve the feasibility of the algorithm in a practical implementation.

In [48], a comparison is provided for FOCUSS with OMP in terms of Mean Square Error (MSE) of the recovered samples. It is shown that the MSE of FOCUSS is much lower than OMP. In [42] proof of convergence is given for FOCUSS algorithm. Also, in FOCUSS the initial estimate calculated ($\mathbf{x}_0$) is not simply increased as the algorithm advances. In fact the largest entries in $\mathbf{x}_0$ can also become zero when the algorithm converges to $\hat{\mathbf{x}}$ [42]. Significant improvement in computation of the algorithm can be achieved along with better convergence and performance properties can be gained by pruning the diminishing entries at each iteration [42]. The FOCUSS algorithm converges asymptotically to a fixed point for any starting point $\mathbf{x}_0$ as proven in [42]. It is seen that by initializing sufficiently closer to the solution, only few iterations are needed in order to converge to the true solution.

In [45], an extensive study is done comparing the performance of FOCUSS algorithm with other algorithms which also includes OMP for multiple measurement vectors. It is seen that FOCUSS performs much better than OMP in terms of achieved MSE and also the authors state that there is no significant increase in the computational efficiency of FOCUSS with multiple measurement vectors(multiple snapshots extracted from different Range-Doppler measurement over time from single sensor) as there is still only one pseudo inverse computation per iteration. With the availability of multiple measurement vectors in time from the same sensor in future, to extend the FOCUSS algorithm is fairly easy and also computationally efficient. Also a detailed study is performed in the angular resolution achieved in DOA estimation using a single ULA and sparse array radar unit for different algorithms in [15]. To compare the two algorithms few important characteristics of the algorithms are used like mean square error, false alarms and probability of resolution. These parameters will help determine the performance of the algorithms. It can be seen that for both ULA and sparse array configuration FOCUSS has much better angular resolution performance than OMP.

Thus, it is seen that using FOCUSS over greedy algorithms like OMP has much to be gained in performance for a very small increase in computational efficiency. FOCUSS provides a relatively inexpensive way to accurately estimate the sparse signals [42]. This is the reason why we chose to extend the FOCUSS algorithm to be used for estimating the signal from multiple snapshots which are sparse at the same location (block sparse) instead of using existing algorithms like BOMP.

3.4. Simulation

A simple simulation is performed to demonstrate the results obtained using Block FOCUSS. Two targets placed at a range of 20 m from the radar and separated by 3° in DOA is considered. The frequency used is 78 GHz and the Bandwidth is 250 MHz. A high SNR scenario of 30 dB is considered in this simulation. Two radar sensors separated by a baseline of 128λ is used where each sensor consists of 3 transmitters and 4 receivers forming 12 virtual antenna elements. To find the theoretical resolution a study of the ambiguity function (AF) is performed. The details about AF and how it is calculated is explained in Appendix B. Fig

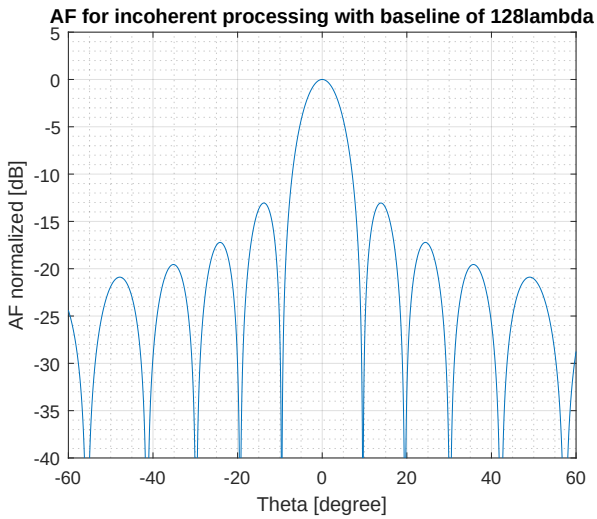

Figure 3.2: AF for incoherent processing

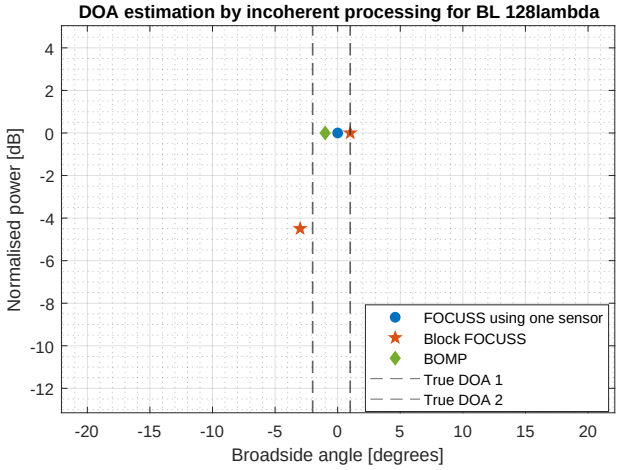

Figure 3.3: DOA estimation using incoherent processing

3.2 depicts the AF obtained from incoherent processing of the responses obtained from the two sensors. As shown in the plot, the AF is equivalent to that of an AF of the sub-aperture present in the system for incoherent processing. This is because Block FOCUSS performs incoherent processing, thus the distributed sensors are not treated as one large aperture. This restricts the resolution to the sub-aperture used in the distributed system. The theoretical resolution that can be achieved is calculated by measuring the MLW of the AF which is $\sim 8.5^\circ$ (which agrees with the theoretical limit for a sensor consisting of 12 ULA). The Block FOCUSS algorithm is a super resolution algorithm, thus the resolution obtained should be better than the theoretical resolution. The dictionary spacing is 1° with scan angles from -45° to $+45^\circ$. By performing incoherent processing there is a spatial diversity gain that is still beneficial, which will help in attaining better resolution than using a single sensor [3]. Having multiple sensors that are looking at the same target from different angles can bring in different perspective and can help resolve the two closely spaced targets. This is depicted in Fig 3.3, the two targets are placed at 1° and -2° shown by the dotted lines in the plot. The output of the FOCUSS algorithm by processing data from a single sensor is shown along with the output of the Block FOCUSS and the BOMP algorithms which process the 4 responses (2 mono-static and 2 bi-static) from the two sensors incoherently. The single sensor case fails to resolve these two targets separated by 3°, whereas the Block FOCUSS algorithm succeeds in resolving them. It is shown that the BOMP algorithm fails to resolve the two targets as well. To study and compare the performance of the algorithms, Monte Carlo runs are performed and parameters like probability of resolution, root mean square error and probability of false alarms are calculated which is presented in Chapter 5.

3.5. Conclusions

In this chapter, block sparsity is explained and how it can be used to fuse data from multiple radar sensors is discussed. Block sparsity works on the principle that the DOA to be estimated from multiple sensors is sparse at the same location, namely, they have the same support. Block sparsity does not assume that the RCS of targets seen is same from all the sensors. Thus, it can be used as a general algorithm for all cases of system coherency and for isotropic or non-isotropic targets. The FOCUSS algorithm which uses l_p-norm optimization is explained and the steps to perform the algorithm are discussed. The Block FOCUSS is derived from the FOCUSS algorithm by combining the estimated signal from virtual apertures in each iteration, by performing a $l_{2,1}$-norm. In each iteration the signal obtained after performing $l_{2,1}$-norm on all the virtual apertures, is used to define the new weighting matrix. Performance of the Block FOCUSS algorithm and comparison of the same with state of the art BOMP algorithm is studied. The study shows that FOCUSS performs much better in terms of convergence to the true solution for a small increase in computational complexity when compared to OMP. Thus, Block FOCUSS algorithm which is an extension of FOCUSS is preferable over BOMP which is an extension of OMP, in order to estimate targets in the angular domain for a distributed system. In simulation it is shown that, for a system with baseline of 128λ and an effective aperture of 6λ, the Block FOCUSS algorithm can resolve two targets separated by 3°, whereas single sensor and BOMP algorithm fails to do so.

4

Coherent processing of signals

This chapter introduces a special case of signal processing for data obtained from a distributed system, when the sub-systems are fully coherent. In the previous chapter a way to perform DOA estimation of targets by incoherently combining the data from multiple sensors was presented. In this method the resolution that can be obtained is still limited by the largest sub-aperture in the distributed system. This chapter provides a way to combine the data coherently such that the resolution achieved is proportional to the aperture of the distributed system. It provides a way to achieve higher angular resolution when the radars are fully synchronized and targets are isotropic. This is possible when the targets are seen to be isotropic with respect to the distributed system as discussed in Section 2.2. Section 4.1 discusses the properties of system and targets to perform coherent processing and also the pre-processing steps needed to ensure coherency are discussed. In Section 4.2 a Coherent FOCUSS algorithm is introduced. The ambiguity function of a distributed system and the limitations of coherent processing are discussed in Section 4.3. Section 4.4 presents a way to combine mono-static and bi-static responses of the system in an incoherent and coherent fashion respectively by employing Fusion FOCUSS algorithm. Coherent FOCUSS and Fusion FOCUSS algorithms in the way they are presented in this thesis are novel. Section 4.6 concludes the chapter.

4.1. Coherency of system and targets

In Chapter 3, the Block FOCUSS algorithm was proposed to solve the problem of DOA estimation using data from multiple radar systems. In this method the coherency of the system is not necessary, i.e., the sub-systems can be mutually incoherent and still the Block FOCUSS algorithm can be applied for the mono-static responses. If the radars are fully coherent then multi-static responses can also be combined to get a better estimate of true positions of the targets. In this algorithm the targets should be visible by both the radars but the nature of the target is not considered as it does not matter if the RCS seen by different apertures are not same.

In this section, we introduce a special way to process the data if it is known a prior that the system is fully coherent and the target is perceived in an isotropic way by the entire system, i.e., the RCS of the targets observed by all the sub-systems within the system is same. When the system is fully coherent it is important to decide if coherent combining of data needs to be performed based on the properties of the target. This is indeed not an easy way to determine, the conditions under which a target is considered isotropic is discussed in Section 2.2. In this thesis we propose the coherent combining of the data assuming we are able to determine the isotropic nature of targets and the system is fully coherent. Under these conditions the distributed system can be treated as one large sparse array, with a large number of elements missing in between the sub-systems

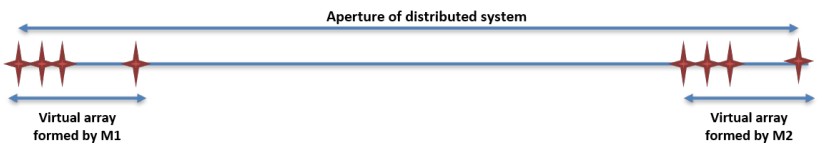

Figure 4.1: Combined physical aperture of the distributed system

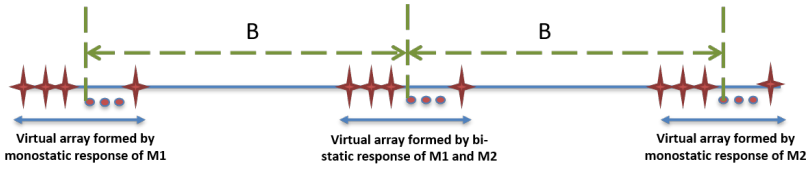

Figure 4.2: Mono-static and bi-static response of distributed system

(the number of missing elements depends on the separation of the sensors in the distributed system). This is depicted in Fig 4.1, where the virtual elements formed by sensors M1 and M2 are shown, which are separated by a distance referred to as the baseline. Baseline represents the physical aperture of the system i.e., if the sub-systems together are considered to form one large virtual array with elements missing in the center, then the physical aperture that can be achieved is depicted by the baseline separation between M1 and M2. Thus we can benefit from this as the azimuth resolution that can be achieved is directly proportional to the array virtual aperture that is formed by the 2 sensors.

- **Coherency of system**

  In order to perform DOA estimation by treating the distributed system as one large array, it is extremely important that the sub-systems are fully coherent. Only then we ensure that an isotropic target can be processed in a coherent way. Achieving complete coherency between the sub-systems is not easy, however it is not impossible either. [20] provides detailed steps that can be followed to achieve the synchronization and coherency between all the sub-systems. In this thesis, we assume that the sub-systems used in the distributed system are mutually coherent.

  When the sub-systems are mutually coherent, the chirps transmitted from one sub-system can be received and properly dechirped as explained in Section 2.3 by the other sub-systems without any anomalies (like frequency offset, time offset, phase offset). Moreover the bi-static responses of the system provide additional data points and helps to get a better estimate of the true signal.

- **Isotropic property of targets**

  In Section 2.2, the isotropic nature of targets is studied in detail. To recall, if the RCS of a target at a certain distance is identical regardless from which angle it is observed, the target is called isotropic, if not it is said to be non-isotropic, Fig 2.4. When the target is isotropic in a certain angular sector, the responses received by all the sub-systems are correlated and the RCS seen by all the sub-systems remains the same in the given angular sector. For a given baseline separation of the radar system, the distance of the target at which the target is perceived in an isotropic manner can be calculated using Eq 2.5.

  If it is known that the target is isotropic as seen from the distributed radar then we can perform coherent processing on the received signal by combining data from all the sub-systems coherently in order to achieve higher angular resolution.

4.1.1. Distributed array configuration

In the system geometry discussed in Section 2.1, M1 and M2 sensors are considered to be identical (can differ in orientation) and placed at equidistant from the center, separated by a distance of B as shown in Fig 2.1. Then the virtual apertures of the mono-static and bi-static responses are as shown in Fig 4.3 [20]. The two bi-static responses of M1 and M2 forms a virtual ULA in the center of the system. The responses of mono-static and bi-static can be generated using Eq 4.1 [5], where d_{Tx} and d_{Rx} represents the transmitter and receiver element positions in the sensor. If a sensor comprises of N_{Tx} and N_{Rx} transmitter and receiver elements respectively, then the virtual array with these elements can be calculated as

$$d^{\text{Virt}} = d^{\text{Tx}} \oplus d^{\text{Rx}} := \left[d_1^{\text{Tx}} + d_1^{\text{Rx}}, d_1^{\text{Tx}} + d_2^{\text{Rx}}, \cdots, d_{N_{\text{Tx}}}^{\text{Tx}} + d_{N_{\text{Rx}}}^{\text{Rx}} \right] \tag{4.1}$$

Extending the Eq 4.1 for a distributed system with 2 sensors separated by a baseline B it can be shown that the virtual array for the mono-static and bi-static responses can be calculated as explained in the below steps. If $d_1^{Tx}, d_1^{Rx}, d_2^{Tx}, d_2^{Rx}$ are the absolute positions of the antenna elements when the 2 sensors are in the center. M1 sensor comprises of d_1^{Tx}, d_1^{Rx} and M2 sensor comprises of d_2^{Tx}, d_2^{Rx} elements then we have the following

- For the left sensor M1 we have

$$d_{M1}^{Tx} = d_1^{Tx} - B/2$$
$$d_{M1}^{Rx} = d_1^{Rx} - B/2$$
$$d_{M1}^{Virt} = \left(d_1^{\mathrm{Tx}} \oplus d_1^{\mathrm{Rx}}\right) - B$$

- For the right sensor M2 we have

$$d_{M2}^{Tx} = d_2^{Tx} + B/2$$
$$d_{M2}^{Rx} = d_2^{Rx} + B/2$$
$$d_{M2}^{Virt} = \left(d_2^{\mathrm{Tx}} \oplus d_2^{\mathrm{Rx}}\right) + B$$

- For the bi-static response where M1 is transmitting and M2 is receiving (Left to Right or in short L2R) we have

$$d_{M1}^{Tx} = d_1^{Tx} - B/2$$
$$d_{M2}^{Rx} = d_2^{Rx} + B/2$$
$$d_{M1M2}^{Virt} = \left(d_{M1}^{\mathrm{Tx}} - B/2\right) \oplus \left(d_{M2}^{\mathrm{Rx}} + B/2\right) = d_{M1}^{\mathrm{Tx}} \oplus d_{M2}^{\mathrm{Rx}}$$

- For the bi-static response where M2 is transmitting and M1 is receiving (Right to Left or in short R2L) we have

$$d_{M2}^{Tx} = d_2^{Tx} + B/2$$
$$d_{M1}^{Rx} = d_1^{Rx} - B/2$$
$$d_{M2M1}^{Virt} = \left(d_{M2}^{\mathrm{Tx}} + B/2\right) \oplus \left(d_{M1}^{\mathrm{Rx}} - B/2\right) = d_{M2}^{\mathrm{Tx}} \oplus d_{M1}^{\mathrm{Rx}}$$

From the above expressions, it is shown that the baseline value cancels in the bi-static responses and thus B has not influence on the relative positions of the virtual antenna elements of the two bi-static responses.

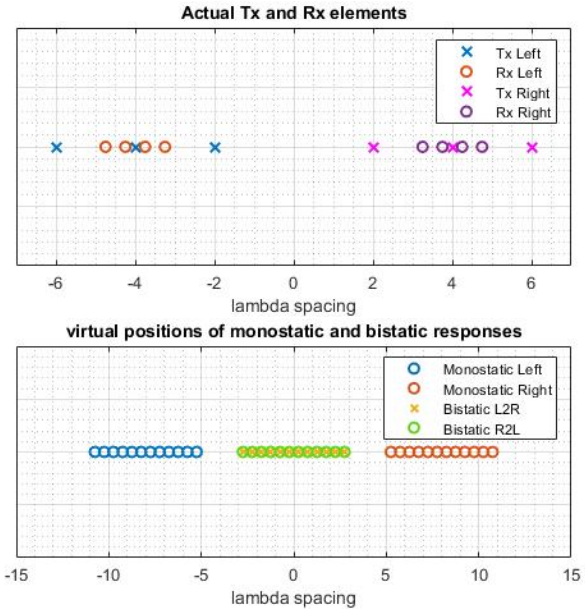

Figure 4.3: Mono-static and bi-static response for a 3 × 4 MIMO sub-system M1 and M2

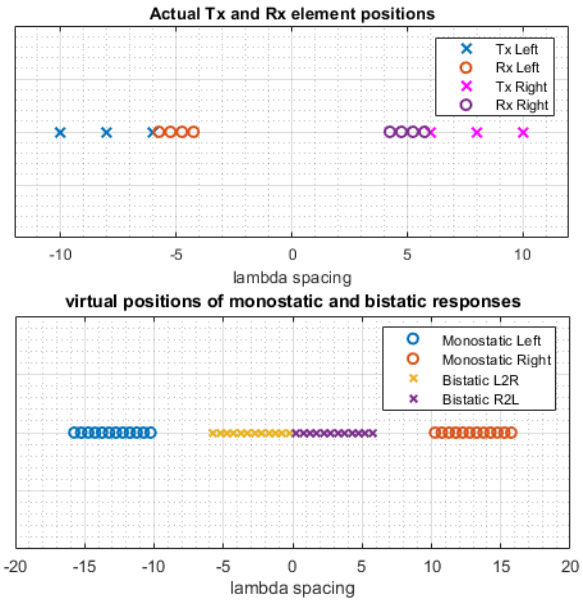

Figure 4.4: Mono-static and bi-static response for a 3 × 4 identical sub-systems M1 and M2 which have different orientation

But for the mono-static responses B is present in the expression, hence for coherent processing of all responses, B has to be known exactly. But for coherent combining of just the bi-static responses and also for incoherent combining of responses we need not know the absolute value of B. Also if the orientation of M1 and M2 sensors are different, as seen from the above expressions it is shown that the 2 bi-static responses are not the same.

Fig 4.3 (top) shows an example explaining Eq 4.1 for a distributed system as discussed in above steps. M1 and M2 are identical sensors and both have $3Tx's$ and $4Rx's$ spaced as shown in figure. The baseline separation between M1 and M2 is 8λ. The resultant virtual positions from the mono-static and bi-static responses are as shown in the Fig 4.3 (bottom). From the figure, the 2 bi-static responses from M1 and M2 sensors are seen to overlap, this is because the positions of transmitting and receiving elements in M1 and M2 are symmetrical around the origin. Thus, we see that by using 2 mono-static and 2 bi-static responses from the sensors we can achieve a large virtual aperture consisting of 4 small virtual apertures as shown in Fig 4.3.

Fig 4.4 shows an example explaining Eq 4.1 for a distributed system as discussed in above steps. M1 and M2 are identical sensors which are mirrored in their orientation and have a certain offset in the receiver elements as shown in the top of figure. The baseline separation between M1 and M2 is 16λ. The resultant virtual positions from the mono-static and bi-static responses are as shown in the Fig 4.4 (bottom). From the figure, the 2 bi-static responses from M1 and M2 sensors are seen to form a larger aperture in the center and do not overlap as in Fig 4.3, this is because the positions of transmitting and receiving elements in M1 and M2 are not centered around the same location and the 2 sensors are mirrored.

4.1.2. Signal Model for DOA estimation by coherent processing

For coherent processing, the sensing matrix can be written as a matrix consisting of columns with beam steering vectors representing the virtual elements of the whole array. For example if we have M1 and M2 both containing 12 element virtual ULA, then the sensing matrix will be made up of columns of size 4×12 elements, where 2 of them represent the mono-static virtual arrays and the other 2 the bi-static virtual arrays, i.e., the entire system is treated as one big array. For the system defined in Fig 2.1 the steering matrix for each of the virtual response is discussed in Section 2.4.2 which is given by Eq 2.15, 2.16, 2.19 and 2.20. The steering matrix for the mono-static responses of M1 and M2 are represented as $\mathbf{A}_1$ and $\mathbf{A}_2$ respectively, the bi-static response obtained when M1 is transmitting and M2 is receiving is represented by $\mathbf{A}_3$ and the bi-static response with M2 transmitting and M1 receiving is given by $\mathbf{A}_4$. Since the RCS observed by all the responses are assumed to originate from isotropic targets we can write the optimization problem as seen by one large array with virtual responses as shown in Fig 4.3.

$$\mathbf{y}_c = \mathbf{A}_c\mathbf{x} + \mathbf{n} \tag{4.2}$$

$$\begin{bmatrix} \mathbf{y}_1 \\ \mathbf{y}_3 \\ \mathbf{y}_4 \\ \mathbf{y}_2 \end{bmatrix} = \begin{bmatrix} \mathbf{A}_1 \\ \mathbf{A}_3 \\ \mathbf{A}_4 \\ \mathbf{A}_2 \end{bmatrix} [\mathbf{x}] + \mathbf{n} \tag{4.3}$$

$$\mathbf{y}_c \in \mathbb{C}^{4N\times 1}; \mathbf{x} \in \mathbb{C}^{N_s\times 1}; \mathbf{A}_c \in \mathbb{C}^{4N\times N_s}$$

In Eq 4.2 $\mathbf{y}_c$ is obtained by stacking snapshots from the 4 apertures in a single column, $\mathbf{A}_c$ is obtained by stacking the sensing matrices of 4 virtual arrays vertically as shown in Eq 4.3. Here the $\mathbf{x}$ to be estimated is the same for all apertures. Thus, by solving this system of equation $\mathbf{x}$ can be estimated using CS techniques which is discussed in Section 4.2.

4.1.3. Phase compensation due to path length difference

In order to perform DOA estimation in a coherent fashion as discussed in previous section it is important that the initial phase of received signal from all the apertures are same, else the DOA estimation will lead to errors. In Section 4.1 the coherency of system and isotropic property of targets are explained which ensures that all apertures experience the same phase of a target. However, the phase perceived by the apertures can still be different which arises from the path length difference. To correct for this we need to know the distance to the target for each aperture. With Range-Doppler processing a coarse estimation of range is obtained whose uncertainty is related to the range resolution. Due to this inability to precisely measure the range of the target we do not exactly know what the path length difference is and hence cannot be corrected. Range resolution is inversely proportional to the bandwidth of the signal used, hence even if the radar uses a bandwidth of $3GHz - 5GHz$ (typically considered to be large BW), the range resolution that can be achieved is limited to few centimetres. This means that the target can be present anywhere in the range cell whose resolution is few centimetres. Thus, there is an error in the range measurement of the target when compared to the true target position that occurs due to the quantization of the target to center of the range cell. The wavelength of the signal used for automotive radar is usually in the millimetre (mm) range, even an error of few millimetres can make the phase of the signal to wrap around multiple times (a factor of 2π) as it travels back from the target to radar. This is called as Range-Angle coupling as explained in [36]. Fig 4.5 depicts this phenomenon for a system with 2 sensors M1 and M2. The shaded elliptical regions show the single range cell of the 2 sensors at range $R1$ and $R2$. When the target is at position T1 or T2 as shown in the figure, the target is detected at T0 by the sensors as it is quantized to the center of the range cell. Thus, the actual distance of a target from the sensors is different than the one measured by the sensor if the target is not at the center of the range cell. Because the range of the target measured by sensors M1 and M2 can vary in multiples of wavelengths (based

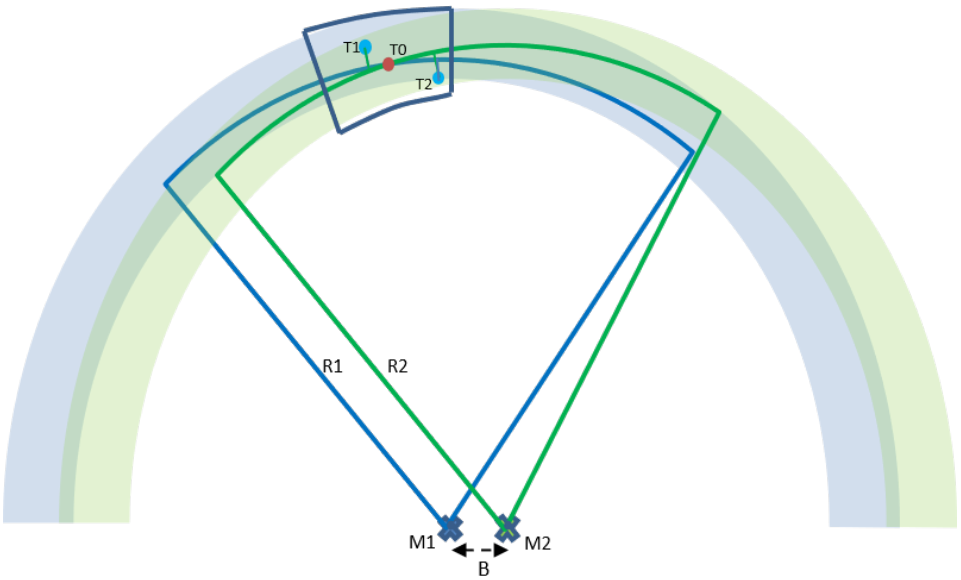

Figure 4.5: Phase change due to path length difference between target and the 2 sensors

on the resolution of range cell), the phase of the waveform received is also different. This phase change due to the path length difference needs to be corrected in order to process the signal coherently. From Eq 2.6 the phase (β), which is the total phase is given as follows

$$\beta = f_c\tau + 1/2\alpha\tau^2 \tag{4.4}$$

In the above equation, f_c is the carrier frequency of the transmitted signal, τ is the time delay or round trip delay given as $2R/c$, where R is the range of the target from radar and c is the constant for speed of electromagnetic wave, α is the ratio of bandwidth to chirp duration. For the 4 responses that are obtained for the system explained in Section 2.1 (Fig 2.1) the τ value can be calculated as

$$\begin{aligned} \tau_1 &= 2R_1/c \\ \tau_2 &= 2R_2/c \\ \tau_3 &= (R_1+R_2)/c \\ \tau_4 &= (R_1+R_2)/c \end{aligned} \tag{4.5}$$

In the above equation, τ_1 and τ_2 are the round trip delay for the 2 mono-static responses, τ_3 and τ_4 are the round trip delay for the 2 bi-static responses. As the range R_1 and R_2 cannot be precisely estimated due to the range quantization error discussed, there will be a phase difference in the received signal as seen by different responses. This phase difference needs to be compensated in order to coherently process the signals. From Eq 4.5 τ_3 and τ_4 have the same value and hence the phase of the bi-static responses due to the path length difference will be same. The phase difference of the mono-static responses can be compensated with respect to the bi-static responses by multiplying with the phase difference observed between the two. If β_1, β_2, β_3 and β_4 are the phase differences of the 2 mono-static responses and 2 bi-static responses respectively due to the path length difference as given in Eq 4.4, then the difference between the mono-static and the bi-static responses can be approximated as

$$\begin{aligned} \beta_1 - \beta_3 &\approx f_c(R_1-R_2)/c = (R_1-R_2)/\lambda \\ \beta_2 - \beta_3 &\approx f_c(R_2-R_1)/c = -(R_1-R_2)/\lambda \\ \Delta\beta &= (R_1-R_2)/\lambda \end{aligned} \tag{4.6}$$

In the above equation only β_3 is used, but note that the value of β_3 and β_4 is same. Also, the τ^2 term in the difference is left out as the value is too small and hence the difference between them is negligible. The modelled phase difference can be compensated for each response by accounting for it in the definition of sensing matrix, by multiplying each column of the sensing matrix with the corresponding phase difference. The steps for this is explained below:

1. For every θ in the dictionary of sensing matrix $\mathbf{A}$, the corresponding angles and range of the target with respect to 2 sensors is calculated using Eq 2.1 - Eq 2.4
2. The phase difference due to different path lengths between the responses is calculated for each column (θ), given as $\Delta\beta_n$ ($n = 1 : N_s$) using Eq 4.6 ($\Delta\beta_n = (R_{1n} - R_{2n})/\lambda$)
3. The new sensing matrix is defined by multiplying each column of the sensing matrix with the corresponding phase difference that is calculated in Step 2. This is represented below, where Eq 2.15 and Eq 2.16 for sensing matrix is re written as

$$\mathbf{A}_1^* = \mathbf{A}^*(\varphi) = \left[\mathbf{a}(\varphi_1)\cdot e^{-j2\pi\beta_1}\,;\,\mathbf{a}(\varphi_2)\cdot e^{-j2\pi\beta_2};\ldots;\mathbf{a}(\varphi_{\mathrm{Ns}})\cdot e^{-j2\pi\beta_{Ns}}\right] \tag{4.7}$$

$$\mathbf{A}_2^* = \mathbf{A}^*(\psi) = \left[\mathbf{a}(\psi_1)\cdot e^{j2\pi\beta_1}\,;\,\mathbf{a}(\psi_2)\cdot e^{j2\pi\beta_2};\ldots;\mathbf{a}(\psi_{\mathrm{Ns}})\cdot e^{j2\pi\beta_{Ns}}\right] \tag{4.8}$$

   Note that $\mathbf{A}_3$ and $\mathbf{A}_4$ remain the same as the phase difference between mono-static responses are calculated with respect to the bi-static responses

By following the above mentioned steps, the phase difference caused due to path length difference observed by the radar sensors is compensated for every DOA of the target that is considered in the dictionary defined for sensing matrix. Thus making the phase of the targets as perceived by the sensors to be coherent. Please note that this compensation works for a radar with infinite range resolution or a sensor which can estimate the range of the target to millimeter precision in this case. We propose a method to compensate for the phase change that occurs due to path length difference, in order to do so it is important to determine precisely the true range of the target else there might be ambiguities that arise due to the applied phase compensation.

4.2. Coherent FOCUSS

As discussed in Section 4.1, coherent processing can be done to improve the angular resolution if the targets and the system are isotropic and coherent respectively. In this section the steps involved in performing coherent processing using FOCUSS algorithm is discussed in detail. In Section 3.2.1 the steps involved in FOCUSS algorithm for a system in the form $\mathbf{y} = \mathbf{A}\mathbf{x} + \mathbf{n}$ is discussed. From Eq 4.2 the problem formulation for coherent processing of the virtual apertures is given. Section 4.1.3 discusses the phase compensation that needs to be applied to the columns of the sensing matrix for mono-static apertures. Thus the system of equations to solve the problem in a coherent fashion can be written as

$$\begin{bmatrix} \mathbf{y}_1 \\ \mathbf{y}_3 \\ \mathbf{y}_4 \\ \mathbf{y}_2 \end{bmatrix} = \begin{bmatrix} \mathbf{A}_1^* \\ \mathbf{A}_3 \\ \mathbf{A}_4 \\ \mathbf{A}_2^* \end{bmatrix} [\mathbf{x}] + \mathbf{n} \tag{4.9}$$

In Eq 4.9 $\mathbf{A}_1^*$ and $\mathbf{A}_2^*$ are given by Eq 4.7 and Eq 4.8 respectively. The Eq 4.9 can be re-written by defining a new vector $\mathbf{y}_c$ comprising of all the snapshots stacked and a new sensing matrix $\mathbf{A}_c$ by stacking the 4 sensing matrices as in Eq 4.9. The new equation is given as

$$\mathbf{y}_c = \mathbf{A}_c\mathbf{x} + \mathbf{n} \tag{4.10}$$

To solve the above Eq 4.10, we can make use of the FOCUSS algorithm discussed in Algorithm 1 where $\mathbf{y}$ and $\mathbf{A}$ are now replaced by new vector $\mathbf{y}_c$ and new sensing matrix $\mathbf{A}_c$.

4.3. Ambiguity function of the distributed system

By performing coherent processing of multiple apertures, a higher angular resolution can be obtained as the virtual aperture of the array is now equivalent to that of twice the baseline of the system. This can be validated by looking at the ambiguity function of the distributed array. The ambiguity function can be calculated as a matched filter response as explained in Appendix B. If we have 2 sensors M1 and M2 separated by a baseline separation of 16λ, then the virtual aperture for this is shown as in Fig 4.6. In this configuration shown, the receiver element positions of the sub-system in the uniformly distributed MIMO are offset by a multiple of lambda relative to the transmitter element positions. This is done in order to get a virtual array in which the 2 bi-static responses don't overlap. The virtual element positions for the 2 mono-static and 2 bi-static responses are depicted in the Fig 4.6 with the notation 'Left to Left (L2L)', 'Right to Right (R2R)' , 'Left to Right (L2R)' and 'Right to Left (R2L)' respectively. The ambiguity function for such an array is depicted in Fig 4.7. In the Figure

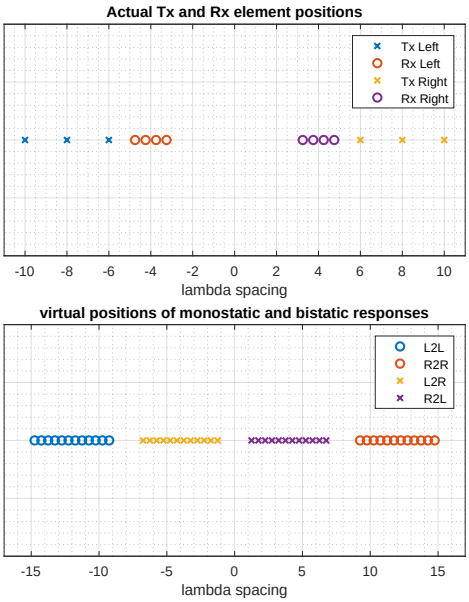

Figure 4.6: Mono-static and bi-static response for a 3 × 4 MIMO sub-system M1 and M2

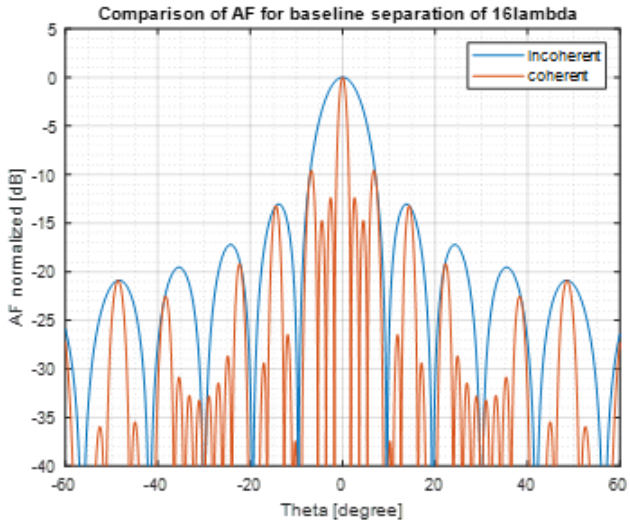

Figure 4.7: Ambiguity function for coherent and incoherent processing for 16λ baseline

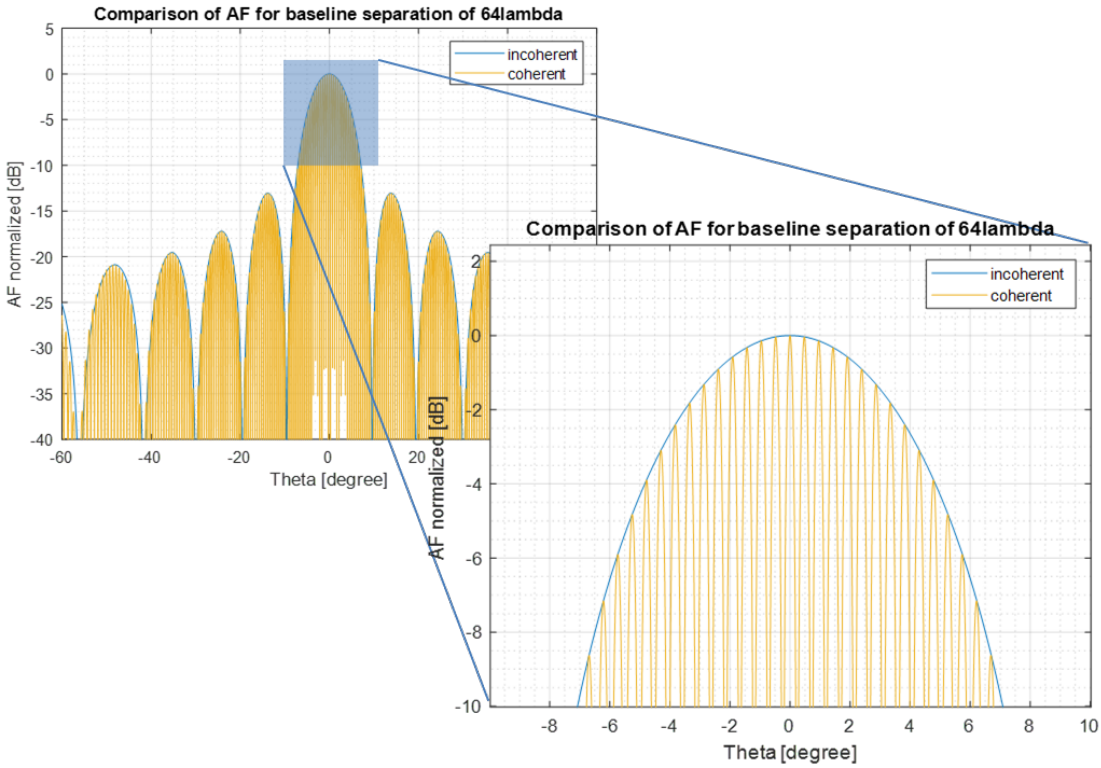

Figure 4.8: Ambiguity function for coherent and incoherent processing for 64λ baseline (mono-static responses only)

the plot "incoherent" (blue plot) shows the AF for the individual mono-static array, it has the same AF and forms an envelope for the coherent array. The plot "coherent" (red plot) shows the AF obtained by coherent processing of the data as studied in Section 4.2.

From the Fig 4.7, the Main Lobe Width (MLW) of the coherent processing is much narrower than that of the incoherent processing. The MLW of the incoherent processing is ~ 8.5° and that of the coherent processing is ~ 1.6°. From this it can clearly be inferred that coherent processing has a much better resolution capability than incoherent processing as it has a larger virtual aperture. The MLW will reduce further with increase of the baseline in order to get a larger virtual aperture, but this comes at a cost of increase in Side Lobe Level (SLL). The increase in SLL can be understood, because when the baseline increases, the virtual array becomes

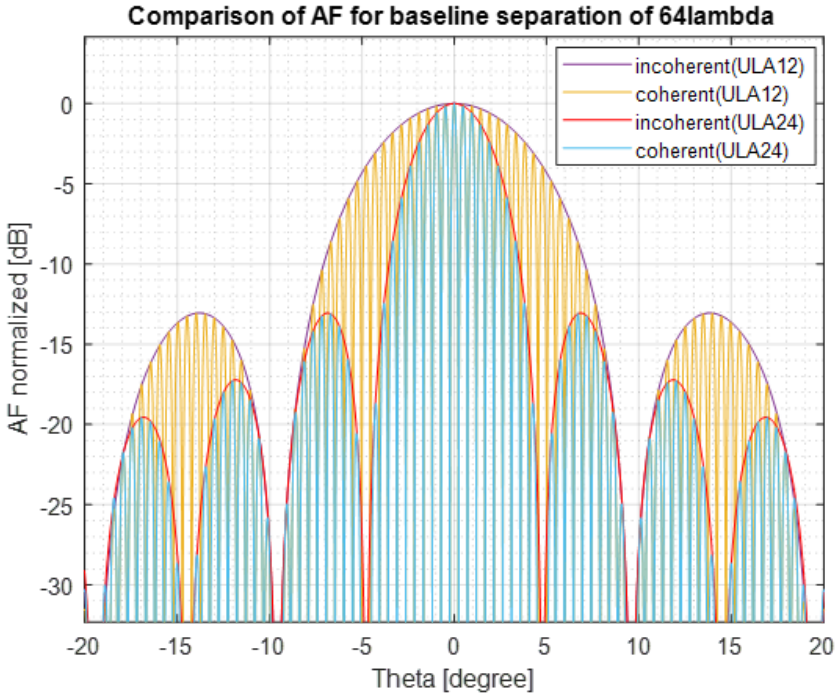

Figure 4.9: Comparison of AF for different sub-apertures with baseline separation 64λ

more sparse. For a sparse array, high SLL is a problem, Fig 4.8 shows the AF response of just the mono-static responses with a baseline of 64λ. In this context the side lobes of the overall response is seen to be very high which is caused due to the grating lobes of the sparse distributed aperture. It is seen that the MLW is narrower but the side lobes have significantly increased which is caused by the absence of more elements between the 2 sensors due to increased baseline when compared to 16λ baseline. Having such high number of side lobes can lead to pointing errors in the DOA estimation. What this means for coherent processing is explained next.

In [21], the AF response for a distributed system with one large virtual aperture consisting of multiple smaller sub-apertures (formed by the sub-systems) is explained in detail. The key take-away from this is that the overall AF response of the coherent processing is a product of individual sub-systems aperture and a two element array with a spacing of $2B$. Since a 2 element array with $2B$ spacing is highly sparse it will result in multiple grating lobes. This is demonstrated in Fig 4.9, where the AF for a distributed system with 2 different sub-apertures is depicted. A sub-system forming a 12 element ULA and a 24 element ULA is considered for comparison, note that the aperture of 24-ULA is double than that of the 12-ULA. The coherent processing suffers from high side lobes in this as discussed, but the side lobes follow the AF response of the incoherent processing (which is nothing but the response of the sub-system aperture or sub-aperture). Thus, the side lobes are suppressed in the overall response due to the sub-aperture MLW. Thus the side lobes is a function of the baseline of the distributed array, but the entire response is a product of 2 element array with an aperture of $2B$ and the sub-aperture. The ratio of the distributed aperture (baseline) to the aperture of the sub-system needs to be defined appropriately to avoid the problems of side lobes. Note that in Fig 4.8 and Fig 4.9 only the mono-static responses are considered to understand the concept, by adding the bi-static responses some of the side lobes are further suppressed as the sparsity in the distributed array reduces, as it can be seen as addition of 2 more array elements in between the $2B$ separated sensors.

These very high SLL caused by the grating lobes of the sparse distributed array can lead to pointing errors when estimating the DOA of the target. The SNR needs to be very high in order to not land in one of these side lobes while estimating the DOA, which in general is hard to achieve.

This problem of side lobes can also be reduced by introducing more sensors in the system, in this study we consider only 2 sensors, but by introducing another sensor in the center of the system the number of multi-static responses will increase in the powers of 2, thus reducing the sparsity and in turn the side lobes in the distributed array. Another method is to design the system in such a way that the ratio of distributed aperture and sub-aperture is reasonable and acceptable.

4.4. Coherency of bi-static responses

In previous section, it was shown that the AF response of the coherent processing of all the sub-apertures can lead to very high side lobes for larger baseline separation and it is very difficult to suppress them for higher baselines. This can be a problem in applications like automotive radar where the sensor positions cannot be very closely spaced, the manufacturers of the automobile might prefer to separate the sensors by optimal placement of them on the car fascia which can lead to high SLL as seen in Section 4.3. In such scenarios coherent processing of the entire aperture can be inefficient due to very large side lobes, which can cause pointing errors especially for lower SNR values as the side lobe is very close to the main lobe and the target DOA can be wrongly estimated to fall in one of the adjacent side lobe. One possible solution for this is to process only the bi-static responses coherently and the 2 mono-static responses incoherently.

In [49], the coherency of bi-static response is discussed in detail. The conditions under which the bi-static responses can be assumed to be coherent are stated as follows:

- The mono-static responses are strongly correlated
- Bi-static angle is very small (less than 10°). The bi-static angle is the angle made between the transmitter, target and receiver in the distributed radar where the transmitter and receiver are not co-located.
- Individual reflectors present in the imaging scene are omni-directional and are not in the shadow of each other

When the above conditions are satisfied for a given system and imaging scene, it can be assumed that the bi-static responses are coherent. Fig 4.11 shows the AF response for the incoherent processing of the mono-static responses and coherent processing of bi-static responses. The sensors M1 and M2 have receiver positions offset from the uniform array position in order to obtain twice the virtual aperture formed by the 2 bi-static responses [20] as shown in Fig 4.10 (for a MIMO sensor with 3 transmitter and 4 receivers). From Fig 4.11 it is seen that the MLW of the bi-static responses that are coherently processed is half that of individual mono-static responses that are incoherently processed. This implies that we have a factor of 2 improvement in the angular resolution that can be gained by processing the bi-static responses coherently.

4.4.1. Fusion FOCUSS

Previous section shows that by processing only the bi-static responses coherently, the angular resolution can be increased by a factor of two. To perform the DOA estimation by fusion of data i.e., processing the mono-static responses incoherently and the bi-static responses coherently a modified version of FOCUSS is provided in this section, which is called the Fusion FOCUSS. Fusion FOCUSS profits from the large virtual aperture of the coherent bi-static responses but avoids the complications of exploiting coherence from all

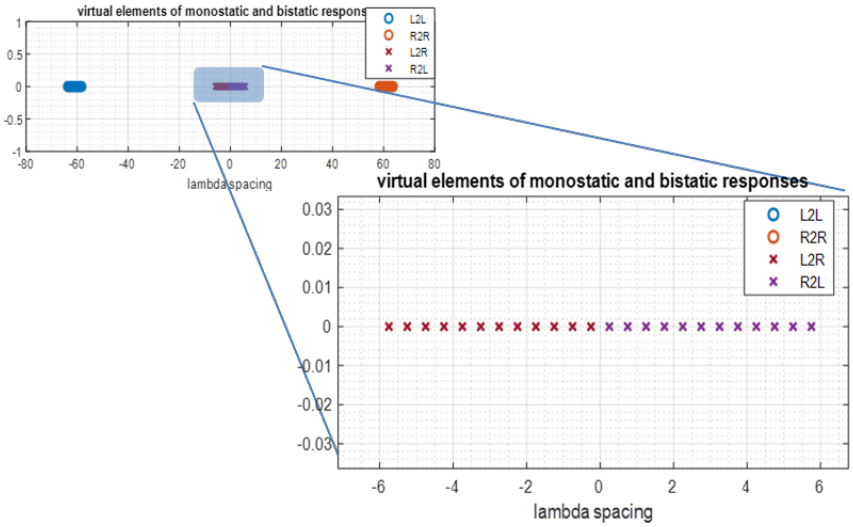

Figure 4.10: Virtual positions of mono-static and bi-static apertures formed by 2 sensors with 3Tx and 4Rx elements

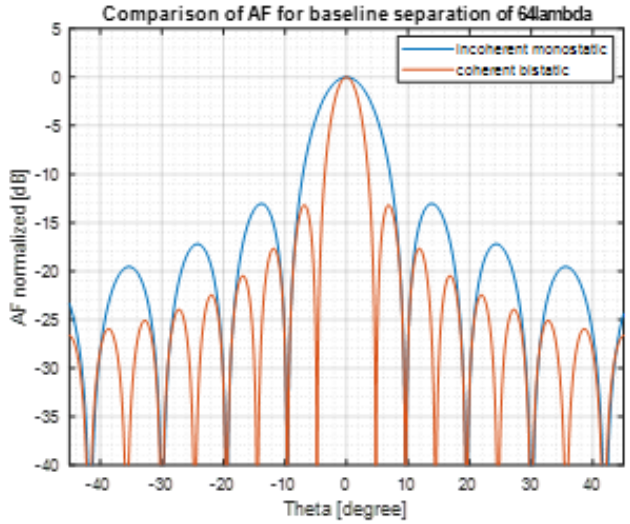

Figure 4.11: Comparison of AF for mono-static and bi-static responses for 64λ baseline

Algorithm 5 Fusion FOCUSS algorithm for incoherent combining of mono-static and coherent combining of bi-static responses (with noise)

1: Initialize $k = 0$; $\mathbf{W}_0 = \mathbf{I}$; $\delta_t = 10^{-8}$; $\delta_0 = 1$; λ = noise variance
2: Construct $\mathbf{y}_b$ and $\mathbf{A}_b$ from bi-static responses as in Eq 4.11
3: **while** $\delta_k > \delta_t$ **do**
4: $k = k + 1$
5: **for** $l = [1, 2, \ldots L]$ **do** ▷ Eg: l = 1,2 for $\mathbf{y}_1$, $\mathbf{y}_2$ and $l = 3$ for $\mathbf{y}_b$
6: $\mathbf{q}_{k,l} = \mathbf{A}_{k,l}^H \left(\mathbf{A}_{k,l} \mathbf{A}_{k,l}^H + \lambda \mathbf{I} \right)^{-1} \mathbf{y}_l$ Where $\mathbf{A}_{k,l} = \mathbf{A}_l \mathbf{W}_k$ with $\lambda \geq 0$
7: $\mathbf{x}_{k,l} = \mathbf{W}_{k-1} \mathbf{q}_{k,l}$
8: Calculate $\mathbf{W}_k \rightarrow \|\mathbf{v}_k\|_2$ for all $x_{k,l} (l = 1, \ldots, L)$ from Eq 3.3
9: Calculate $\mathbf{W}_k \rightarrow \mathbf{W_k} = diag\left(\|\mathbf{v}_k\|_p\right)$
10: $\delta_k = \frac{\|\mathbf{x}_k - \mathbf{x}_{k-1}\|_2}{\|\mathbf{x}_{k-1}\|_2}$

the responses (path length difference compensation problem). Fusion FOCUSS is same as Block FOCUSS except that the sub-apertures now have different number of spatial samples, the bi-static responses have twice the number of spatial samples as that of the mono-static responses. The concept in this remains the same as Block FOCUSS, a common grid of dictionary elements is defined for all the sub-apertures, the sensing matrices for each of them is defined which has same number of columns and the DOA estimation is performed by trying to minimise the l_p-norm of $\mathbf{x}$ as shown in Eq 3.8. There is however an extra step involved in this, which is the construction of the sensing matrix for the bi-static responses. If the assumption that the bi-static responses are coherent holds, as discussed in Section 4.4, then the system of equations for bi-static responses can be combined as

$$\begin{bmatrix} \mathbf{y}_3 \\ \mathbf{y}_4 \end{bmatrix} = \begin{bmatrix} \mathbf{A}_3 \\ \mathbf{A}_4 \end{bmatrix} [\mathbf{x}] + \mathbf{n} \tag{4.11}$$

$$\mathbf{y}_b = \mathbf{A}_b \mathbf{x} + \mathbf{n} \tag{4.12}$$

Eq 4.11, gives the system of equations for the bi-static responses that are coherent. A single measurement vector $\mathbf{y}_b$ is constructed by taking the spatial samples from the same Range-Doppler bin of both bi-static modes. A single sensing matrix $\mathbf{A}_b$ is obtained by stacking the two sensing matrices $\mathbf{A}_3$ and $\mathbf{A}_4$ which are given in Eq 2.19 and Eq 2.20. For a system with 2 sensors such as the one shown in Fig 2.1 there will be now 3 apertures in total instead of the 4 that was discussed in Section 3.2.2. The 2 apertures from the 2 mono-static responses which are considered to be mutually incoherent and the other aperture is the combined, coherently assumed, 2 bi-static responses. Thus now we have $L = 3$ instead of $L = 4$ which was the case for

Block FOCUSS algorithm where all the responses were treated to be mutually incoherent. After this step, the steps for Fusion FOCUSS are same as Block FOCUSS which is explained in detail in Algorithm 5. The dimension of the estimated vector $\mathbf{x}_l$ is same for each L even though the size of the measurement vector $\mathbf{y}_l$ and sensing matrix $\mathbf{A}_l$ are different as the same dictionary is used for all the apertures (refer to Algorithm 5).

4.5. Simulation

A simple simulation is performed to demonstrate the results obtained by using Coherent FOCUSS. Two targets placed at a range of 20 m from the radar and separated by 1° in DOA is considered. The frequency used is 78 GHz and the bandwidth is 250 MHz. A high SNR scenario of 30 dB is considered in this simulation. Two radar sensors separated by a baseline of 64λ is used where each sensor consists of 3 transmitters and 4 receivers forming 12 ULA. The theoretical resolution for a baseline separation of 64λ is shown to be $\sim 1.6°$ in Section 4.3. The simulation results of coherent processing is depicted in the Fig 4.12, the two targets are placed at 0° and −1° which is shown by the dotted lines in the plot. The dictionary spacing is 1° with scan angles from −45° to +45°. The output of the Coherent FOCUSS algorithm is shown along with the output of the Block FOCUSS and the BOMP algorithms for comparison. From the figure it is shown that Coherent FOCUSS is able to resolve the two closely spaced targets separated by 1°, whereas the Block FOCUSS and the BOMP fails to resolve the targets. The result from the Block FOCUSS and the BOMP is hard to distinguish in the plot as they have the same result. This shows that Coherent FOCUSS has better resolution capability than incoherent processing, which is inline with the theory explained in this chapter. To study and compare the performance of the algorithms, Monte Carlo runs are performed and parameters like probability of resolution, mean square error and probability of false alarms are calculated which is presented in Chapter 5.

Simple simulation is performed to evaluate the functionality of the Fusion FOCUSS and the results are depicted in Fig 4.13. Similar setup described above for coherent processing is used, but now the two targets are placed 2° apart, one at 1° and the other at −1° depicted by dotted lines. The sensors are designed with a receiver offset and are mirrored in orientation with respect to each other such that, the bi-static aperture is double than that of a single mono-static aperture as depicted in Fig 4.4. It is ensured that the RCS received by both the bi-static responses are same in this scenario. Thus, the bi-static responses are processed coherently, whereas the mono-static responses are processed incoherently. The Fusion FOCUSS is employed to perform this combined coherent and incoherent processing. It is shown in the Fig 4.13 that the Fusion FOCUSS is able to resolve the two targets separated by 2°, whereas the Block FOCUSS fails to do so. Block FOCUSS detects a single target at −1° and fails to detect the target at 1°. Thus, we get better resolution by processing the bi-static responses coherently as they form a virtual array with virtual aperture double than the mono-static response as explained in Section 4.4.

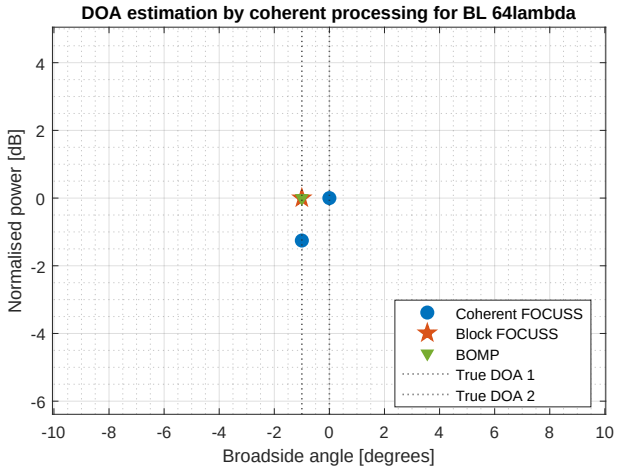

Figure 4.12: DOA estimation using coherent processing

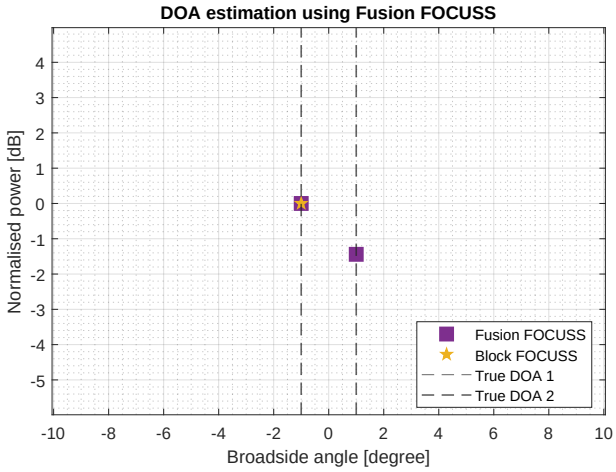

Figure 4.13: DOA estimation using Fusion processing of coherent and incoherent apertures

4.6. Conclusions

In this chapter, the necessary conditions to perform coherent processing of the data in order to estimate the DOA of targets is discussed. The condition is that the system consisting of multiple sensors should be fully coherent and the target present in the imaging scene must be isotropic. When this condition is met the coherent processing can be performed by ensuring the phase of the reflected signal from the target is same across both the sensors. But due to the path length difference of the target to the two sensors, the phase of the target as seen by the virtual apertures can vary. As we cannot determine the range of the target precisely due to range quantization errors, finding the phase difference caused by the path length difference of the wave is nearly impossible. In this chapter, a method to compensate for the phase difference due to the path length difference is provided by defining a new sensing matrix. This sensing matrix accounts for this phase difference by compensating for the difference in every possible DOA defined in the dictionary of the sensing matrix. Coherent FOCUSS algorithm is then performed using this new sensing matrix to estimate the DOA of targets. Coherent processing has a much better resolution than the incoherent processing, the gain in resolution is proportional to the baseline separation between the sensors. But this method is limited by the high side lobes that are produced with increase in the baseline. The high side lobes next to each other for low SNR cases will cause pointing errors. Also, due to the range quantization error it is impossible to exactly correct for the phase difference observed due to path length difference, which makes coherent processing of mono-static responses difficult. A new method of processing is introduced in order to avoid the high side lobes, which exploits the bi-static responses to be coherent and treats the mono-static responses as being mutually incoherent. By choosing the appropriate array design for the sensors, the bi-static responses can be designed to have double the aperture than the individual mono-static responses. Thus, it gives a factor of two improvement in angular resolution that can be achieved when compared to the single aperture case. But the theoretical resolution is still lower in Fusion FOCUSS when compared to coherent processing. The steps involved in the Fusion FOCUSS algorithm is discussed, which solves the coherent-incoherent combining of the bi-static and mono-static responses respectively. In simulation it is shown that, for a system with an effective aperture of 64λ, the Coherent FOCUSS algorithm can resolve two targets separated by $1°$, whereas Block FOCUSS and BOMP algorithm fails to do so as their effective aperture is 6λ (equivalent to that of the sub-system used). Simulation results also show that Fusion FOCUSS with the coherent bi-static aperture of 12λ (twice that of individual mono-static response) resolves two targets separated by $2°$, whereas Block FOCUSS fails to do so.

5

Performance analysis of DOA estimation

In this chapter, the performance analysis of the Block FOCUSS and the Coherent FOCUSS algorithms that are discussed in Chapter 3 and 4, are presented. Comparison of the proposed Block FOCUSS and Coherent FOCUSS algorithm is done alongside the BOMP algorithm using MATLAB software. Monte Carlo runs are performed to evaluate the performance parameters RMSE, probability of resolution and probability of false alarm for the proposed algorithms and the BOMP algorithm. The performance parameters for varying scenarios are studied. An experiment that is performed in the anechoic chamber to evaluate the performance of the Block FOCUSS algorithm is presented. Section 5.1 discusses the simulation parameters used in MATLAB to design the radar system. In Section 5.2 the simulation results obtained for various scenarios is analysed along with the effects of SNR. Section 5.3 explains the penalty incurred in performing coherent processing on a non-isotropic target. In Section 5.4 the drawback of using an on-grid algorithm when the target is not exactly on the grid is discussed and a possible solution to overcome this problem is presented. Section 5.5 presents the results obtained from performing an experiment to estimate the DOA of the targets in the lab of TU Delft by using trihedral reflectors as targets.

5.1. Simulation parameters

The system parameters used for the MATLAB simulation are given in Table 5.1. Two sub-systems are used where each sensor has 3 transmitters and 4 receivers uniformly spaced as shown in Fig 4.3 in each sensor. The overlapping FOV of the sensors is considered to be $-45°$ to $+45°$. Different baseline separation values are considered for the performance analysis as mentioned in the table. The parameters of the FMCW waveform used for the simulation is given in Table 5.2.

5.1.1. Performance evaluation parameters

In order to evaluate the performance of the algorithms, Monte Carlo runs are executed and the parameters RMSE, probability of resolution, probability of false alarm and average number of false alarms are considered. The algorithm outputs the possible detected target positions. A thresholding operation is performed where only the targets detected with the signal power greater than the defined threshold is considered as a valid target. For example if the algorithm outputs four possible targets and two of them have a normalised power level above -15 dB and two of them below -15 dB then only two targets are considered as valid detections.

Table 5.1: Parameters for the distributed system used in MATLAB simulations

Parameter	Value
Number of sub-systems (M)	2
Number of Tx in each sensor (N_{Tx})	3
Number of Rx in each sensor (N_{Rx})	4
Baseline values (BL)	$16\lambda, 128\lambda$
Joint Field of View	$-45°$ to $45°$
System coherency	Fully coherent

Table 5.2: Parameters for the FMCW waveform used in MATLAB simulations

Parameter	Value
Center frequency (f_c)	78 GHz
Bandwidth (BW)	250 MHz
Number of chirps	256
Number of samples per chirp	256
Acquisition time	25.6 μs
Settle time	5 μs
Reset time	5 μs

Table 5.3: Parameters for MATLAB simulations and algorithm parameters

Parameter	Value
Number of experiments in each Monte Carlo trial (N_{mc})	500
Detection Window (DTW)	$[-3°, +3°]$ around the ground truth
Detection threshold	-15 dB
Dictionary used for sensing matrix	$-45°$ to $45°$ with $1°$ spacing

Going forward only the targets detected after the thresholding operation are considered. The thresholding level used in this thesis for the simulation is -15 dB unless mentioned otherwise, this is the chosen value as most of the runs use SNR of 15 dB and higher except for in Section 5.2.3 when appropriate value is chosen based on SNR. A detection window (DTW) of $-3°$ to $+3°$ is defined around the ground truth of the target for each Monte Carlo run, this is the value chosen based on the state of the art comparison [5]. If the estimated value from the output of the algorithm falls in the DTW then the target is said to be detected and the closest of all such declarations is considered as the detected target. If multiple detections are found in a given DTW then only the closest detection to the ground truth is treated as actual target and the rest of them will be added to the list of false alarms (along with other false alarms that might be found outside DTW). If no targets are detected in the DTW then the target is considered as not detected and the resolution capability of the algorithm for such a scenario is 0 as the algorithm fails to detect the target. The simulation parameters used for the Monte Carlo runs and the algorithm parameters used are given in Table 5.3. A single Monte Carlo run or trial consists of multiple experiments where each experiment has different realisation of noise and phases of the targets simulated. Hence all the performance parameters are calculated for each run or trial which consists of N_{mc} experiments in each run. The description of these parameters are given below

1. **Root Mean Square Error (RMSE)**: The root mean square error determines the error in the DOA estimation of the target. It is obtained by taking the square root of the mean of the square of error between the ground truth of the target and the detected target by the algorithm. Mathematically it is given as depicted below. Here x is the ground truth of the target and $\hat{x}$ is the estimated position of the target found within the DTW defined for each run. The equation below is given for a Monte Carlo run with N_{mc} experiments in each trial where the number of times the target is detected in the DTW for a given Monte Carlo run is given by N_d. If the target is not detected in the DTW then the RMSE is not calculated for that experiment.

$$\text{RMSE} = \sqrt{\frac{1}{N_d}\sum_{i=1}^{N_d}(x_i - \hat{x}_i)^2}$$

2. **Probability of Resolution (PR)**: The probability of resolution is defined as the ratio of number of times the target is detected in the DTW defined to the total experiments in a Monte Carlo run. It is given as

$$\text{PR} = \frac{\text{Number of times } \textit{all} \text{ the targets are detected in DTW}}{\text{Total number of experiments in a Monte Carlo run}}$$

PR is thus a number between 0 and 1, it is 1 if all the targets are detected in all the experiments in the trial and 0 if none of the targets are detected even in one single experiment. For example, if we run 500 experiments in a Monte Carlo trial and 400 times all the targets are detected, then PR for this example would be 400/500, which is 0.8. Higher the PR, better is the algorithm performance.

3. **Average number of False alarms (Avg FA)**: The average false alarm is defined as the average number of detections found in the entire FOV minus the number of detected targets. Along with the PFA this gives an idea on the average number of undesired targets that are detected. This can be mathematically expressed as

$$\mathrm{FA}_{\mathrm{Avg}} = \frac{1}{N_{mc}} \sum_{i=1}^{N_{mc}} (D_i - K)$$

In the above equation D is the total detections found in the FOV for each experiment and K is the actual number of targets detected within the DTW. If there is more than one target that is detected in the DTW, then one of them is considered as an actual target and the other as a false alarm. The equation is given for a Monte Carlo trial with N_{mc} experiments. Average FA can be any number greater than 0. Lower this number, better is the algorithm performance. If we see a lot of false targets being detected then the Average FA will increase significantly and that is not desirable.

4. **Probability of False alarm (PFA)**: The probability of false alarm is defined as the ratio of the number of times more than the actual number of targets are detected in the total FOV to the total experiments in a Monte Carlo run. It is given as

$$\mathrm{PFA} = \frac{\text{Number of times more than actual targets are detected in an experiment}}{\text{Total number of experiments in a Monte Carlo run}}$$

PFA is thus a number between 0 and 1, it is 1 if always more targets are detected than the actual number of targets in the experiment and 0 if the number of detections always match the actual number of targets present. For example, if we have two targets in the imaging scene where we run 500 experiments in a Monte Carlo trial and 400 times two targets are detected and the remaining 100 times more than two targets are detected in the FOV, then PFA for this example would be 100/500, which is 0.2. Lower the PFA, better is the algorithm performance.

5.2. DOA simulations

In this section, the results obtained by MATLAB simulations are presented. Monte Carlo runs are executed for different target positions, baseline and SNR values. The performance evaluation parameters discussed in the previous section for each scenario are presented. We use two targets in all the simulations and the phase of each target RCS is chosen to be random in each experiment as given in the signal model in Chapter 2 Eq 2.10. The SNR value mentioned is the SNR that is achieved after the Range-Doppler processing is performed.

5.2.1. Spatial diversity gain with distributed radar setup

This section explains the gain obtained by having distributed sensors to perform the DOA estimation over a single sensor. A simple simulation is performed to understand how the phase difference between the targets effect the resolution capability of closely placed targets. This will also help us understand the results in further sections. For this simulation a single sensor is considered which constitutes of 3 Transmitter and 4 Receivers placed at the center i.e., instead of two sensors separated by a baseline, we replace it with single sensor at the center of this system. Two point targets are considered, phase of one target is kept constant at zero and the phase of the second target is varied from zero to 2π radians. Hence the phase difference between the two targets is equal to the phase of the second target. To measure the resolution capability we record the probability of resolution for this simulation. The SNR used is greater than 30 dB and hence it can be considered as a noiseless case, this is done to ensure that the resolution capability is not effected due to the presence of noise. The two targets are separated by a difference of 2° in the broadside. Fig 5.1 shows the resolution capability of the FOCUSS algorithm (note that it is the existent FOCUSS algorithm and not the new one introduced in this thesis) with single sensor for 2 closely placed targets whose phase is varying. It is shown that when the phase difference between the 2 targets that are closely placed is almost the same (closer to 0 or 2π) the sensor is unable to resolve them as two separate targets, this is because the received signal from the 2 targets are highly correlated as the RCS seen is similar for 2 targets in this region of 0.23π radians. Note that this is mainly seen in targets that are very closely spaced as we are within the beam width of the AF for a given sensor (For this case the Half Power Beam Width (HPBW) is $\sim 8.5^\circ$).

In this case we have considered the sensor present at the center. When the sensors are distributed like in the distributed system that we consider in the thesis, there is an additional phase term that gets added to the target phase which is due to the path length difference that is present between the target and the 2 sensors.

Based on how this phase gets added to the original phase of the target we will see a phase difference between the targets in each sensor which is a combination of these 2 phases. In such scenarios we can gain from the spatial diversity by combining the data from the 2 sensors as we do in the Block FOCUSS algorithm. Consider a scenario where the combined phase difference of path length travelled and the target RCS adds up in a way that the phase difference between the 2 targets as seen by sensor 1 is closer to zero and the phase difference between the 2 targets seen by sensor 2 is not closer to 0 or 2π. In this case the sensor 1 will not be able to resolve the 2 targets, where as the sensor 2 will successfully resolve the 2 targets, thus the combined result of both the sensors will help us resolve the 2 targets. This effect is validated with experimental results as well (Section 5.5 Fig 5.18). A second simulation is performed to visualise this, where 2 sensors M1 and M2 are considered. The resolution capability of having just M1 or M2 is shown in Fig 5.2 represented by dotted lines. In this we make sure that M1 and M2 sensors both see the two targets at different phase difference. M1 is able to resolve the 2 targets when M2 fails and vice versa, the combined resolution capability is the best of both and hence always resolves the 2 targets. This is the spatial diversity gain that is achieved by combination of data from multiple sensors using block sparse method.

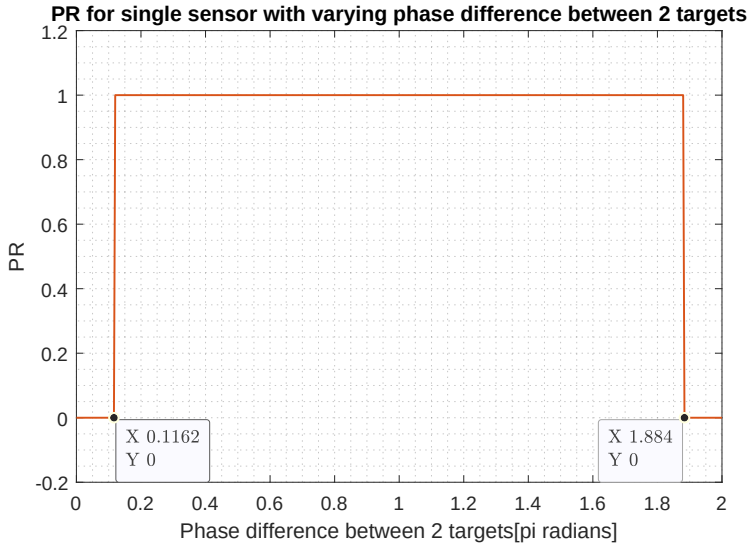

Figure 5.1: PR for single sensor with phase difference between the 2 closely placed targets

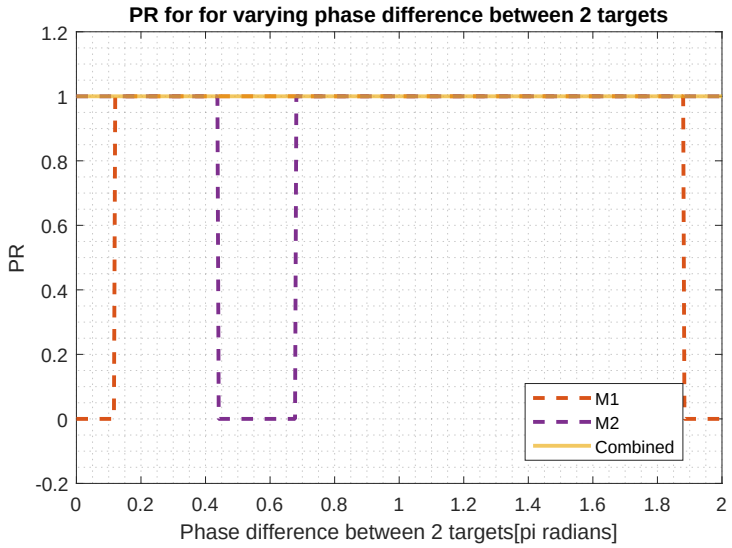

Figure 5.2: PR for 2 individual sensors and the combined PR

5.2.2. Comparison of algorithms

The simulation results are provided for the algorithms Block FOCUSS and Coherent FOCUSS that are discussed in Chapter 3 and Chapter 4. Also the performance of the BOMP algorithm is presented for comparison with the proposed algorithms. BOMP is chosen as the comparison algorithm as it is also a CS algorithm that combines the data in a block sparse manner and is the current state of art chosen in the thesis, which fuses the data from multiple sensors.

In these simulations, the targets are placed at a range of 20m in the y co-ordinates from the system and the x co-ordinates are changed according to the desired DOA separation needed as per system defined in Fig 5.13. The DOA separation in these simulations is varied from zero degree to 14° in steps of 1°, for zero degree separation we expect to see a single target and verify the same. The range of the target is chosen such that the target is closer to the center of the range bin as we do not have infinite range resolution for the chosen bandwidth, if it is not placed appropriately then we see some undesirable results in the coherent processing of the results which is discussed in Section 5.3. By placing it appropriately in range the problem from compensating the path length difference is reduced. In these simulations the complete radar processing chain is simulated and it is not a generation of snapshot directly. Some of the main steps involved in these simulations are the chirp generation, reflection to the target, dechirped signal from the target reflection, range and Doppler processing for each virtual channel, extraction of the snapshot and then the DOA estimation is performed using these extracted snapshots. In this simulations setup if the target is non-isotropic or the phase of the signal observed by different sensors are not the same then there will be errors when performing coherent processing, which is discussed in Section 5.3. The simulation results from Monte Carlo runs for different SNR values (30 dB, 20 dB and 15 dB) are provided for a distributed system with baseline (BL) values of 16λ and 128λ. Note that a fully coherent system is considered for simulation, hence 2 mono-static responses and 2 bi-static responses are used for DOA estimation in these runs.

Also for the given system and sub-system used for simulation, we can theoretically find the expected

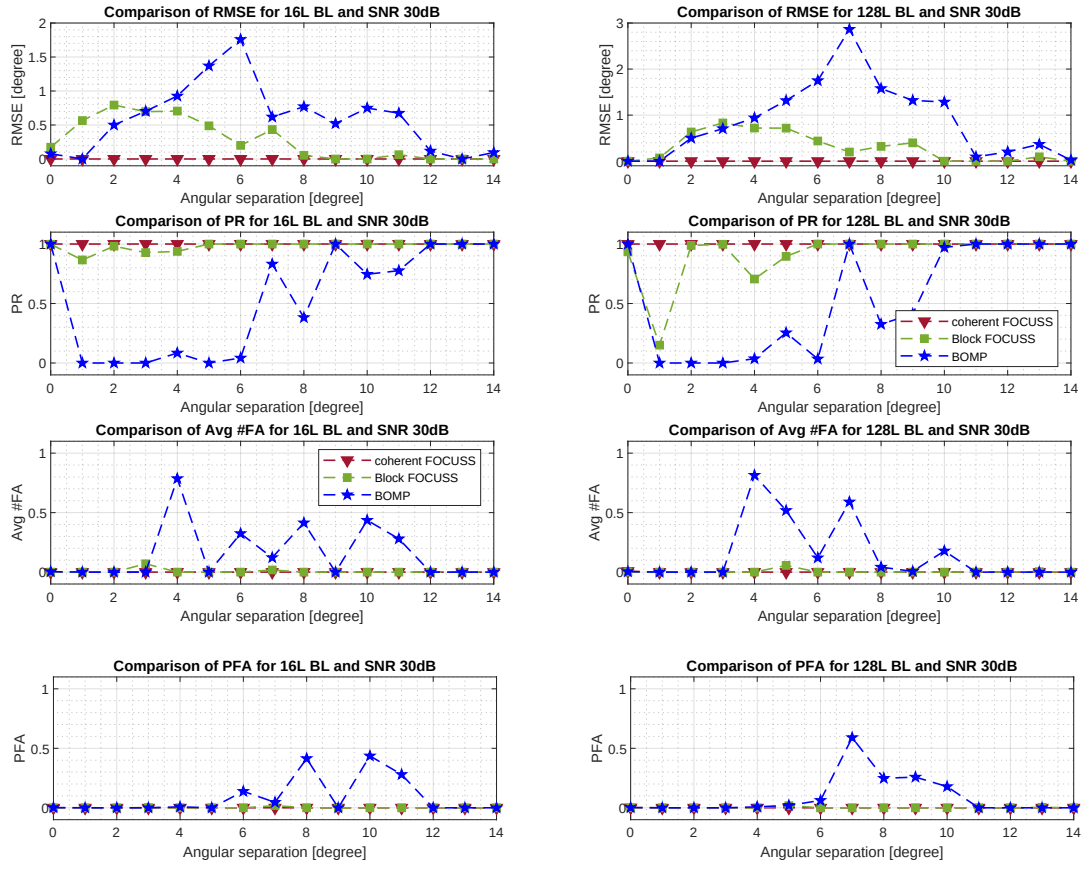

(a) 16λ BL (b) 128λ BL

Figure 5.3: Results from Monte Carlo simulations for a baseline separation of 16λ and 128λ for SNR of 30 dB for a target at 20m

resolution capability based on the aperture of the sensors. The azimuth resolution is inversely proportional to the aperture of the sensors used. For an array with 3 Transmitter and 4 Receivers separated by a distance of $\lambda/2$ in the virtual array has main lobe width of ~ 8.5° in the AF. This is the resolution that can be obtained by the beam forming method, but the algorithms used here have super high resolution capability as discussed in previous chapters, thus we should see a resolution that is less than this value. For coherent processing as the aperture is equivalent to the baseline used, we should be able to achieve a very high theoretical resolution of ~ 0.9° for the baseline of 128λ, but this is limited by the dictionary spacing that can be used as the AF has very high side lobes for a large baseline separation of sensors and hence a finer dictionary will lead to errors as discussed in Section 4.3. Thus we can expect a resolution capability closer to 1° for coherent processing as the dictionary spacing used for the simulations is 1° as given in Table 5.3.

From the Fig 5.3, Fig 5.4 and Fig 5.5 it can be observed that Coherent FOCUSS performs the best of the 3 algorithms for both the baselines. Block FOCUSS performs better than BOMP in incoherent combining of the data for all the cases. A SNR of 30 dB is an idealistic case and can be considered close to noiseless case, thus the performance of the algorithms are discussed first without the dominant effect of noise. It is shown in Fig 5.3 the performance of the algorithms Coherent FOCUSS and Block FOCUSS for this case is also very idealistic with PR close to 1 for all the DOA separations and PFA is close to zero. But the BOMP algorithm fails to resolve the targets that are separated by less than 6° for this SNR value. In Fig 5.4 and Fig 5.5, for Coherent FOCUSS algorithm the probability of resolution is greater than 80 percent for SNR of 20 dB and 15 dB for all DOA separations with PFA also being below 30 percent, which is desirable. The PR achieved by Block FOCUSS algorithm is better than BOMP algorithm for all the cases. Block FOCUSS provides a resolution capability of 5° with PR greater than 80 percent for DOA separations of 5° and above with a PFA below an acceptable value for most cases. It is seen that as the SNR value reduces the PFA increase, which is not desirable. The effect of SNR on the variation of parameters is studied in detail in Section 5.2.3. Also for the BOMP algorithm the information is a prioiri made available that there are a maximum of 3 targets in the imaging scene to ensure the algorithm stops at the right stage as it is a greedy algorithm and it suffers from more errors if this is not specified. This upper bounds the number of FA's to 3 for BOMP algorithm. By specifying the right threshold

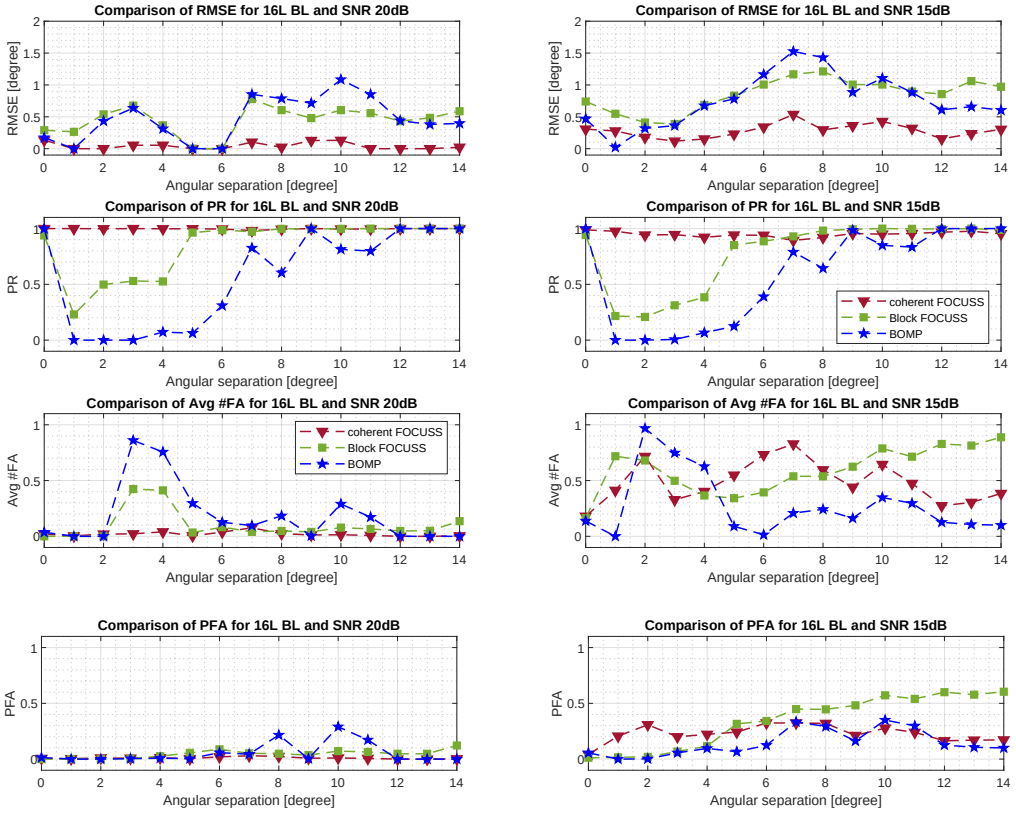

(a) SNR 20 dB (b) SNR 15 dB

Figure 5.4: Results from Monte Carlo simulations for a baseline separation of 16λ and SNR values of 20 dB and 15 dB for a target at 20m

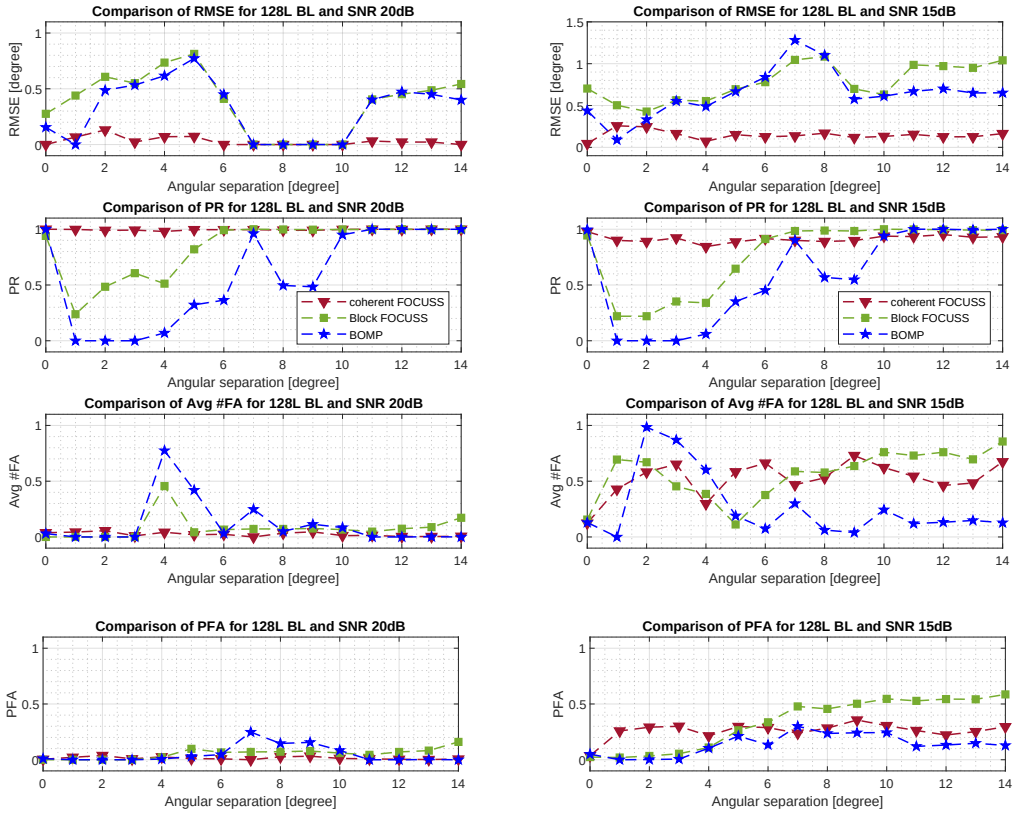

(a) SNR 20 dB (b) SNR 15 dB

Figure 5.5: Results from Monte Carlo simulations for a baseline separation of 128λ and SNR values of 20 dB and 15 dB for a target at 20m

to stop the algorithm this a-prioiri information can be removed, but there was no enough time to sort this out in the scope of the thesis. Thus we see that the average FA does not increase as in the case of Block FOCUSS for lower SNR values. If the a priori information is not given to the BOMP algorithm then the BOMP will also suffer from high false alarms for lower SNR values. The performance of Block FOCUSS is seen to be better as compared to BOMP, this is in accordance with the literature and theory that is studied in Section 3.3. Even though both BOMP and Block FOCUSS perform incoherent combining of the data thus having the same theoretical resolution capability, Block FOCUSS outperforms BOMP. BOMP is a greedy algorithm and is seen to converge faster and might lead to errors, FOCUSS is not a greedy algorithm and tries to find the most optimal solution.

5.2.3. Evaluation for different SNR

To study the performance of the proposed algorithms for variations in SNR a simulation study is performed. In this scenario the baseline used is 128 λ and 2 targets with varying phase difference are simulated as discussed in Section 5.2. The SNR is varied from 1 dB to 30 dB for target DOA separations of 2°. A Monte Carlo run is performed with 500 experiments for each SNR value for different realisations of noise and varying target phase. The performance parameters RMSE, PR, PFA and average FA are plotted against varying SNR values for Block FOCUSS, BOMP and Coherent FOCUSS for the different DOA separations considered.

From Fig 5.6, it is noted that the RMSE of Coherent FOCUSS reduces as SNR increases and also the PFA and Average FA reduces significantly with increase in SNR for Coherent FOCUSS. As the targets considered here are on grid with a dictionary of 1° spacing, if SNR is sufficiently large the RMSE will go to zero. But when the targets are off-grid there will be some error due to quantization of the target to the closest grid. In this case the maximum error will be half of the dictionary spacing used for a uniformly distributed targets in the dictionary bin for large SNR values. The RMSE of Block FOCUSS however slightly increases with increase in SNR, this is because of the increase in PR. If we see the PR for Block FOCUSS it is above 50% after SNR of 22 dB and this is when there is an increase in the RMSE curve as well. For lower PR as the 2 targets are not resolved we do not have enough measurements to get a true estimate of the RMSE, higher the number of measurements closer

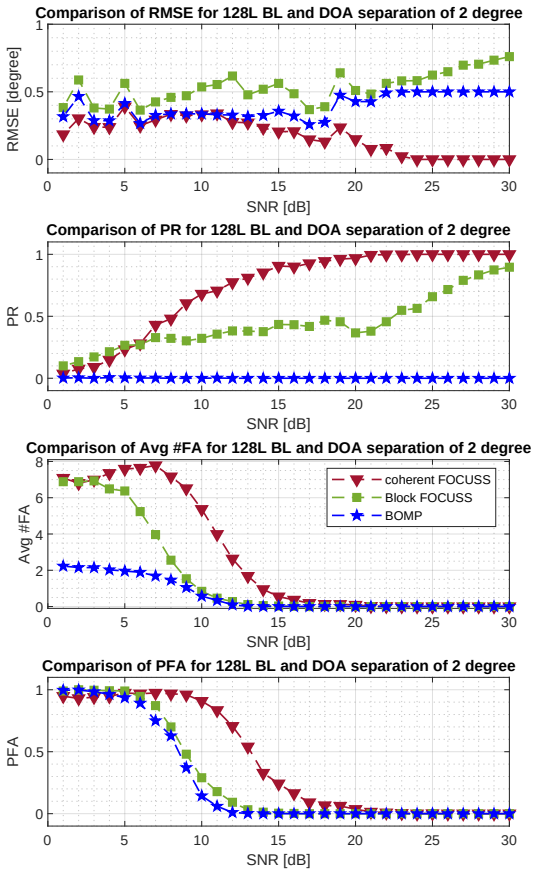

Figure 5.6: Results from Monte Carlo simulations for a baseline separation of 128λ and varying SNR for a target at 20m

is the RMSE to the true value (ideally N_{mc} should be closer to infinity but this is practically not feasible). Also as the two targets are starting to resolve, they bias the estimation of the other target and thus an observed increase in RMSE. Note that BOMP algorithm fails to resolve the two targets at 2° separations, thus the RMSE plot depicts the RMSE observed for a single target from the expected ground truth. Also would like to remind the reader again that BOMP has been provided with a-priori information that maximum number of targets are 3 and thus the average number of FA is less even though PFA is high. For Block FOCUSS the PFA and average number of false alarms is significantly reduced for SNR values greater than 10 dB. But Coherent FOCUSS suffers from higher false alarms for lower SNR values. The number of false alarms is reduced for SNR values above 15 dB for coherent processing where as it is reduced above 10 dB for Block FOCUSS, this indicates that coherent processing suffers from more false alarms at lower SNR values. This is in accordance with the AF study performed in Section 4.3, where it is shown that for a baseline separation of 128λ the side lobe levels are very high and thus for lower SNR values it can easily lead to false alarms as one of the side lobes can get detected as a possible target.

5.3. Coherent processing of non-isotropic targets

In Chapter 4, the conditions and methods to perform coherent processing are discussed. To recall: the targets and the system should be completely coherent in order to perform coherent processing. Ensuring system coherency has been discussed in literature [20] and is something that can be verified as well, but ensuring the targets are perceived in an isotropic manner by the entire distributed system is difficult. Even if the target is isotropic, there will be a phase difference that occurs due to the path length difference and it is hard to compensate as we cannot estimate the range of the target precisely as discussed in Section 4.1.3. Hence it will be interesting to see what happens when the phase due to path length difference is wrongly compensated or the target itself is non-isotropic.

In this section, through simulation the errors observed in processing a non-isotropic target coherently are presented. For this a single target is considered at bore sight (to ensure it has the same path length) which

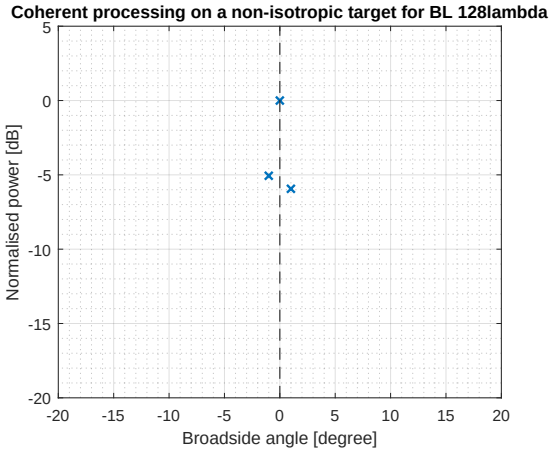

Figure 5.7: Coherent processing on a non-isotropic target at 0 degree for a baseline of 128 λ

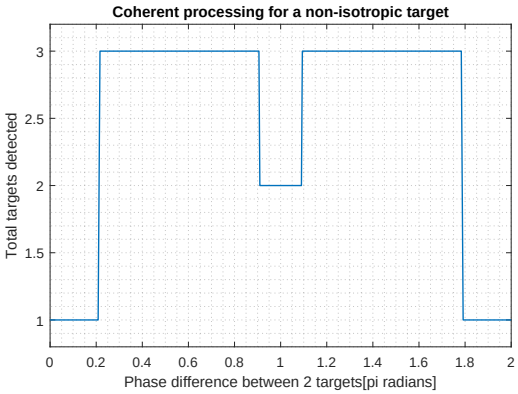

Figure 5.8: Coherent processing on a non-isotropic target for a baseline of 128 λ

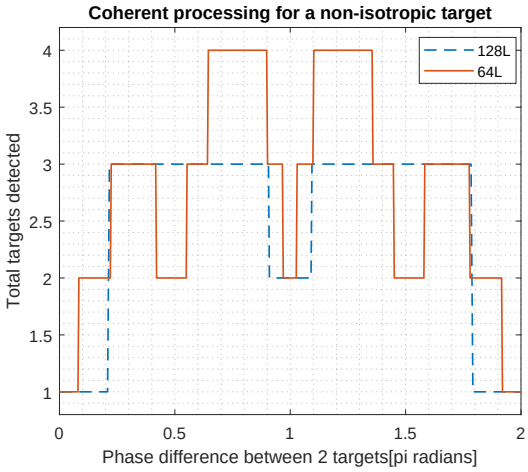

Figure 5.9: Coherent processing on a non-isotropic target for a baseline of 64 λ

is observed by 2 sensors separated by a baseline of 128λ. A high SNR value greater than 30 dB is considered in order to eliminate the effect of noise on the result. The phase of the single target as seen by sensor M1 is fixed at a certain value and the phase observed by sensor M2 for the same target is varied such that the phase difference between responses seen at M1 and M2 is varied from 0 to 2π radians. The consequence of doing the coherent processing on a target that is non-isotropic is an increase in the number of false alarms, i.e., more unwanted targets are observed in the result from running the Coherent FOCUSS algorithm and

it becomes very difficult to detect the true target as the false alarms are very close to the true target, this is depicted in Fig 5.7 for one of the scenarios where the dashed lines represents the ground truth. When we look at the number of targets detected, by varying the phase difference between the targets from 0 to 2π it is seen from Fig 5.8 that up to a certain phase difference between the targets the Coherent FOCUSS performs well.

The number of expected targets is 1 as we have a single target in the scene, but as the phase difference of this single target as seen by the 2 sensors increases the number of targets detected also increases, which leads to false alarms. The phase difference up to which the coherent processing performs as expected is coupled to the virtual aperture size of the system configuration, and it changes for different configurations. Fig 5.8 only shows this for a baseline of 128λ but this can vary for different baseline. Fig 5.9 shows the variation of number of targets detected for a baseline of 64λ in comparison with 128λ baseline.

5.4. Solution to the problem of off-grid targets

The compressive sensing algorithms that are used in this thesis are grid based algorithms, which means a pre defined grid is used and a search for the target is made on these grid points. The grid based algorithms are known to suffer from off-grid problems, that is when a target is not located exactly on the defined grid then there will be an error in the estimation of the DOA of target [13]. In this section the problem of off-grid target

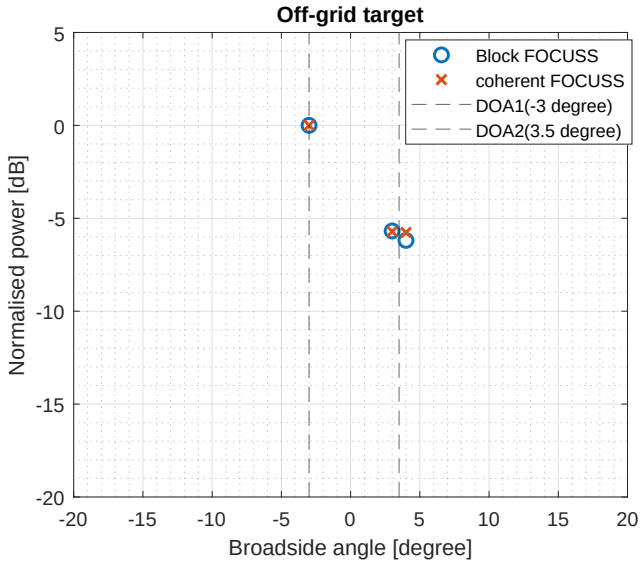

Figure 5.10: Off-grid target present at 3.5° for a dictionary with 1° spacing

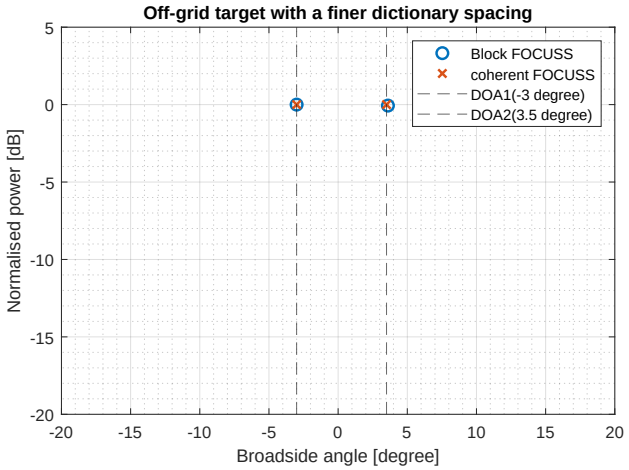

Figure 5.11: Off-grid target present at 3.5° for a dictionary with refined spacing around targets

is explained and a solution is proposed to overcome this problem. When a target is not present on the grid, we see two kinds of errors, one where the target gets detected on the nearest grid point to the target and thus shows up as an error in the estimation of DOA. The second type of error can occur where the energy is spread out into two adjacent grid points and thus we see more than one target. The scenario where we see 2 targets instead of one single target is depicted in Fig 5.10, where a dictionary spacing of 1° is used and the adjacent grids are at 3° and 4° for a target which is present at 3.5°, one single target shows up on 2 adjacent grid points in this case and leads to false detections.

One of the solution that can be implemented to solve this off-grid problem is to follow a 2 step process in the estimation of the DOA of targets as explained in [50]. In the first step we have a coarse dictionary spacing in order to satisfy the coherency condition of the sensing matrix as discussed in Appendix A. Once the targets are detected, the algorithm is called again to re-estimate the DOA of the targets by defining a finer grid only around the region where the target is detected. In the example Fig 5.10 there are 3 targets being detected, one at $-3°$ and the other two at 3° and 4°. Thus, we refine the dictionary around $-3°$, $+3°$ and $+4°$ to be finer, say in steps of 0.1° as compared to previously defined 1° spacing. After estimating the DOA of the target with this new dictionary, the results obtained are depicted in Fig 5.11. Once we are sure that a target is present in that region, by refining the grid and looking at the region where the target is detected gives in a zoom in effect of looking at the target positions. If there are 2 targets present within the dictionary spacing considered then it is a different problem which depends on the resolution capability of the system and the algorithm and this is not discussed here.

The drawback of this method is the added computational effort (hence reducing the efficiency), thus it might not be the best method to solve this problem. The off-grid compresseive sensing techniques like Atomic norm might be worthwhile to explore and to consider in the future works [13].

5.5. Experimental evaluation

An experiment was conducted in the anechoic chamber of TU Delft to validate the Block FOCUSS algorithm proposed in this thesis. The system coherency could not be achieved in the time frame of the thesis and thus only Block FOCUSS could be validated. Block FOCUSS as discussed in previous chapters is an incoherent method of fusing the data from multiple sensors. A radar module based upon the NXP TEF810X car radar transceiver is used to transmit and receive the reflected signal back from the target [51]. Two trihedral reflectors mounted on a bar were used as the targets. The experimental setup and the results are explained in detail in the remaining of this section.

5.5.1. Experiment setup

- **Radar setup**

  A radar module based upon the NXP TEF810X car radar transceiver is placed at one end of the room. The TEF810X is a fully integrated single-chip RFCMOS 77 GHz automotive FMCW radar transceiver [51]. This device is intended for usage in short, medium and long range radar applications covering the full automotive radar frequency band from 76 GHz to 81 GHz. The TEF810X radar transceiver is a low

Table 5.4: Radar configuration used for experimental evaluation

Parameter	Value
Center frequency	78.8 GHz
Decimation Rate	1
Bandwidth	1.01 GHz
Acquisition time	23.8 μs
Dwell Time	1 μs
Reset time	5 μs
Number of samples per chirp	512
Sampling frequency	40 MHz
Number of chirps	128
Number of Rx	4
Number of Tx	3
FrameRate	400

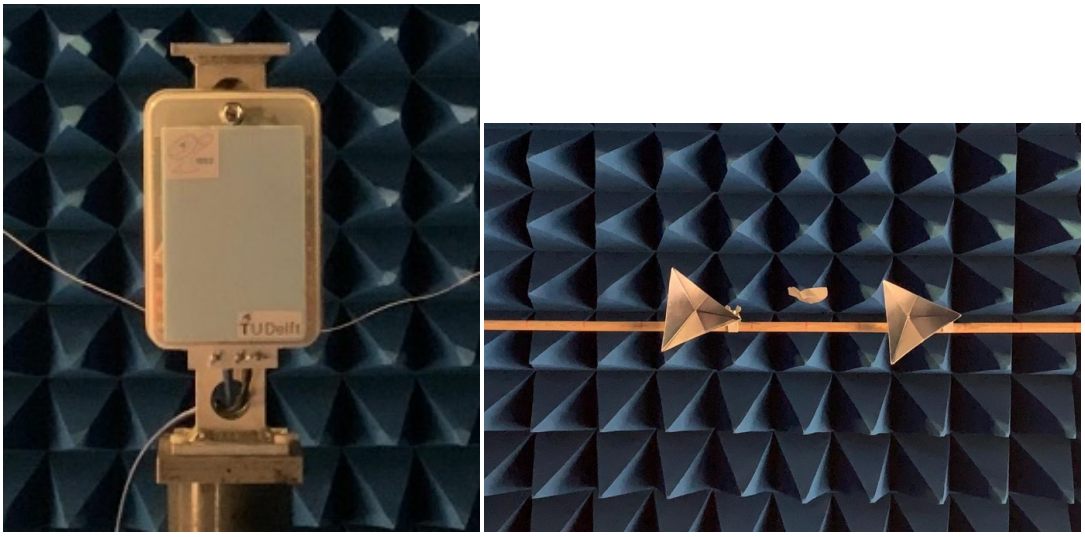

Figure 5.12: Hardware setup in the anechoic chamber. Top: NXP Dolphin radar. Bottom: Two trihedral reflectors used as targets

power radar transceiver which integrates 3 transmitters, 4 receivers, Analog-to-digital converters and low phase noise Voltage Controlled Oscillator (VCO). More details about this radar unit can be found online on the NXP website [51]. The radar is mounted on a motor controlled column at one end of the room. The software controlled motor column is equipped for precise movement of the radar in the x and y direction in steps of 1 millimetre. Thus the radar unit could be precisely positioned at the desired location in the x-direction, this is done in order to capture the data from different positions, to mimic the distributed radar setup. As the targets are stationary this mimics an incoherent distributed setup with a baseline that is controlled by the precise positioning of the radar using the motor control provided in the lab. The maximum baseline achievable using this setup is used for the experiments which is 0.396 m. Once the target positions were fixed, the radar sensor is moved to the extreme ends of this baseline and a measurement is recorded for each end. Thus recreating a scenario with 2 incoherent sensors separated by a baseline of 0.396m($\sim 104\lambda$). Hence, scenarios with distributed radar with baseline up to 104λ can be mimicked. An image of the column mounted with the NXP radar is shown in Fig 5.12. The configurations used on this sensor to perform the experiment is given in Table 5.4. Going forward the radar sensor placed at left side is referred to as the left sensor or M1 and when it is placed at the right side is referred as the right sensor or M2, but it is the same sensor that is being moved.

- **Target setup**

  Two trihedral reflectors were used as targets for this experiment. The image of these reflectors mounted on a stick is shown in Fig 5.12. The trihedral reflector used has an edge length of 8.5 cm. The RCS of the trihedral reflector is calculated using the below equation

$$\text{RCS} = \frac{4\pi a^4}{3\lambda^2}$$

$$\text{RCS}_{\text{dB}} = 10\log_{10}(\text{RCS})$$

  a is the edge length of the trihedral reflector. Substituting the values in the above equation, the RCS of the trihedral reflector used is obtained as 11.8 dB. The targets are placed at the other end of the room such that the distance between the center of the distributed sensor and the target is 4.5 m. The targets are moved along the x co-ordinates with the same y co-ordinates based on the desired DOA separation. This is depicted in the Fig 5.13 with M1 and M2 showing the 2 sensor positions separated by a baseline, R_y is the range of the target in the y-axis which is 4.5 m in this setup. The two targets are placed such that the R_y for both the targets is same. Using basic geometry the position of the target in the x-axis can be calculated for the desired angle θ. To achieve a certain DOA separation between the targets, θ_1 and θ_2 are chosen appropriately and the corresponding R_{x1} and R_{x2} are calculated for the given R_y. The baseline separation between the left and right sensor used here is 0.396 m ($\sim 104\lambda$) for the first part of the experiment, later the baseline is varied to study the effects of varying baseline. For the given

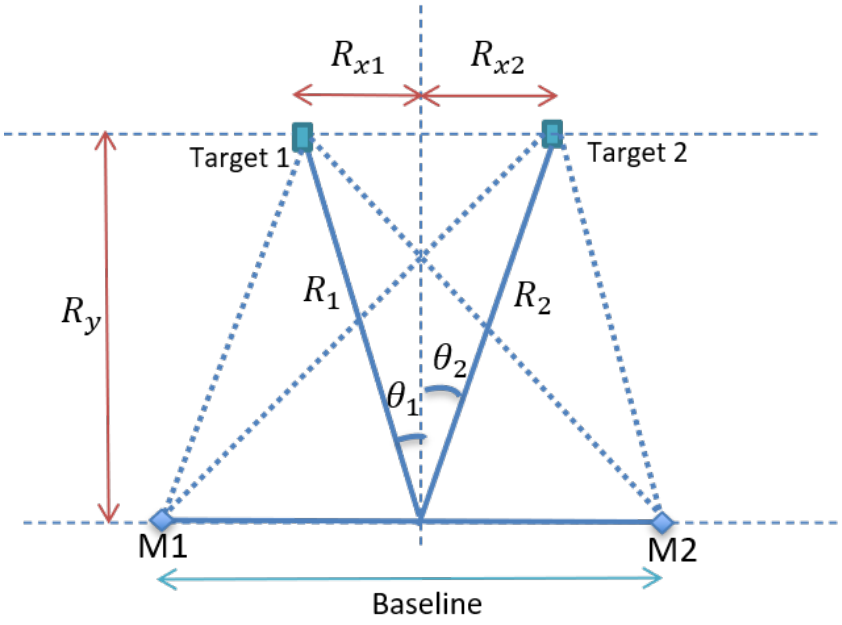

Figure 5.13: Depiction of target setup in the anechoic chamber

Table 5.5: Parameters used for B-FOCUSS algorithm for experimental evaluation

Parameter	Value
Regularization parameter (λ)	Closer to Noise variance ($\sim 10^{-3}$)
Detection threshold	-15 dB
Dictionary used for sensing matrix	$-40°$ to $+40°$ with $0.5°$ spacing

baseline and the wavelength the target is in the near field region of the distributed system as discussed in Section 2.1.1.

5.5.2. Processing of the data

The data captured from the sensor is saved in the form of a radar data cube. Range processing is performed by taking FFT along the fast time samples and Doppler processing is performed by taking FFT along the slow time dimension as explained in Section 2.3.1. It is verified that the highest energy is present at the range bin that matches the distance of where the target is placed, and Doppler bin matches the zero velocity. The snapshot consisting of the spatial samples are extracted from the Range Doppler bin with the highest energy, this is the bin where the targets are present. This is done for both the sensors, left and right sensor. Once we have the spatial samples we can process the 24 samples (12 samples for each sensor consisting of 3 transmitters and 4 receivers) in order to estimate the direction of arrival (DOA) of the two targets using compressive sensing algorithm discussed in section 3.2.2. In this experiment we use Block FOCUSS in order to estimate the DOA of two targets as the distributed system used is not synchronized, additionally the targets are present in the near field and can have different RCS as seen from the left and the right sensor positions. Hence the coherency is lost and coherent processing cannot be performed. Thus, Block FOCUSS is used which does not require the coherency in system or targets to perform DOA estimation of targets in the imaging scene. BOMP algorithm is also applied in order to compare the performance of the two algorithms. The parameters used for the Block FOCUSS algorithm is given in Table 5.5. The SNR value observed after Range-Doppler processing for the experiments is in the range of 15 dBm to 20 dBm for both the sensor positions.

5.5.3. Analysis of results

- **DOA estimation of Single target**

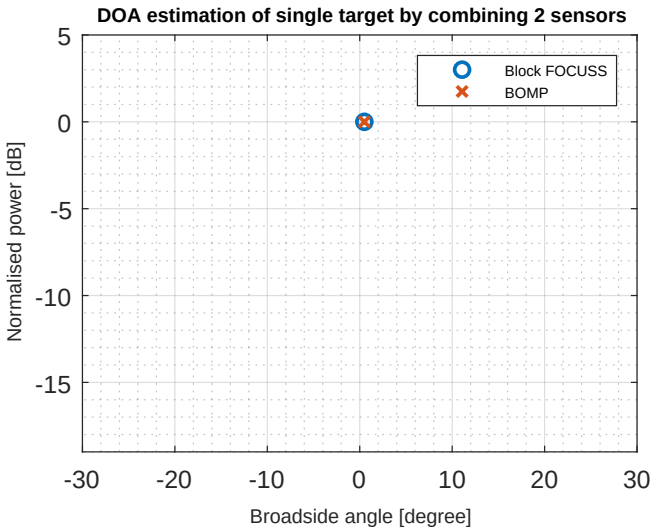

Figure 5.14: DOA estimation of single target placed at the center of the distributed system

At first a single target is placed at a distance of 4.5 m from the center of the two sub-systems. This is done in order to mark the zero degree and to estimate the error in DOA for a single target. Fig 5.14 shows the estimated target DOA by using Block FOCUSS. It is seen that the target is estimated with an error of 0.5°. This is because the target is not precisely at zero degree and the estimated DOA is mapped to one of the nearest grid points. As the defined dictionary spacing is 0.5°, the target is mapped to the nearest grid point from where it is present which is 0.5° in this case.

This position is marked as zero degree in the setup and the targets are placed along the same x axis where this target is placed as shown in Fig 5.12. Experiments are performed for two targets separated by a certain distance in the x axis such that the DOA of the targets from the center of the distributed system is varied in steps of 1°, from 2° up to 11° by moving the targets along the x axis as explained using Fig 5.13.

- **DOA estimation of two targets**

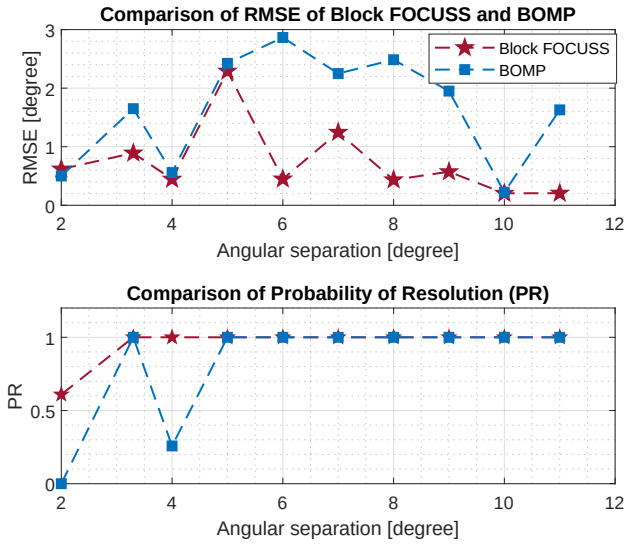

Figure 5.15: RMSE and PR of 2 targets after DOA estimation using Block FOCUSS and BOMP algorithms

As the targets are stationary and the SNR observed is good after range processing of the data (SNR of 16 dB), we make use of different chirps in the radar data cube to perform statistical analysis of the data for different realization of noise. Range processing is performed on the samples in each chirp and the DOA estimation is performed on snapshot extracted from each chirp. The root mean square error (RMSE), probability of resolution(PR) and probability of false alarm (PFA) is then calculated on these different realizations for the DOA estimation of targets. The definitions of these parameters is explained in detail in Section 5.1.1.

Fig 5.15 shows the RMSE and the PR of the targets for varying DOA separations. The difference in DOA of the targets is plotted in the x axis, which is varied from 2° to 11° by moving the target along the x axis, keeping the y axis distance fixed. It is seen from the plot that a DOA separation of 3° and above is always resolved by Block FOCUSS algorithm. The DOA separation of 2° is resolved 60 percent of the time by Block FOCUSS where as BOMP fails to resolve this. The RMSE plot shows that the error in DOA estimation is below 1° for all the cases except when the targets are separated by 5°. Note that an error of 0.5° can occur as we use grid based estimation and the grid spacing is 0.5°, which means the target estimate is quantized to one of the nearest grid points. Also the RMSE of the DOA estimation for Block FOCUSS is lower than the BOMP algorithm.

- **DOA estimation of two targets away from broadside**

To further investigate the performance of the algorithm, the targets are placed away from the broadside by ~ 10° to both left extreme from the broadside and to the right extreme from the broadside. This is done to verify if the performance of the DOA estimation is similar to that of the targets placed at broadside for different DOA separations as 10° is not very far away from broad side. A Figure depicting this setup is shown in Fig 5.16 whereas Fig 5.13 shows the setup where the targets are placed in broadside. Fig 5.17 shows the comparison of the DOA estimation for these 3 positioning of the targets, Left side placement from broadside is marked as 'Left' in the plot, right side placement from broadside is marked as 'Right' and the broadside placement is marked as 'Broadside'. From the PR plot in Fig 5.17 it is seen that the targets separated by 3° and higher are always resolved. Targets separated by 2° are resolved when away from broadside for this experiment. False alarm rate is slightly higher for DOA separation of 3° when the target is placed at the left extreme of broadside, this is dependent mainly on how the phase of the targets is received by the 2 sub-systems and it is nothing to do with the target placement, as it is not seen for other DOA separations.

By looking at the RMSE plots it is observed that the RMSE of this particular experiment is slightly higher when compared to that of the one shown in Fig 5.15, this is because the SNR of this experiment is also

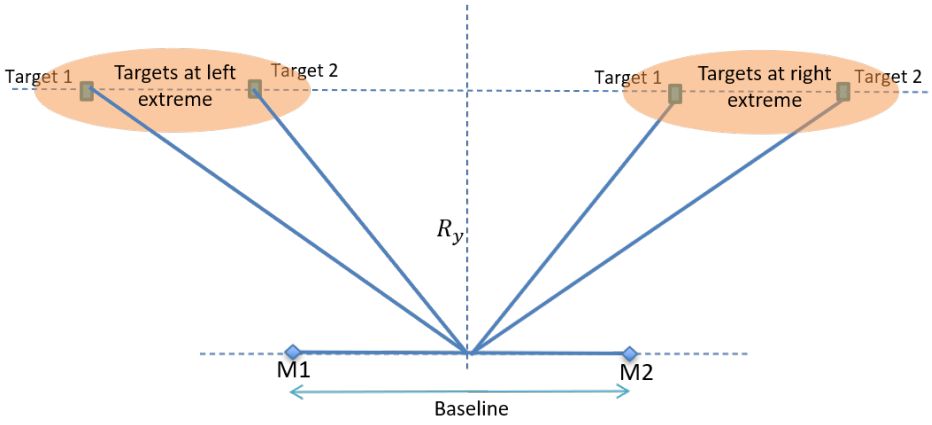

Figure 5.16: Depiction of target placed away from broadside in the anechoic chamber

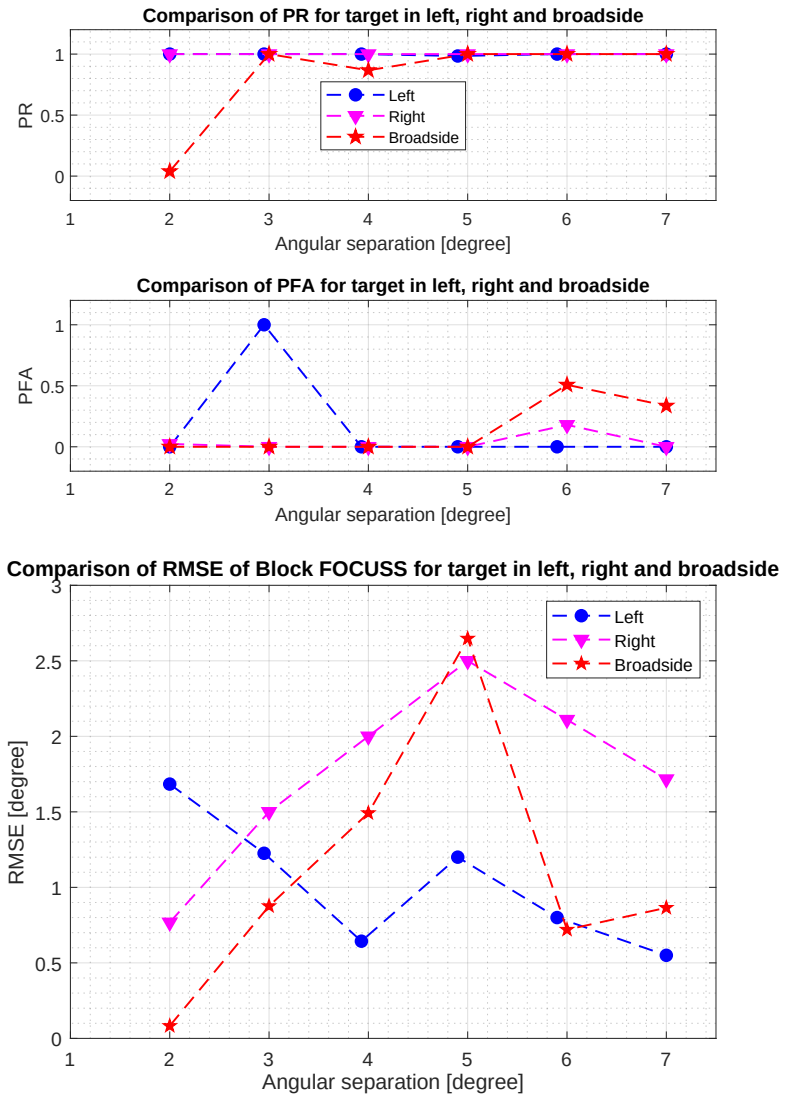

Figure 5.17: DOA estimation of targets in broadside and away from broadside

lower. The SNR for this experiment is 13 dB, it could be because of target not being in the center of the range bin. An important observation here is that when targets are placed to the left extreme of the

broadside direction, the performance is better when compared to the broadside placement or to the placement on the right extreme of the broadside direction. A possible explanation that can be given for this is the way the hardware setup is used. The hardware used does not have enough absorbers to reduce the effect of the possible radiations from the connecting wires to the chip, which acts as interference and effects the beam pattern generated from the antennas. Another point to notice from the RMSE plot in Fig 5.17 is that for the DOA separation of 5° between the targets the RMSE is higher when compared to other separations in all three positioning of the target. Hence, it can be inferred that the beam pattern for this particular DOA separation suffers more from interference than the rest.

- **Comparison of single sensor vs distributed setup**

  In the setup, as we are incoherently combining the data from the two sub-systems separated by a baseline of 0.396 m, we do not increase the aperture of the system, but we gain from the spatial diversity as we now have more data points for the same imaging scene. This comparison can be done by processing the data captured from the 2 sub-systems individually and comparing the results with the combined processing for 2 targets separated by certain DOA separation and placed in the broadside region of the sensors. Fig 5.18 shows the probability of resolution and probability of false alarm of the data processed by left sensor and right sensor as standalone systems using FOCUSS algorithm along with the combined DOA estimate performed using Block FOCUSS.

  From Fig 5.18 it can be seen that combining the data from the 2 systems will help to reduce the false alarm ratio. It is seen that the combined DOA estimation has lower false alarms as compared to the two sub-systems estimating the DOA's individually. It can also be seen from the probability of resolution plot that the resolution we obtain by a combined estimate is a combination of the 2 systems. For example, DOA separation of 3° is always resolved by the left sensor, where as the right sensor fails to resolve it. But the combined DOA estimation using Block FOCUSS resolves the two targets, this is the spatial diversity gain that is achieved.

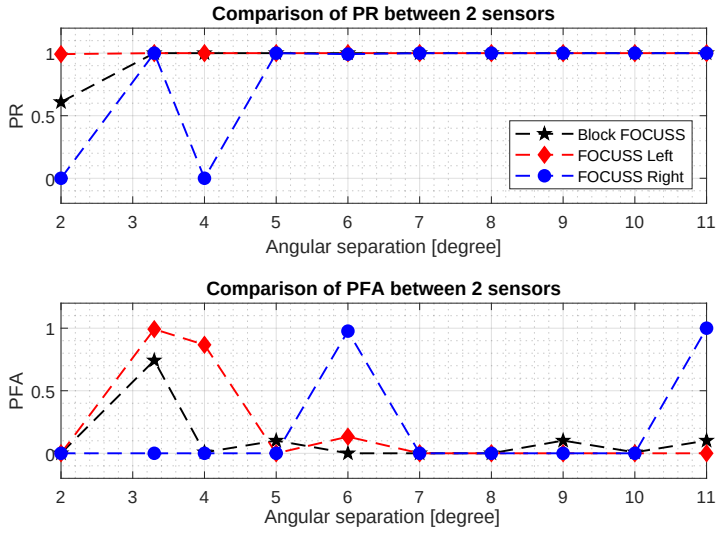

Figure 5.18: Comparison of PR and FA for single sensor vs distributed system

5.5.4. Effect of varying baseline

In this experimental setup as discussed in previous section we process the data incoherently, which means the resolution that we obtain is still limited by the aperture of the sub-system and we only benefit from the spatial diversity gain by doing a combined estimate of data from 2 sensor positions. In this type of combining the positioning of the 2 sub-systems plays a role in the spatial diversity that can be achieved. This means the way in which targets phase is perceived by the 2 sensors will effect the resolution capability of the sensors. There are 2 factors here that can influence how the phase of the targets are perceived by the sub-systems, one being the RCS of the target itself. Second one is the exact distance of the target from the sensor. As we are operating in the mm wave frequency range, even a small displacement in range of the target can change the phase of the targets as perceived by the sensors drastically. Thus eventually the phase of the targets seen by the sensors is dependent on both the RCS of the target and the path length travelled by the reflected wave. If the phase difference between the 2 targets is closer to zero, then the sensor might not be able to resolve the 2 closely spaced targets as the signals received by the 2 targets are strongly correlated, whereas if the target phases differ by a factor of pi then the resolution probability will increase. Thus by increasing the number of sensors used to estimate the DOA the resolution capability of the system is increased as it provides a diversity in the received phase and thus in resolution.

An experiment is conducted by placing 2 targets at a fixed DOA separation in the broadside and at 4.5 m from the center of the distributed system. The baseline (BL) separation between the 2 sub-systems is varied and the same target is observed with different baseline separations. The processed data is studied to see the effect of probability of resolution of the 2 targets with varying baseline separation. Fig 5.19 shows the plot of probability of resolution for baseline separations varying from 30 mm to 100 mm. This experiment is performed for targets with DOA separation of 2°, 3° and 4°.

Fig 5.19 indicates that the targets separated by 2° in azimuth is resolved by baseline separation of 40 mm and 100 mm. Targets separated by 3° have reduced probability of resolution for baseline separation of 60 mm and 80 mm. Targets separated by 4° are well resolved by all baseline separations except at 50 mm baseline separation which has lower probability of resolution. This plot clearly indicates that the baseline separation plays a role in how the targets are perceived by the 2 sub-systems. This is also explained in detail with some simple simulations in Section 5.2.1.

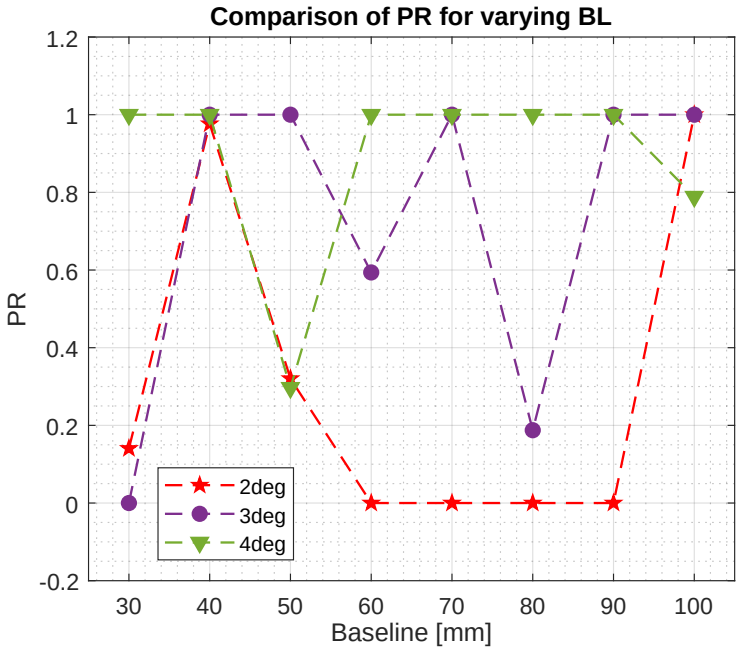

Figure 5.19: PR for varying baseline separation between the 2 sensors

5.6. Conclusions

Monte Carlo runs are executed by simulating the target scene and the radar signal in MATLAB for two targets, present at the range of 20 m from the radar sensors. Performance parameters like RMSE, probability of resolution, probability of false alarm and average false alarm are studied for different SNR and baseline scenarios. It was successfully demonstrated from simulation that the Coherent FOCUSS has the best resolution capability (1°) compared to Block FOCUSS and BOMP. This is in line with the theory as the aperture used for coherent processing is equivalent to the baseline (128λ) of the distributed system which is much larger than the effective aperture of each sub-system. Coherent FOCUSS however suffers from large false alarms if the SNR is lower than 15 dB. Processing a non-isotropic target in a coherent manner leads to large false detections which is shown through simple simulations.

Block FOCUSS has a resolution capability of 5° with PR greater than 80 percent and PFA less than 15 percent, for a sub-system with effective aperture of 6λ and SNR of 20 dB. It is shown that the performance of the proposed Block FOCUSS algorithm is thus better than the existing BOMP algorithm, which provides a DOA resolution of 9° for the same configuration. Block FOCUSS and BOMP algorithms also suffer from higher false alarms for lower SNR values (less than 15 dB) and hence might not be effective for lower SNR scenarios. The algorithms used in this thesis are grid based algorithms and thus suffer from errors in DOA estimation for targets not present on the grid. A possible solution existing in literature is discussed, which can be used to overcome the error caused by the off-grid target. It is done by having a two level estimation process, once with coarse dictionary grid and then with the finer grid of dictionary. This approach can be applied to real life scenarios when the targets are not on the grid by refining the grid further to estimate the true DOA.

Experiments are conducted in the anechoic chamber in TU Delft by placing two trihedral reflectors as targets and using the NXP Dolphin MIMO radar with 3 transmitters and 4 receivers (effective aperture of 6λ) as the radar sub-system. The radar sensor was moved to two different positions to mimic the distributed system setup with a baseline of 0.396 m. The sensor placed in two positions are thus not synchronized, and moreover the targets used are not coherent. Hence, we use algorithms which perform incoherent combining of the two mono-static responses. The DOA estimation is performed for targets separated from 2° to 11° in azimuth by using Block FOCUSS and BOMP. The two algorithms are compared and it is seen that Block FOCUSS has better probability of resolution and RMSE when compared to BOMP algorithm. The Block FOCUSS algorithm can resolve targets separated by 3° or higher in the azimuth, whereas BOMP can resolve only from 5°. Further comparison is done for probability of resolution and probability of false alarm for single subsystem versus distributed system. It is seen that combined DOA estimate from distributed system performs better as it benefits from the spatial diversity gain. An experiment is also performed for varying baseline separation between the two sub-systems. It is observed that the baseline separation between the sensors affects the spatial diversity gain and thus the resolution. It is to be noted that for the same effective aperture, the Block FOCUSS achieves a better angular resolution in experiments compared to simulations. This is because the simulation results are obtained after Monte Carlo runs with targets having varying phases, whereas the experimental results do not cover this varying phase scenario.

6

Conclusions and future work

This chapter concludes the work done in this thesis by summarizing the novelties and results in Section 6.1. Section 6.2 provides some recommendations to further investigate the problem.

6.1. Results and novelties

In the last decade the interest in safety of drivers, passengers, pedestrians and other road users has increased significantly with the growth in automotive industry and economy of the nations. Radars play an important role in the safety of autonomous driving as they can be used for detection of pedestrians, cyclists, other automobiles and other road objects. While radars are able to perform high resolution estimation of range and velocity of the objects, the systems are currently limited by the angular resolution. A primary reason is that, the aperture of a single sensor cannot be increased as it is cost ineffective and large sensors are high undesirable by the car manufacturers. This work introduces three novel algorithms to improve the angular resolution of the radar system, while maintaining a small physical aperture per sensor through sensor fusion. The proposed algorithms work on single snapshot data obtained after Range-Doppler processing, allowing easy integration and compliance. The radar scene can be assumed to be sparse as there will be only few targets with the same range and velocity. Hence, in this work sparse signal processing techniques are utilized to solve the DOA estimation problem using a single snapshot.

For a distributed radar system, the target in the imaging scene cannot always be assumed to be in the far field, as its virtual aperture is much larger than that of a single sensor. Therefore, more complex near field assumption is considered when estimating the DOA of targets, by defining the corresponding DOA of the target to each sensor in the distributed system. Additionally, if the system is fully coherent then the bi-static responses from the sensors can be utilized along with the mono-static responses to improve the DOA estimation, when compared to using only the mono-static responses. The target can be perceived as isotropic or non-isotropic based on the distance of the target to the radar, the radar aperture and the dimensions of the target. Through theoretical modelling, it is shown that coherent processing is feasible only when the target is isotropic, and hence incoherent processing of the sensor data also needs to be considered. Thus, in this thesis three methods of combining the data from multiple sensors are proposed namely, incoherent processing, coherent processing and a combination of both coherent and incoherent processing. Feasibility of the algorithms are validated through Monte Carlo simulations of a testbench developed in MATLAB that models the hardware and the target scenario.

The incoherent processing can be performed irrespective of whether the system is fully coherent or the target is isotropic. The effective aperture of the incoherent processing is proportional to the aperture of the largest sub-system and is independent of the baseline, but it can still benefit from the spatial diversity gain. Block sparse algorithms can be used to perform combined DOA estimation of the targets, since the virtual array response from both the sensors have the same support basis. The current state of art block sparse algorithms like BOMP (extension of OMP) suffer from low resolution capability and low noise tolerance. A novel Block FOCUSS algorithm is proposed to address these drawbacks, which is an extension of an alternative algorithm called FOCUSS. The FOCUSS algorithm was extended for data fusion from multiple sensors since, it converges to the true DOA of the targets by selecting the columns of sensing matrix that best represents the true DOA, unlike the greedy algorithms like OMP. It is to be noted that OMP is computationally efficient when

compared to FOCUSS algorithm, but the aim of this work is to improve the resolution capability. For a system with two sensors with an effective aperture of 6λ (theoretical resolution of ~ 8.5°), the Block FOCUSS algorithm consistently outperforms the BOMP algorithm achieving 2° angular resolution for SNR greater than 30 dB (3x BOMP resolution) and 5° angular resolution for SNR between 15 dB to 30 dB (2x BOMP resolution). Block FOCUSS has PR of more than 80 percent for DOA separations of 5° or more, with PFA less than 15 percent, when the effective aperture of each sensor is 6λ for SNR of 20 dB. Whereas, BOMP has a PR of more than 80 percent only for DOA separation of 9° or more for the same configuration.

An experimental evaluation was performed using NXP radar (consisting of 3 transmitter and 4 receivers in each sensor, forming an effective aperture of 6λ) and trihedral reflectors as targets, inside an anechoic chamber. As the two distributed sensors are not synchronized, only the mono-static responses are used to perform incoherent processing. Hence, only the performance of the Block FOCUSS and BOMP algorithms are evaluated using this experimental setup. The Block FOCUSS achieves an angular resolution of 3° or more in azimuth for the targets in near field (4.5 m for a baseline of 0.396 m) using single snapshot from each sensor. Whereas in the same scenario, BOMP could only achieve an angular resolution of 5° or more. It is to be noted that for the same effective aperture, the Block FOCUSS achieves a better angular resolution in experiments compared to simulations. This is because the simulation results are obtained after Monte Carlo runs with targets having varying phases, whereas the experimental results do not cover this varying phase scenario.

The coherent processing can be performed when the system is fully coherent and the targets are isotropic. When the target is in the near field, the path length difference between the target and the sensors leads to phase difference between the snapshots from the sensors. Presence of this phase difference can impede coherent processing even though the target is isotropic. In this thesis, a novel algorithm called Coherent FOCUSS is introduced, which compensates the phase difference observed due to the path length difference. This method has an effective aperture equivalent to the baseline of the distributed system, thus it provides higher angular resolution compared to the incoherent processing. For a baseline of 128λ(theoretical resolution of ~ 0.9°) and a sub-system aperture of 6λ, Coherent FOCUSS achieves an angular resolution of 1° for SNR values greater than 15 dB, which is two times better than the Block FOCUSS. For lower SNR values (below 15 dB), both Block FOCUSS and Coherent FOCUSS suffer from ghost targets that appear in the DOA estimation of targets. Coherent FOCUSS suffers more in lower SNR (below 15 dB) cases compared to Block FOCUSS.

In coherent processing, the finite range resolution of the radar sensor limits the accurate estimation of the path length difference. This practical constraint leads to high false alarms in coherent processing. Moreover, coherent processing also suffers from high side lobe levels that increase with the increase in baseline. To overcome these limitations a novel Fusion FOCUSS algorithm is proposed, which combines the bi-static responses coherently along with the incoherent mono-static responses of the system. By appropriately designing the sensor elements in each sensor, the bi-static responses together can have twice the aperture of the individual mono-static responses. Thus, this method improves the angular resolution by a factor of two, when compared to incoherent processing of both mono-static and bi-static responses.

With the simulation and experimental results the performance of Block FOCUSS is validated. With the simulation results the Coherent FOCUSS is validated and a Fusion FOCUSS method is proposed to overcome some of the drawbacks of Coherent FOCUSS. Hence, demonstrating the robustness of the algorithms in practical scenarios.

6.2. Recommendations for future work

Based on the work done in this thesis, several recommendations are provided here to investigate and further improve the solution.

- Stationary objects are considered in this thesis, the work can be extended to consider moving targets. When the targets are in motion, the main difference to be considered is the phase change that occurs due to the migration of the target. This phase change can be perceived differently by different sensors. This can have a major impact on the coherent processing of the data. [52] shows a study of the effect of target displacement on the DOA estimation. It is non negligible and thus needs to be addressed to complete the problem for application in practical scenarios. [53] also provides a way to correct for errors in the estimation based on the target positions in oceans, this idea can be expanded in automotive radar as well. Another aspect of moving targets, is that the individual radar sensors perceive the target with different radial velocity. Moreover, similar to range quantization there will be errors due to Doppler quantization. Hence, the coherency corrections for range have to be extended with corrections

for Doppler. This will further complicate the coherent processing of the data.

- In this thesis the AF and the resolution achieved is studied for a uniformly distributed array in each sensor. Instead, sensors made up of sparsely distributed elements can be utilized which will provide higher virtual aperture for each sensor, thus providing higher resolution as shown in the study performed by [15]. Also, having sparse arrays can improve the coherency of the sensing matrix (discussed in Appendix A). An optimization problem can be formed to estimate the best configuration of array in the sub-system by considering the baseline and other system parameters. Current state of art mostly discusses about finding the optimized sparse single sensor, instead we can look for optimized sparse sensor configurations for the distributed setup by considering multiple sub-systems in a single optimization problem. Optimal design of the distributed system can enhance the resolution capability and the performance of the algorithm further.
- Grid based algorithms suffer from errors in estimation of DOA when the target is not present on the grid. But the granularity with which a grid can be defined is limited by the properties of sensing matrix [13] and by implementation constraints. In this thesis one of the ways to overcome this problem is presented by having a refined grid spacing around the estimated target position, but this is not the most efficient way to estimate the DOA. Hence, grid-less algorithms suggested in [13] like atomic norm minimization can be explored for data fusion to overcome the off-grid problems by extending the algorithms for block sparsity.
- The regularization parameter (λ) chosen in all the variants of the FOCUSS algorithms can be further optimized in each iteration of the algorithm to achieve better convergence [42]. Currently only single value of the optimization parameter is used in the algorithms for all the apertures, which is selected as the minimum of the noise variances from all apertures.
- The performance of the Fusion FOCUSS algorithm for varying array configurations can be studied, in order to determine the best array configuration that can be used without increasing the side lobe levels than the defined threshold. The evaluation of the performance of Fusion FOCUSS for varying SNR, baseline and varying phase of the target can be studied.

Appendices

A

Coherency of sensing matrix

To ensure that the unique solution can be found by solving the under determined set of equations to obtain the sparse solution, it is necessary that the sensing matrix **A** satisfies the uniqueness conditions. One of the ways to find this uniqueness condition is by checking if the sensing matrix satisfies the restrictive isometric property (RIP). But this is computationally very ineffective to implement [13]. In this thesis we thus use the mutual coherence [13] or what we call as the coherence index of the sensing matrix ($\mu(\mathbf{A})$). The coherence index quantifies the correlation between the atoms (or columns) of **A**. The coherence index ($\mu(\mathbf{A})$) of **A** is given by the largest absolute correlation between any two columns of **A** (normalized sensing matrix). It is given as

$$\mu(\boldsymbol{A}) = \max_{i \neq j} \frac{\left|\langle \boldsymbol{a}_i, \boldsymbol{a}_j \rangle\right|}{\|\boldsymbol{a}_i\|_2 \left\|\boldsymbol{a}_j\right\|_2} \tag{A.1}$$

where $\langle .,. \rangle$ denotes the inner product of 2 vectors.

Intuitively, if the 2 columns of the matrix A are highly correlated then it will be difficult to distinguish their contribution to the measurements **y**, thus making it hard to attain the unique solution. If the two columns are completely coherent then it will be impossible to attain the sparse solution as it is impossible to distinguish their contributions to **y**. Therefore, to ensure a successful recovery of the sparse signal the value of $\mu(\mathbf{A})$ should be small.

If the signal to be reconstructed is K - sparse, i.e., in automotive radar if we have K targets that needs to be recovered, then the necessary condition for a successful recovery is

$$K < \frac{1}{2}\left(1 + \frac{1}{\mu}\right) \tag{A.2}$$

For a normalized matrix **A** the coherence index can also be calculated as the maximum absolute off-diagonal element of $\mathbf{A}^H\mathbf{A}$ [41]. The visualization of the values of coherence index for matrix **A** is explained in detail in [41]. An important point that we would like to bring the attention from [41] is that, the coherence index has been derived for several independent worst case scenarios in order to provide an easily interpretable bound for uniqueness. In some of the practical applications the value of the coherence index can be typically relaxed further. [41] provides some real world examples with statistical distribution of the data to prove this point. If the coherence index is not small enough, as the cardinality of the sparse signal increases the misdetection probability also increases.

Fig A.1 depicts the coherence index of the sensing matrix for incoherent and coherent processing for a distributed sensor with baseline of 128λ and for a target present in the near field region. The sensing matrix consists of a dictionary that looks at targets from $-45°$ to $+45°$ by dividing this filed of view equally into multiple points, which make up the dictionary of **A**. The x axis in the figure plots the dictionary size and the y axis plots the coherence index for the dictionary size. As the dictionary size increases, the number of atoms (or columns) in the sensing matrix increases thus reducing the angular spacing between the 2 adjacent columns. This increases the correlation between the columns and thus makes it hard to find the sparse solution as discussed above. For example when the dictionary size is 3 there are only 3 columns each spaced out equally in the FOV, thus the correlations between these columns is almost zero. Note that lower coherence index is desirable as it increases the probability of attaining the right sparse solution and reduces the misdetection

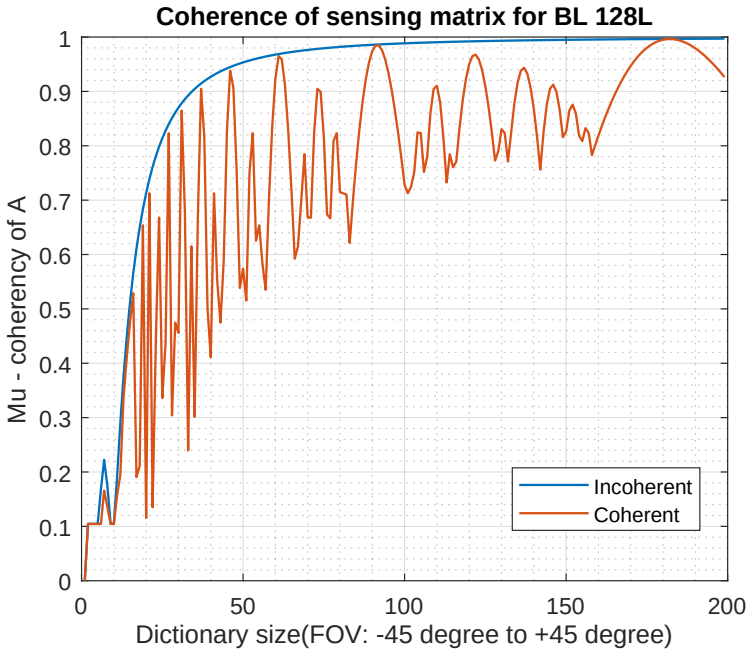

Figure A.1: Coherence index of **A** for baseline 128λ

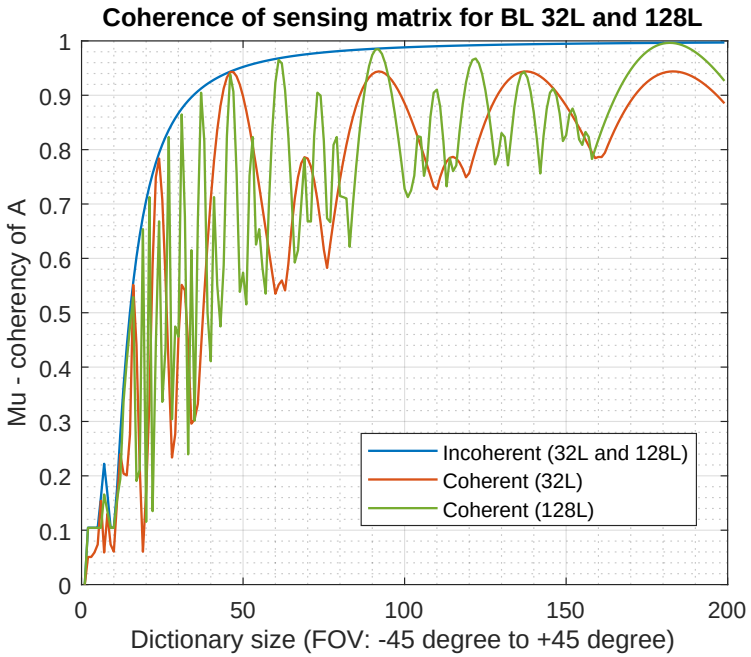

Figure A.2: Coherence index of **A** for baseline 128λ and 32λ

probability. Also from the figure it is shown that the coherence index of the incoherent processing increases smoothly with the increase in dictionary size, whereas for the coherent processing we see more variations. In coherent processing we are looking at a large aperture with very few antenna elements, thus making the large aperture a sparse array. This sparsity leads to the variation of the coherence index as well, based on the dictionary points that we chose. If we look at the AF for coherent processing as shown in Fig 4.8 it is seen that it has multiple side lobes that are placed very close to the main lobe. If the dictionary of the matrix **A** is made to coincide with the nulls of the side lobes, then the correlation between the columns can be reduced, as the ambiguities in DOA estimation reduces as well. These are represented by the dips in the coherence index for

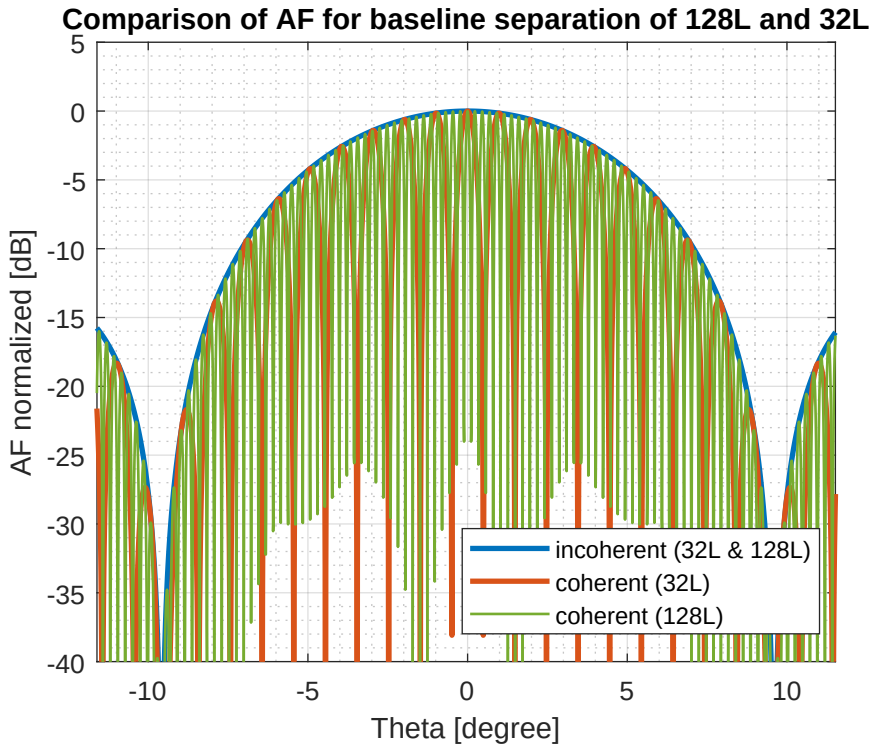

Figure A.3: AF for baseline 128λ and 32λ

coherent processing plot in the Fig A.1.

Looking at the coherence index, it is shown that picking the right dictionary is important to guarantee the recovery of a sparse signal. It can be seen that having an extremely fine grid increases the coherence index and is not desirable, even though it helps to avoid off-grid problems. Thus defining the dictionary grid that has sufficiently less coherency and still having as fine a grid as possible can be challenging. To understand the variation of coherence index for varying baseline we can look at the Fig A.2. From the plots it is shown that the coherence index for incoherent processing does not vary with varying baseline, this is because the sensing matrix for each sub-aperture is defined separately. As long as the array design for the sub-system remains same the coherence index also will remain the same for all the sub-apertures. However, for coherent processing we see that the variations in coherence index with dictionary size reduces with reduction in baseline, this is because as the baseline reduces the sparsity in the virtual aperture of the distributed system reduces (as the number of elements remain the same and they are now spaced more closely). As the baseline reduces further, the coherence index variations move closer to that of incoherent processing. The variation in coherence index for coherent processing can be linked to the AF of the same. Fig A.3 depicts the AF response of the coherent processing for baseline of 128λ and 32λ. From the plots it is seen that the number of side lobes next to the main lobe reduces as the baseline decreases, thus reducing the ambiguities in the measurements. A similar pattern is observed in the Fig A.2 where the variations in coherence index with dictionary spacing is reduced for a 32λ baseline when compared to 128λ baseline.

Hence, it is important to understand that choosing the right array design and the right dictionary spacing needs to be considered to achieve a lower coherence index value. Lower value for coherence index is important as it helps us in achieving the true sparse solution. Thus, exploring sparse array designs for the sub-systems used in the distributed system can be an important step towards achieving lower coherence index of the sensing matrix $\mathbf{A}$.

B

Ambiguity function

To evaluate the impact of the array geometry on the algorithms we can make use of Ambiguity function. AF is motivated by the matched-filter (MF) response defined as the similarity between the signal model $\mathbf{a}(\theta)$ evaluated at an assumed target position θ_T and the hypothesis θ. For a steering matrix $\mathbf{A}$ defined as in Eq 2.13, which consists of the steering vectors as the columns of the matrix, the AF is defined as given below

$$AF(\theta_i, \theta_T) = |MF[i]| = \left|\mathbf{a}(\theta_i)^H \mathbf{a}(\theta_T)\right| \tag{B.1}$$

For incoherent processing (Block FOCUSS) the AF is calculated as the aggregated matched-filter response from all the virtual apertures L (2 mono-static and 2 bi-static for a coherent system with 2 sensors). An effective ambiguity function is found by calculating the aggregated matched-filter norm across all the apertures defined by the below equation

$$AF_{incoh}(\theta_i, \theta_T) = MF[i] = \left(\sum_{l=1}^{L} \left(AF^l(\theta_i, \theta_T)\right)^2\right)^{1/2} \tag{B.2}$$

In the Eq B.2, AF^l is calculated for each virtual aperture as given in Eq B.1. The ambiguities that exist between the hypothesis θ_T and θ_i in the Block FOCUSS atom selection is produced by a high value of Eq B.2, and the peak values are the side lobes. For the case when the targets are on grid, the main lobe is centered at the true hypothesis ($\theta_i = \theta_T$). Note that for the symmetric array designs that are discussed in this thesis has a symmetry in AF around the main lobe. The AF obtained by incoherent processing for a system with 2 sensors is depicted in Fig 3.2. In this figure the true position of the target is considered as zero degree, which is where the main lobe is centered at. The side lobe levels indicate the ambiguity in the measurement of the DOA of a target, higher value for side lobes indicate a higher ambiguity and therefore making it difficult to measure the true DOA.

For coherent processing, the matrix $\mathbf{A}_c$ is obtained by stacking the sensing matrix from all the virtual apertures as shown in Eq 4.2. As all the steering vectors are now combined in a single matrix $\mathbf{A}_c$, we can write the AF for coherent processing as shown in Eq B.3, where $\mathbf{a}_c(\theta)$ represents the columns of $\mathbf{A}_c$, which constitutes the steering vectors from all the virtual apertures.

$$AF_{coh}(\theta_i, \theta_T) = |MF[i]| = \left|\mathbf{a}_c(\theta_i)^H \mathbf{a}_c(\theta_T)\right| \tag{B.3}$$

In coherent processing of a distributed system it should be noted that the sparsity in the total virtual aperture formed increases with increasing baseline. The effect of this on the AF is discussed in detail for coherent processing in Section 4.3. Fig 4.8 depicts the AF response from coherent processing for a distributed system with a baseline of 64λ. From this figure it is shown that the main lobe width for this response is much narrower than that of the incoherent processing, this means a better resolution can be achieved using such a large virtual array. However, it is also seen that the side lobe levels are very close to the main lobe, thus creating lot of ambiguities. Due to this, the target might be detected to be in one of the side lobe levels in scenarios with noise, leading to errors in the DOA estimation.

Bibliography

[1] Christian Waldschmidt, Juergen Hasch, and Wolfgang Menzel. "Automotive Radar — From First Efforts to Future Systems". In: *IEEE Journal of Microwaves* 1.1 (2021). DOI: 10.1109/jmw.2020.3033616.

[2] Mike Köhler et al. "Feasibility of automotive radar at frequencies beyond 100 GHz". In: *International Journal of Microwave and Wireless Technologies* 5.1 (2013). ISSN: 17590787. DOI: 10.1017/S175907871200075X.

[3] Alexander M. Haimovich, Rick S. Blum, and Leonard J. Cimini. "MIMO Radar with Widely Separated Antennas". In: *IEEE Signal Processing Magazine* 25.1 (2008), pp. 116–129. DOI: 10.1109/MSP.2008.4408448.

[4] C. Jacobs. *From ADAS to Driver Replacement-Is Actual Radar Performance Good Enough?* 2020. URL: https://www.analog.com/en/technical-articles/from-adas-to-driver-replacement.html.

[5] David Mateos-Núñez et al. "Design of mutually incoherent arrays for DoA estimation via group-sparse reconstruction". In: *2019 IEEE Radar Conference (RadarConf)*. 2019, pp. 1–6. DOI: 10.1109/RADAR.2019.8835842.

[6] Xiaofei Zhang and Renzheng Cao. "Direction of Arrival Estimation: Introduction". In: *Wiley Encyclopedia of Electrical and Electronics Engineering*. John Wiley & Sons, Inc., Feb. 2017, pp. 1–22. DOI: 10.1002/047134608x.w8343.

[7] Francesco Belfiori, Wim Van Rossum, and Peter Hoogeboom. "Coherent MUSIC technique for range/angle information retrieval: Application to a frequency modulated continuous wave MIMO radar". In: *IET Radar, Sonar and Navigation* 8.2 (2014). ISSN: 17518784. DOI: 10.1049/iet-rsn.2013.0121.

[8] S. Unnikrishna Pillai and Byung Ho Kwon. "Forward/Backward Spatial Smoothing Techniques For Coherent Signal Identification". In: *IEEE Transactions on Acoustics, Speech, and Signal Processing* 37.1 (1989). ISSN: 00963518. DOI: 10.1109/29.17496.

[9] Richard Roy and Thomas Kailath. "ESPRIT—Estimation of Signal Parameters Via Rotational Invariance Techniques". In: *IEEE Transactions on Acoustics, Speech, and Signal Processing* 37.7 (1989). ISSN: 00963518. DOI: 10.1109/29.32276.

[10] Wenjing Liao and Albert Fannjiang. "MUSIC for single-snapshot spectral estimation: Stability and super-resolution". In: *Applied and Computational Harmonic Analysis* 40.1 (Jan. 2016), pp. 33–67. ISSN: 1096603X. DOI: 10.1016/j.acha.2014.12.003.

[11] Shengzhi Xu, Jianping Wang, and Alexander Yarovoy. "Super resolution DOA for FMCW automotive radar imaging". In: *2018 IEEE Conference on Antenna Measurements and Applications, CAMA 2018*. 2018. DOI: 10.1109/CAMA.2018.8530609.

[12] Joachim H.G. Ender. "On compressive sensing applied to radar". In: *Signal Processing* 90.5 (May 2010), pp. 1402–1414. ISSN: 01651684. DOI: 10.1016/j.sigpro.2009.11.009.

[13] Zai Yang et al. *Sparse methods for direction-of-arrival estimation*. Dec. 2017. DOI: 10.1016/B978-0-12-811887-0.00011-0.

[14] Stefano Fortunati et al. "Single-snapshot DOA estimation by using compressed sensing". In: *Eurasip Journal on Advances in Signal Processing* 2014.1 (2014). ISSN: 16876180. DOI: 10.1186/1687-6180-2014-120.

[15] David Mateos-Nunez et al. "Sparse array design for automotive MIMO radar". In: *EuRAD 2019 - 2019 16th European Radar Conference*. 2019.

[16] Matthias Weiß. "Passive wireless local area network radar network using compressive sensing technique". In: *IET Radar, Sonar and Navigation* 9.1 (Jan. 2015), pp. 84–91. ISSN: 17518784. DOI: 10.1049/iet-rsn.2014.0073.

[17] Matthias Weiß. "Single frequency surveillance radar network using an adapted ℓ minimization approach for extended targets". In: *2016 4th International Workshop on Compressed Sensing Theory and its Applications to Radar, Sonar and Remote Sensing, CoSeRa 2016*. Institute of Electrical and Electronics Engineers Inc., Nov. 2016, pp. 153–157. ISBN: 9781509029204. DOI: 10.1109/CoSeRa.2016.7745719.

[18] Sandeep Gogineni and Arye Nehorai. "Target estimation using compressive sensing for distributed MIMO radar". In: *Conference Record - Asilomar Conference on Signals, Systems and Computers*. 2010, pp. 793–797. ISBN: 9781424497218. DOI: 10.1109/ACSSC.2010.5757674.

[19] André W. Gunst and Mark J. Bentum. "The LOFAR phased array telescope system". In: *IEEE International Symposium on Phased Array Systems and Technology*. 2010. DOI: 10.1109/ARRAY.2010.5613300.

[20] Michael Gottinger et al. "Coherent Automotive Radar Networks: The Next Generation of Radar-Based Imaging and Mapping". In: *IEEE Journal of Microwaves* 1.1 (Jan. 2021), pp. 149–163. DOI: 10.1109/jmw.2020.3034475.

[21] Chih-Heng Lin. *MONTEREY, CALIFORNIA THESIS DISTRIBUTED SUBARRAY ANTENNAS FOR MULTI-FUNCTION PHASED-ARRAY RADAR*. Tech. rep. 2003.

[22] Christian R Berger and José M F Moura. *Noncoherent Compressive Sensing with Application to Distributed Radar*. Tech. rep.

[23] D ; Liu et al. *Sparsity-driven distributed array imaging*. Tech. rep. 2015. URL: http://www.merl.com.

[24] Jiadi Zhang. *Super-resolution Algorithms for Target Localization using Multiple FMCW MIMOs*. Tech. rep. URL: http://repository.tudelft.nl/..

[25] Aitor Correas-Serrano and Maria A. Gonzalez-Huici. "Experimental evaluation of compressive sensing for DoA estimation in automotive radar". In: *Proceedings International Radar Symposium*. Vol. 2018-June. IEEE Computer Society, Aug. 2018. ISBN: 9783736995451. DOI: 10.23919/IRS.2018.8448197.

[26] Krishnasamy T. Selvan and Ramakrishna Janaswamy. "Fraunhofer and Fresnel Distances : Unified derivation for aperture antennas." In: *IEEE Antennas and Propagation Magazine* 59.4 (2017), pp. 12–15. DOI: 10.1109/MAP.2017.2706648.

[27] Wanjun Zhi and Michael Yan Wah Chia. "Near-field source localization via symmetric subarrays". In: *IEEE Signal Processing Letters* 14.6 (June 2007), pp. 409–412. ISSN: 10709908. DOI: 10.1109/LSP.2006.888390.

[28] Harry L. Van Trees. *Optimum Array Processing*. 2002. DOI: 10.1002/0471221104.

[29] A.G. Stove. "Linear FMCW radar techniques". English. In: *IEE Proceedings F (Radar and Signal Processing)* 139 (5 Oct. 1992), 343–350(7). ISSN: 0956-375X. URL: https://digital-library.theiet.org/content/journals/10.1049/ip-f-2.1992.0048.

[30] Minqiu Chen, Xingpeng Mao, and Liang Xin. "Underdetermined passive localisation of emitters based on multi-dimensional spectrum estimation techniques". In: *IET Radar, Sonar and Navigation* 11.11 (2017). ISSN: 17518784. DOI: 10.1049/iet-rsn.2017.0186.

[31] Sangdong Kim, Daegun Oh, and Jonghun Lee. "Joint DFT-ESPRIT Estimation for TOA and DOA in Vehicle FMCW Radars". In: *IEEE Antennas and Wireless Propagation Letters* 14 (2015). ISSN: 15361225. DOI: 10.1109/LAWP.2015.2420579.

[32] J Ruoyu Feng. *Target Localization Using MIMO-monopulse Application on 79 GHz FMCW Automo-tive Radar*. Tech. rep. URL: http://repository.tudelft.nl/..

[33] Geun Ho Park, Young Kwang Seo, and Hyoung Nam Kim. "Range-doppler domain-based DOA estimation method for FM-band passive bistatic radar". In: *IEEE Access* 8 (2020). ISSN: 21693536. DOI: 10.1109/ACCESS.2020.2981957.

[34] J. Li and P. Stoica. *MIMO Radar Signal Processing*. Wiley - IEEE. Wiley, 2008. ISBN: 9780470391433. URL: https://books.google.nl/books?id=g6uLLWb-TqYC.

[35] Hamid Krim and Mats Viberg. "Two decades of array signal processing research: The parametric approach". In: *IEEE Signal Processing Magazine* 13.4 (1996). ISSN: 10535888. DOI: 10.1109/79.526899.

[36] Andre Durr et al. "Range-Angle Coupling and Near-Field Effects of Very Large Arrays in mm-Wave Imaging Radars". In: *IEEE Transactions on Microwave Theory and Techniques* 69.1 (Jan. 2021), pp. 262–270. ISSN: 15579670. DOI: 10.1109/TMTT.2020.3022938.

[37] E.J. Candes and M.B. Wakin. “An Introduction To Compressive Sampling”. In: *IEEE Signal Processing Magazine* 25.2 (2008). ISSN: 1053-5888. DOI: 10.1109/msp.2007.914731.

[38] David L. Donoho. “Compressed sensing”. In: *IEEE Transactions on Information Theory* 52.4 (Apr. 2006), pp. 1289–1306. ISSN: 00189448. DOI: 10.1109/TIT.2006.871582.

[39] Ying Wang, Geert Leus, and Ashish Pandharipande. “Direction estimation using compressive sampling array processing”. In: *IEEE Workshop on Statistical Signal Processing Proceedings*. 2009, pp. 626–629. ISBN: 9781424427109. DOI: 10.1109/SSP.2009.5278497.

[40] Gilbert Strang. “Introduction to Applied Linear Algebra: Vectors, Matrices, and Least Squares [Bookshelf]”. In: *IEEE Control Systems Magazine* 40.6 (2020). ISSN: 1941-000X. DOI: 10.1109/MCS.2020.3019153.

[41] Ljubisa Stankovic et al. “Demystifying the Coherence Index in Compressive Sensing [Lecture Notes]”. In: *IEEE Signal Processing Magazine* 37.1 (2020). ISSN: 15580792. DOI: 10.1109/MSP.2019.2945080.

[42] Irina F Gorodnitsky and Bhaskar D Rao. *Sparse Signal Reconstruction from Limited Data Using FOCUSS: A Re-weighted Minimum Norm Algorithm*. Tech. rep. 3. 1997.

[43] Joachim H. G. Ender. “A compressive sensing approach to the fusion of PCL sensors”. In: *21st European Signal Processing Conference (EUSIPCO 2013)*. 2013, pp. 1–5.

[44] Stefan Brisken and Joachim Ender. “Block-sparse 3-D ISAR image reconstruction in a non-coherent multistatic scenario”. In: *IEEE National Radar Conference - Proceedings*. Vol. 2015-June. June. Institute of Electrical and Electronics Engineers Inc., June 2015, pp. 265–269. DOI: 10.1109/RADAR.2015.7131007.

[45] Shane F. Cotter et al. “Sparse solutions to linear inverse problems with multiple measurement vectors”. In: *IEEE Transactions on Signal Processing* 53.7 (2005). ISSN: 1053587X. DOI: 10.1109/TSP.2005.849172.

[46] Bhaskar D. Rao et al. “Subset selection in noise based on diversity measure minimization”. In: *IEEE Transactions on Signal Processing* 51.3 (2003). ISSN: 1053587X. DOI: 10.1109/TSP.2002.808076.

[47] Irina F. Gorodnitsky, John S. George, and Bhaskar D. Rao. “Neuromagnetic source imaging with FOCUSS: a recursive weighted minimum norm algorithm”. In: *Electroencephalography and Clinical Neurophysiology* 95.4 (1995). ISSN: 00134694. DOI: 10.1016/0013-4694(95)00107-A.

[48] Xuebing Han, Hao Zhang, and Gang Li. “Fast Algorithms for Sparse Recovery with Perturbed Dictionary”. In: *arXiv preprint arXiv:1111.6237* (2011).

[49] Robert E Kell. *PROCEEDINGS OF THE IEEE O n the Derivation of Bistatic RCS from Monostatic Measurements*. Tech. rep.

[50] Dmitry Malioutov, Müjdat Çetin, and Alan S. Willsky. “A sparse signal reconstruction perspective for source localization with sensor arrays”. In: *IEEE Transactions on Signal Processing* 53.8 (Aug. 2005), pp. 3010–3022. ISSN: 1053587X. DOI: 10.1109/TSP.2005.850882.

[51] NXP Semiconductors. *TEF810X Product Data Sheet*. May 2019. URL: https://www.nxp.com/docs/en/data-sheet/TEF810XDS.pdf.

[52] Haoqing Liu et al. “Effects of Target Displacement on Single-Snapshot DOA Estimation in Automotive Radar”. In: *2021 IEEE Topical Conference on Wireless Sensors and Sensor Networks, WiSNeT 2021*. 2021. DOI: 10.1109/WiSNeT51848.2021.9414108.

[53] Jinyan Du et al. “Attitude correction method in DOA estimation of single vector hydrophone”. In: *2018 OCEANS - MTS/IEEE Kobe Techno-Oceans, OCEANS - Kobe 2018*. 2018. DOI: 10.1109/OCEANSKOBE.2018.8559051.